

Water and heat transport of paved surfaces

vorgelegt von:

M.Sc.

Anne Timm

ORCID: 0000-0002-5279-3642

von der Fakultät VI - Planen Bauen Umwelt
der Technischen Universität Berlin
zur Erlangung des akademischen Grades

Doktorin der Naturwissenschaften

- Dr. rer. nat.-

genehmigte Dissertation

Promotionsausschuss:

Vorsitzender: Prof. Dr. Reinhard Hinkelmann

Gutachter: Prof. Dr. Gerd Wessolek

Gutachter: Prof. Dr. Markus Weiler

Gutachterin: PD Dr. Patricia Göbel

Tag der wissenschaftlichen Aussprache: 05. April 2019

Berlin 2019



An example of urban pavement

Acknowledgements

First, I would like to thank Prof. Gerd Wessolek for many things, including the opportunity for this research and the good advice throughout these intense three years. I am most thankful however, for the trust put into me and the freedom to develop my own ideas and make my own mistakes.

I had the great pleasure to work on this thesis within the Graduate School *Urban Water Interfaces*, a joint project by TU Berlin and IGB Berlin, funded by the German Research Foundation DFG (GRK 2032). Everyone involved made this time interesting and easier. I am especially grateful to Prof. Dr. Reinhard Hinkelmann, Dr. Gwendolin Porst, the other doctoral students and the Internal Steering Committee who showed continued engagement for the project. Thank you all.

I am grateful to everyone who is or has been at the chair of soil conservation at the TU Berlin. Your previous work and support during my research has been instrumental for everything. Dr. Thomas Nehls and Dr. Yong Nam Rim, for installation and gradual improvement of the two lysimeters used in this study during previous research, which provided a perfect foundation for my own experiments. Everyone who helped me during the lysimeter reconstruction in April 2016, especially: Sven Glawion, Dr. Steffen Trinks and Joachim Buchholz. Dr. Björn Kluge and Reinhild Schwartengräber for always having an open door and good advice. Dr. Basem Aljoumani for making our office home. Dr. Andre Peters for providing the AWAT filter routine and always being available for questions concerning it, as well as teaching a specific course and supervising my Masters thesis, which lead to my love for data processing and R.

For everything concerning R, the community at *stackoverflow.com* has been a robust and reliable help. As is tradition by now, I am very lucky to be able to count on Sinah Ruhнау for proof-reading and general support.

Outside of work, my friends, RPG groups and the Critical Role community were essential. Thank you for times in which my thoughts could walk different paths.

As always, I am grateful to my family for believing that I could achieve whatever I set my mind to.

And finally - Floh. For unconditional love and support for 12 years, including the first two of this phase. Sometimes a dog is the best listener and taking walks at night solves problems.

Summary

The urban soil-atmosphere is typically paved with varying materials. This alteration has drastic effects on the urban hydrological balance. With a focus on stormwater management, most existing models treat all types of pavements identically when estimating runoff and neglect losses caused by evaporation and infiltration processes.

A literature review reveals that very few studies have been published that measured all components of the hydrological balance and water transport processes of pavements. Combining these studies with other research focussed on individual processes showed that pavements have varying impacts.

Within this project, two common pavement types were studied: cobblestones and concrete slabs. A combination of high-resolution weighable lysimeters and sensors measuring soil water content and temperature was used to gain new insights into their hydrological balance, as well as water and heat transport processes. Annually, cobblestones evaporated 25 % and rarely produced runoff (3 %). Concrete slabs tended to produce more runoff (16 %) and less evaporation (22 %). Both surfaces led to similar infiltration (62 %). Upward water transport from underlying soil layers led to evaporation processes during dry periods. This effect contributed 47 % of evaporation for cobblestones and 13 % for concrete slabs. Both surfaces led to higher soil temperatures compared to natural surface covers, with concrete slabs tending to slightly higher temperatures.

Estimating evaporation from paved surfaces may be accomplished by reducing the common grass-reference evapotranspiration. For annual estimations, the pre-existing TUBGR model yielded good results.

Pavements are more than a runoff generator. The urban soil-atmosphere interface is an active system with varying impacts on the urban hydrological balance. Understanding and utilising these differences has the potential to improve the design of urban areas.

Kurzfassung

Die urbane Grenzfläche zwischen Boden und Atmosphäre ist meist mit verschiedenen Materialien versiegelt. Diese Veränderung beeinflusst den urbanen Wasserhaushalt in hohem Maße. Mit einem Fokus auf starke Niederschläge und Überflutung gehen die meisten existierenden Modelle davon aus, dass sich alle Arten von Pflasterung gleich verhalten und Verdunstung und Versickerung vernachlässigt werden können.

Eine Analyse der Literatur ergibt dass bisher nur wenige Studien publiziert sind in denen alle Komponenten des urbanen Wasserhaushaltes gemessen wurden. Die vorhandenen Studien zeigen auf, dass verschiedene Arten von Versiegelung abweichende Auswirkungen haben.

Innerhalb des Projektes wurden zwei Pflasterungen näher untersucht: Bernburger Mosaik und Betonplatten. Dazu wurden hochauflösende wägbare Lysimeter mit zusätzlichen Sensoren ausgestattet, um Wassergehalt und Temperatur des Bodens zu messen. Mit dieser Kombination von Methoden wurde angestrebt, neue Erkenntnisse zum urbanen Wasserhaushalt und zu relevanten Wasser- und Wärmetransportprozesse zu gewinnen. Bernburger Mosaik bildete nur selten Oberflächenabfluss (3 %) und 25 % verdunsteten jährlich. Betonplatten bildeten weniger Verdunstung (22 %) und führten häufiger zu Oberflächenabfluss (22 %). Bei beiden Oberflächen versickerten rund 62 %. An der Verdunstung war aufwärts gerichteter Wassertransport von Bodenschichten an trockenen Tagen maßgeblich beteiligt. Bei Bernburger Mosaik wurden 47 % der gesamten Verdunstung an Tagen ohne Niederschlag verzeichnet, bei Betonplatten waren es 13 %. Im Vergleich zu natürlichen Oberflächen führte Versiegelung zu höheren Bodentemperaturen, wobei Betonplatten zu leicht höheren Temperaturen neigten.

Für die Abschätzung von Verdunstung versiegelter Flächen kann eine verringerte Gras-Referenzverdunstung genutzt werden. Dabei lieferte das bereits vorhandene TUBGR Modell gute Ergebnisse für jährliche Werte.

Gehweg- und Straßenpflaster sind mehr als Erzeuger von Oberflächenabfluss. Die urbane Grenzfläche von Boden und Atmosphäre ist ein aktives System mit unterschiedlichen Auswirkungen auf den urbanen Wasserhaushalt. Ein verbessertes Verständnis dieser Auswirkungen und dessen Anwendung hat Potenzial urbane Räume besser zu gestalten.

Table of contents

List of Figures	iii
List of Tables	v
1 Preface	1
2 Introduction	3
2.1 Paved surfaces	5
2.2 Water transport processes	7
2.2.1 Elements and characteristics of pavements	7
2.2.2 Processes	8
2.2.2.1 Runoff	8
2.2.2.2 Infiltration	10
2.2.2.3 Groundwater recharge	10
2.2.2.4 Evaporation	11
2.3 Hydrological balance	12
2.4 Application	16
2.4.1 Sealing degree (SD)	17
2.4.2 Runoff coefficient (RC)	18
2.4.3 Numerical models	18
2.4.4 Data generation	19
2.5 Conclusion	20
3 Material & Methods	21
3.1 Lysimeter studies	21
3.2 Lysimeter station	23
3.2.1 Surface types	23
3.2.2 Lysimeter set-up	25
3.2.3 Built-in sensors	26
3.2.4 Climate station	28
3.3 Surface wetting-drying experiment	28
3.4 Data processing	29
3.4.1 Tools	30
3.4.2 Lysimeter data	30
3.4.2.1 Runoff	30

3.4.2.2	Precipitation, Evaporation & Infiltration	32
3.4.3	Sensor data	36
4	Results	37
4.1	Lysimeter study	37
4.1.1	Climatological conditions	37
4.1.2	Hydrological balance & water transport	38
4.1.2.1	Hydrological balance	38
4.1.2.2	Water transport processes	44
4.1.3	Heat balance & transport	50
4.2	Process interactions	55
4.2.1	Coupled heat and water transport	55
4.2.2	Correlation of processes	60
5	Estimating evaporation of paved surfaces	64
5.1	Grass-reference evapotranspiration ET_0	64
5.2	Relationship between E and ET_0 for paved surfaces	65
5.2.1	TUBGR model	66
5.2.2	Determining the ratio between E and ET_0	67
5.2.3	Outlook	72
6	Conclusion	73
A	Appendices	I
A.1	Extended tables & figures	I
A.2	Lysimeter reconstruction	VII

List of Figures

2.1	Examples of different pavement types	6
2.2	Pavement elements and water transport processes	8
2.3	Hydrological balance in summer & winter	16
3.1	Basic principle of vegetated and paved weighable lysimeters	23
3.2	Lysimeter station	24
3.3	Lysimeter surfaces	24
3.4	Scheme of lysimeter set-up	25
3.5	Sensor placement	26
3.6	Surface wetting	28
3.7	Data processing	29
3.8	Example of raw runoff data	31
3.9	Principle of AWAT filter routine	33
3.10	Precipitation comparison	35
4.1	Rainfall distribution	38
4.2	Hydrological balance	39
4.3	Cumulative hydrological balance	41
4.4	Hydrological balance event intensities	42
4.5	Hourly hydrological balance – period with highest E	45
4.6	Hourly hydrological balance – period with highest P	46
4.7	Evaporation on dry days following rainfall	49
4.8	Annual mean temperature profile	50
4.9	Daily temperature profiles	51
4.10	Differences in monthly mean temperatures	52
4.11	Hourly air, surface & soil temperatures – period with highest E	53
4.12	Monthly air & soil temperatures for different surface covers	55
4.13	Example hourly soil water content and temperatures	56
4.14	Surface wetting-drying process (timeseries)	58
4.15	Surface wetting-drying process (thermal)	59
4.16	Correlation matrix for hourly data	62
4.17	Correlation matrix for daily data	63
5.1	Relationship between daily E and ET_0	68
5.2	Monthly estimation of evaporation (E) with TUBGR model	69

5.3	Deriving monthly κ from T_{air}	70
5.4	Comparison of monthly estimations of E	72
A.1	Hourly air, surface & soil temperatures – period with highest P	V
A.2	Deriving monthly κ_w and κ_d from T_{air}	VI
A.3	Impressions from lysimeter reconstruction in April 2016	VII
A.4	Sensor installation	VIII

List of Tables

2.1	Scientific communities researching pavement	5
2.2	Pavement surface properties	9
2.3	Previous studies of annual hydrological balances	13
2.4	Short period or single component observations of hydrological balances . .	14
2.5	Sealing degrees of paved surfaces	17
3.1	Soil and paver properties	27
4.1	Climatological conditions	37
4.2	Measured annual hydrological balance	40
4.3	Days without events	43
4.4	Soil water content	48
4.5	Evaporation on days with and without precipitation	50
5.1	TUBGR model coefficients for paved surfaces	67
5.2	Annual hydrological balance estimated by TUBGR model	67
5.3	Monthly and annual estimated evaporation	71
A.1	Monthly mean volumetric water content (θ)	I
A.2	Hourly surface & soil temperatures	II
A.3	Monthly mean air, surface & soil temperatures	III
A.4	Ratio evaporation to grass-reference evapotranspiration	IV

List of Abbreviations

Symbols and units

C_d	Constant used in ET_0 calculation [$s\ m^{-1}$]
C_n	Constant used in ET_0 calculation [$K\ mm\ s^3\ Mg^{-1}\ d^{-1}$]
e_a	Actual vapour pressure [kPa]
e_s	Saturation vapour pressure [kPa]
E	Actual evaporation [mm]
E_{COB}	Evaporation from cobblestone surface [mm]
E_{CON}	Evaporation from concrete slab surface [mm]
ET	Actual evapotranspiration [mm]
ET_0	Grass-reference evapotranspiration estimated after Penman-Monteith [$mm\ d^{-1}$]
$E(T)$	Actual evaporation or evapotranspiration, as case may be [mm]
G	Soil heat flux density at soil surface [$MJ\ m^{-2}\ d^{-1}$]
I	Infiltration [mm]
I_{COB}	Infiltration from cobblestone surface [mm]
I_{CON}	Infiltration from concrete slab surface [mm]
M	Mass
M_{lys}	Mass of lysimeter [kg]
M_{out}	Mass of outflow [g] or [kg]
M_{ro}	Mass of runoff [g] or [kg]
P	Precipitation [mm]
P^*	Net precipitation ($P - RO$) [mm]
P_s	Precipitation in summer [mm]
R_n	Net radiation at crop surface [$MJ\ m^{-2}\ d^{-1}$]
R_s	Incoming solar radiation [$MJ\ m^{-2}\ d^{-1}$]
RH	Relative humidity [%]
RO	Runoff [mm]
RO_{COB}	Runoff from cobblestone surface [mm]
RO_{CON}	Runoff from concrete slab surface [mm]
RO_m	Runoff at 1-minute resolution [$mm\ min^{-1}$]
R^2	Coefficient of determination based on Pearson correlation coefficient
ΔS	Change in soil water storage [mm]
T_{air}	Air temperature [$^{\circ}C$]
T_{dew}	Dew point temperature [$^{\circ}C$]

T_{pav}	Temperature at underside of paver [°C]
T_{soil}	Soil temperature [°C]
T_{surf}	Surface temperature [°C]
T_5	Temperature at 5 cm depth below paver [°C]
T_{15}	Temperature at 15 cm depth below paver [°C]
T_{25}	Temperature at 25 cm depth below paver [°C]
u_2	Wind speed at 2 m height [m s^{-1}]
u_{10}	Wind speed at 10 m height [m s^{-1}]
β_s	Infiltration coefficient for summer [-]
β_w	Infiltration coefficient for winter [-]
Δ	Slope of saturation vapour pressure-temperature curve [$\text{kPa } ^\circ\text{C}^{-1}$]
γ	Psychrometric constant [$\text{kPa } ^\circ\text{C}^{-1}$]
κ	Reduction coefficient ($= E/ET_0$) [-]
κ_d	Reduction coefficient for dry days [-]
κ_w	Reduction coefficient for wet days [-]
κ_T	Reduction coefficient derived from air temperature [-]
κ_{COB}	Reduction coefficient for cobblestones [-]
κ_{CON}	Reduction coefficient for concrete slabs [-]
ρ	Spearman correlation [-]
θ	Volumetric water content (VWC) of soil [Vol.-%]
θ_{COB}	VWC of soil under cobblestones [Vol.-%]
θ_{CON}	VWC of soil under concrete slabs [Vol.-%]
θ_5	VWC of soil at 5 cm depth below paver [Vol.-%]
θ_{15}	VWC of soil at 15 cm depth below paver [Vol.-%]
θ_{25}	VWC of soil at 25 cm depth below paver [Vol.-%]

Abbreviations

AWAT	Adaptive Window and Adaptive Threshold – filter routine
COB	Cobblestones
CON	Concrete Slabs
CPP	Classic Permeable Pavement
DPP	Designed Permeable Pavement
GSV	Google Street View
LPP	Low Permeability Pavement
OSM	Open Street Map
RC	Runoff Coefficient
SD	Sealing Degree
VWC	Volumetric Water Content (θ)

1 Preface

Urbanisation has been a central topic across numerous scientific disciplines. One main aspect linked to urban areas are streets and sidewalks, covered in different kinds of paving materials. These paved surfaces are a necessary infrastructure of cities. At the same time, their characteristics lead to an altered hydrological balance compared to rural counterparts. With increasing flood risks, runoff processes and storm water management have become an important topic and subject of numerous models. While these extreme events are clearly relevant given their consequences, a research focus on them also led to missing data for regular conditions and their corresponding hydrological balance. However, the hydrological balance of different pavement types is essential to assess the impact of urbanisation in general and urban design in particular. An improved understanding of underlying processes would enable urban planners to better adapt cities to current and future challenges.

Therefore, central questions are:

- What is the hydrological balance of paved surfaces?
- Which water and heat transport processes take place?
- Are these adequately reflected in common models?
- How can evaporation from paved surfaces be estimated?

This thesis aims to answer all these questions, combining an extensive literature review, own measurements, and an analysis of what this means for estimating evaporation. The review considers all kinds of pavement, own research takes a closer look at two pavement types commonly used for sidewalks.

Chapter 2, a detailed introduction into the hydrological balance of paved surfaces, was published in Timm et al. (2018). It contains a summary of previous studies on this subject and collects the state of the art knowledge of related processes. This literature review revealed that very few measurements of water transport processes are available. It concludes that additional research of these would be valuable for both, process understanding and modelling approaches. Therefore, a detailed study of the hydrological balance, as well as water and heat transport processes, was conducted for two paved surfaces: cobblestones and concrete slabs. A combination of high-resolution weighable lysimeters and sensors installed within the soil column of the lysimeters was utilised to gain new insights. Chapter 3 details the materials and methods of the lysimeter

study and an additional experiment. The results of these are illustrated and analysed in chapter 4. They confirm and enhance many of the observations from previous studies. Additionally, previously disregarded processes are re-evaluated. Resulting from the high resolution and combination of methods, it can be shown that these overlooked processes take place and play an important role for the hydrological balance of these two paved surfaces. Finally, the results of the measurements are used in chapter 5 to evaluate an existing model and develop a new approach for estimating evaporation from paved surfaces. A conclusion is drawn in chapter 6, summarising the most important results of this study and providing an outlook for future research and practice.

2 Introduction

Rapid urbanisation is a process attracting worldwide attention in many different scientific research areas. As of 2014, 54 % of the global population was living in cities, with 59 countries exceeding 80 % urbanisation and some countries like Belgium reaching up to 98 % (UN, 2014). This trend is expected to continue with two thirds of the world population becoming urban by 2050 (UN, 2014). Linked to urbanisation is a significant alteration of our environment which creates many challenges, such as flooding (Haase, 2009; Pistocchi et al., 2015; Qin et al., 2013), air pollution (Rodríguez et al., 2016) and altered, heterogeneous microclimates (Chatzidimitriou and Yannas, 2015).

Of these alterations, soil sealing is often seen as the main driver for the challenges attributed to urbanisation, with many studies from numerous fields focusing on the hydrological impact of paved areas (e.g. Bhaduri et al., 2001; EC, 2012; Scalenghe and Marsan, 2009). Depending on the discipline, pavements may be seen in many different ways, e.g. as necessity for urban life, runoff generator and pollution source, storage for heat and water, or a product to be optimized. Table 2.1 gives an overview of communities researching and designing pavements. While some of these have been dealing with pavements for a long time (e.g. road construction and urban planning), the subject might be relatively new to others (urban water ecology and climatology). Based on different priorities (e.g. safety, function, ecological impact, drainage), they make use of a wide range of measurement scales and methods. From a soil science perspective, soil sealing is considered to irreversibly destroy natural soil functions (Morel et al., 2014) and to reduce the soils ecological functionality (Lehmann and Stahr, 2007). Similarly, urban hydrologists perceive soil sealing as the cause for drastically altered hydrological balances, which is most visible in storm water and flood generation after heavy rainfalls (Hibbs and Sharp, 2012; Salvatore et al., 2015). These impacts illustrate why paved surfaces are seen as the key urban water interface, determining transformation and transport processes of water, matter, and energy between the soil and atmosphere in urban areas (Gessner et al., 2014).

With a focus on addressing safety issues such as flood prevention and increased water pollution, pavements are mostly seen as an impermeable runoff generator (Fletcher et al., 2013; Jacobson, 2011) and pollutant source (Göbel, Dierkes and Coldewey, 2007). Accordingly, over the last few decades models have been developed for water transport at the surface, their input to streams and sewer networks, and the effectiveness of storm

This chapter is the accepted version of an article published in *Landscape and Urban Planning*, (Timm et al., 2018), doi: <http://dx.doi.org/10.1016/j.landurbplan.2018.03.014>. Alterations with new results are marked.

water remediation measures such as localised recharge areas. Soil sealing with any material is often defined as the prevention of any infiltration and evaporation, resulting in very little or no losses in the rainfall-runoff relationship (Fletcher et al., 2013; Mansell and Wang, 2010). However, it is well known in construction and building material science that asphalt and concrete mixtures do take up moisture, which leads to damage to the material and shortening of the service life (Kakar et al., 2015; Liu and Hansen, 2016*b*; López-Montero and Miró, 2016; Penttala, 2006; Xu et al., 2016). Further evidence for the permeability of pavements is provided by studies assessing the overall hydrological balance of paved surfaces in Europe. Under moist mid-latitude (Cfb) climate (updated Köppen-Geiger classification after Kottek et al., 2006), studies (see section 4) have shown that infiltration and evaporation take place for all types of pavement, including asphalt.

Knowledge about these processes could also be used to actively design and utilize pavements for specific purposes. For example, water may be applied to streets in order to increase evaporation and thereby cool cities that struggle with the urban heat island effect (Daniel et al., 2018; Hendel et al., 2016). For storm water mitigation, specifically designed pervious paving materials are used to increase infiltration and reduce runoff volumes (Booth and Leavitt, 1999; Brattebo and Booth, 2003; Haselbach et al., 2006; Solpuker et al., 2014).

Due to increased contaminant loads, water quality of urban runoff has been the subject of hundreds of studies (Göbel, Dierkes and Coldewey, 2007). Kayhanian et al. (2012) analysed storm water runoff from highways and observed an increase of mean concentration of most contaminants with traffic density. While few data is available for sidewalks and bicycle paths, the available studies indicate considerably smaller concentration of most contaminants for these surfaces (Göbel, Dierkes and Coldewey, 2007). Additionally, a large fraction of contaminants is bound to particulate matter (Kayhanian et al., 2012) which can be partly retained by the material filling joints between paving stones (Nehls et al., 2008).

An examination of recent reviews about urban hydrology from the last 15 years, whether focusing on runoff (e.g. Fletcher et al., 2013), catchment modelling (e.g. Salvatore et al., 2015), groundwater recharge (e.g. Lerner, 2002) or the overall impact of urbanisation (Gessner et al., 2014; Jacobson, 2011; Shuster et al., 2005), reveals that they all reach the same conclusion: urban water cycle as well as its basic physical processes are not yet well understood.

Field	“Paving is . . .”	Elements & Keywords	Priority
Urban Planning ^[1]	Necessity for urban life and functions	Land-use, Urban life, Habitat quality, Streetscape	Design, Function, Safety, Public health
Road Construction ^[2]	Product to be optimized	Material properties, Freeze-Thaw-Cycles, Deterioration	Safety, Durability, Cost efficiency
Urban Water Management ^[3]	Runoff generator, Pollution source	Urban water cycle, Water supply, Drainage, Sanitation, Storm water management, Rainwater harvesting	Water quality, Water quantity, Decision tools, Management
Urban Hydrology ^[4]	Runoff generator, Pollution source	Catchment hydrology, Pollution of surface & groundwater, Flooding	Water regime, Flood protection, Hydrological cycle
Urban Climatology ^[5]	Heat & Water storage	Urban heat island, Albedo, Radiation, Evapotranspiration, Heat stress	Cooling (Urban heat island mitigation)
Soil Science ^[6]	Soil sealing, Loss of function	Water & solute transport, Ecosystem functions	Urban ecosystem services

^[1] Fukahori and Kubota, 2003; Jung et al., 2017; Kaparias et al., 2015 ^[2] Corazza et al., 2016; Kardos and Durham, 2015; Kelly et al., 2016 ^[3] Gogate et al., 2017; Willuweit and O'Sullivan, 2013 ^[4] Chen et al., 2017; Jacobson, 2011 ^[5] Qin, 2015 ^[6] Morel et al., 2014; Scalenghe and Marsan, 2009

Table 2.1: Disciplines dealing with water transport processes of paved surfaces

2.1 Paved surfaces

Surfaces, such as streets and sidewalks, can be paved using a wide range of materials. Paving can consist of a single continuous cover (e.g. asphalt or concrete) or an assembly of individual pavers (made of e.g. stone, concrete, or brick). In the latter case, the paved surface will also feature numerous joints of varying width between the pavers. These joints are filled with seam material and may facilitate growth of vegetation. Furthermore, the joints allow water to infiltrate into the underlying soil. Paving with a uniform cover is denoted as Low Permeability Pavement (LPP) and paving consisting of pavers and joints as Classic Permeable Pavement (CPP). CPPs differ from Designed Permeable Pavement (DPP), which refers to (super) porous concrete or asphalt, and other new materials specifically designed as storm water remediation methods allowing more infiltration (Andersen et al., 1999; Bonicelli et al., 2015; Carbone et al., 2014; Haselbach et al., 2006; Yong et al., 2013). In this article, pavement is always defined as surface consisting of paving material and (if present) joints between individual pavers. Examples of various common pavements are shown in figure 2.1. Surfaces with all types of paving are considered sealed soils. The definition of soil sealing often includes a complete absence

Designed Permeable Pavements (DPPs)

grass pavers



open pavers



grass joints pavers



Classic Permeable Pavements (CPPs)

gravel



sett stones



large stone plates



small cobblestones



brick pavers



large concrete pavers



small concrete pavers



mid-size concrete pavers



interlocking concrete pavers



Low Permeability Pavements (LPPs)

asphalt



damaged asphalt



concrete



Figure 2.1: Examples of different pavement types

of infiltration (Salvadore et al., 2015; Scalenghe and Marsan, 2009), or generally refers to any sealing material used for street, parking lots and pavement (Fletcher et al., 2013; Hibbs and Sharp, 2012; Jacobson, 2011) including bricks, concrete and asphalt (Mansell and Rollet, 2009; Yao et al., 2016). While CPPs are examples of pervious materials in some studies (Mansell and Rollet, 2009; Nehls et al., 2006, 2008), they are often grouped together with LPPs. The term pervious paving mostly refers to DPPs.

2.2 Water transport processes

The studies introduced in the previous section are commonly cited to point out that infiltration and evaporation are processes that should not be neglected when assessing urban ‘impermeable’ surfaces (Dupont et al., 2006; Fletcher et al., 2013; Nakayama and Fujita, 2010; Rodriguez et al., 2008; Salvadore et al., 2015). Due to complex interactions between pavement properties, aging processes (cracks and dust) and climatological conditions, as well as difficulties in measurements, not all processes governing the water transport of paved areas are well understood and confirmed. For example, Mansell and Rollet (2009) pointed out that a dynamic interaction between microclimatic conditions above the surface and the distribution of water within the paver influences three vital processes at once: surface wetting, evaporation and infiltration. Figure 2.2 illustrates relevant elements and water and vapour transport processes of paved surfaces, which will be explained in detail in the following sections with the corresponding processes in the schematic figure indicated in square brackets.

2.2.1 Elements and characteristics of pavements

As can be seen in figure 2.2a, the soil-atmosphere interface of paved soils can consist of numerous elements. Most apparent is the paving material itself, which can have a wide array of physical properties affecting its hydrological balance and water storage capacities. Depressions leading to ponding (Mansell and Rollet, 2009; Nehls et al., 2015) and slopes affecting runoff generation (Hollis and Ovenden, 1988*a*; Ramier et al., 2006) also affect infiltration and evaporation. In both cases, cracks can develop over time, altering flow regimes (Hibbs and Sharp, 2012; Hollis and Ovenden, 1988*a*; Ramier et al., 2006). Additionally, the sublayer of the pavement (Starke et al., 2011) as well as the microclimate above the pavement (Nehls et al., 2015) influence exchange processes. At a larger scale, the connection of the pavement to drainage systems, vegetated areas and water bodies has to be considered.

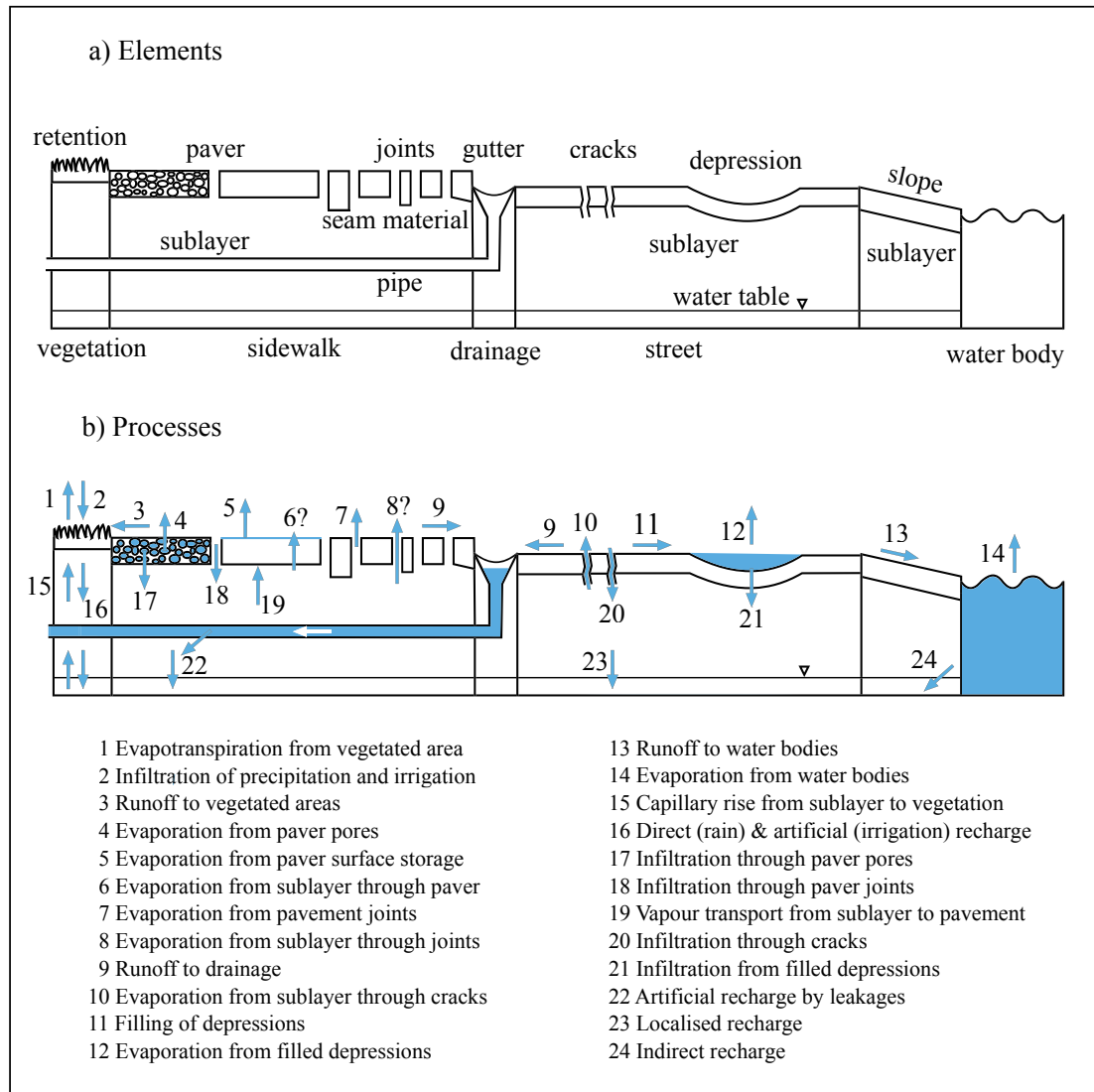


Figure 2.2: a) Elements of the urban soil-atmosphere interface affecting water transport processes, b) water transport processes of paved surfaces. Processes not yet verified are marked with a '?'*

2.2.2 Processes

2.2.2.1 Runoff

The generation of runoff [Number 11 in figure 2.2b] depends on rainfall intensities (Flöter, 2006; Rim, 2011; Ragab et al., 2003; Ramier et al., 2006, 2011), the slope (Ramier et al., 2006) and properties of the pavement surface affecting surface wetting, filling of depressions, infiltration and evaporation (Mansell and Rollet, 2009; Nehls et al., 2015; Ragab et al., 2003). Mansell and Rollet (2009) describe and model four stages of runoff generation depending on surface texture and micro topography of paved surfaces: 1)

*The two processes marked with a '?' were observed during own measurements and are subject of chapter 4

surface wetting, 2) filling of depressions, 3) overflow and runoff generation, and 4) surface drying. Surface wetting describes upper layers of paver and seam material absorbing and detaining water. The duration of the surface being wetted depends on the number, duration and intensity of precipitation events (Wiles and Sharp, 2008). Once this layer is saturated, runoff will start to flow towards local depressions, where some of the water will be lost to infiltration [21] and evaporation [12] (Mansell and Rollet, 2009; Nehls et al., 2015). If rainfall continues, these local depressions will overflow and fill larger depression areas, finally leading to runoff (Mansell and Rollet, 2009). Clearly, slopes will affect the rerouting of water flows on the surface. Further, steep slopes can decrease the surface storage capacities of pavements and hence increase the runoff (Ramier et al., 2006). Additionally, some water will infiltrate through the joints [18] or through the porous paver material [17]. Evaporation losses and hence runoff delay are not only caused by evaporation from filled depressions, but also from heated up paver surfaces [5, 7] (Wessolek and Facklam, 1997).

Numerous works have determined minimum rainfall intensity for runoff generation, surface storage capacity, and the depression storage capacity of different paving material (table 2.2). Minimum rainfall intensities for runoff formation range from 0.01 to 0.2 mm/min, pavement surface storage capacities from 0.05 to 2.0 mm and depression storage capacities from 0.07 to 2.0 mm. Differences for the same material may be caused by the method of determination or by changed properties due to aging processes (Flöter, 2006; Nehls et al., 2006; Wessolek and Facklam, 1997). For example, while granite paving blocks retained 0.4 mm when tested in the lab, under field conditions runoff started to form after 1.2 and 1.8 mm were applied during cold and warm weather, respectively

	Minimum rainfall intensity for runoff formation [mm/min]	Pavement surface storage capacity [mm]	Depression storage capacity [mm]
<i>Low Permeability Pavement (LPP)</i>			
Asphalt	0.1 [6]	0.05 – 1.0 [2][5][6]	0.08 – 2.0 [4][7]
<i>Classic Permeable Pavement (CPP)</i>			
Small concrete pavers	0.16 – 0.20 [1]	0.24 [1]	
Large concrete pavers	0.01 – 0.18 [1][3][6]	0.17 – 1.4 [1][3][5][6]	0.09 [4]
Small natural stone pavers	0.02-0.09 [3][6]	0.93-2.0 [3][6]	0.08 – 0.22 [4]
Brick paving blocks	0.13 [6]	0.8 – 1.3 [5][6]	0.58 [4]
Granite paving blocks		0.4 – 1.8 [5]	0.07 [4]
Rubber paving blocks			0.19 [4]
<i>Designed Permeable Pavement (DPP)</i>			
Porous asphalt		0.43 – 0.45 [2]	
Porous concrete			1.41 [4]

[1] Flöter, 2006, [2] Ramier et al., 2004, [3] Rim, 2011, [4] Nehls et al., 2015, [5] Wessolek and Facklam, 1997, [6] Wessolek, 1994, [7] Hollis and Ovenden, 1988b

Table 2.2: Minimum rainfall intensities for the generation of runoff, surface and depression storage capacities for different pavement types

(Wessolek and Facklam, 1997). On a larger scale, Hollis and Ovenden (1988*a*) investigated the relationship between precipitation and runoff for concrete and macadam roads, and observed initial losses averaging 0.8 mm, but reaching up to 8.8 mm.

2.2.2.2 Infiltration

Infiltration mechanisms have not been studied directly, but infiltration has been mostly attributed to cracks [20] (Wiles and Sharp, 2008) and joints between pavers [18] (Flöter, 2006; Nehls et al., 2006, 2008; Wessolek, 2001). Since infiltration is concentrated at these points, less water and time is necessary to saturate these flow paths, creating preferential flow (Wiles and Sharp, 2008). After passing through the joints, water will be distributed laterally beneath the paver to a certain extent, fully saturating the ‘paving bed’ for small paving stones but not reaching the mid-section of larger paving stones (Flöter, 2006). However, a weak correlation between share of joints and infiltration rates indicates that infiltration occurs not only through cracks and joints (Wessolek and Facklam, 1997), but also through the porous system of the paver [17] (Liu and Hansen, 2016*a,b*; Ramier et al., 2004; Xu et al., 2016).

It has been shown that moisture uptake and hydraulic conductivity of these materials increase in the presence of salt (e.g. introduced as de-icer) and in case of freeze-thaw or other damage to the material (Liu and Hansen, 2016*a,b*; Xu et al., 2016; Zhang et al., 2016). Furthermore, depressions play an important role in infiltrating processes, as they can store significant amounts of water which will mostly evaporate or infiltrate, depending on the hydraulic properties of the pavement, its initial moisture and weather conditions (Nehls et al., 2015). Pavement aging influences infiltration rates, which are reduced because of fine dust particles entering pavers (clogging the pores) and joints (changing seam material properties), as well as the increased evaporation through vegetation growth (Bonicelli et al., 2015; Flöter, 2006; Nehls et al., 2006; Wessolek and Facklam, 1997).

When studying infiltration, drip infiltrometers are used to determine maximum infiltration rates (Wessolek and Facklam, 1997; Wiles and Sharp, 2008). Depending on the material, share of joints and age, infiltration rates of 2 to 288 cm/day have been reported for different paved surfaces (Gilbert and Clausen, 2006; Hollis and Ovenden, 1988*a*; Wessolek, 1993; Wessolek and Facklam, 1997; Wiles and Sharp, 2008).

2.2.2.3 Groundwater recharge

In contrast to natural soils, water that infiltrated paved soils are not stored and later evaporated and transpired through plants and capillary uprising, but instead contribute to groundwater recharge (Flöter, 2006; Hibbs and Sharp, 2012; Wessolek, 2001) if it is not intercepted by subsurface structures or drained into leaking sewer pipes (Bricker et al., 2017; Dirckx et al., 2016). Natural direct recharge, where water infiltrates and recharges at the point of precipitation [16] (Wiles and Sharp, 2008), is limited to adja-

cent vegetated areas. Though direct recharge may be decreased, storm water detention ponds as well as cracks and joints of pavements can act as preferential flow paths, increasing localised recharge [23] (Hibbs and Sharp, 2012; Lerner, 2002; Wiles and Sharp, 2008). Additionally, artificial recharge [22] caused by leaking water supply and drainage networks, as well as over irrigation of parks, further compensates for decreased direct recharge (Lerner, 2002; Wiles and Sharp, 2008). Rates of leakage between 20 and 25 % are common, but can reach up to 50 % in some water mains (Lerner, 2002). Finally, recharge can occur as indirect recharge from losing streams [24] (Hibbs and Sharp, 2012). Flow paths in the sublayer of pavements are governed by numerous factors affecting permeability and hydraulic conductivity, such as the sublayer material, buried structures, fractures and utility line trenches (Wiles and Sharp, 2008).

2.2.2.4 Evaporation

Evaporation from paved areas occurs from the upper surface storage of the pavers [5] (Flöter, 2006; Hassn et al., 2016; Mansell and Rollet, 2009; Ragab et al., 2003; Ramier et al., 2004, 2011), the porous network of the whole paver [4] (Garcia, Hassn, Chiarelli and Dawson, 2015; Hassn et al., 2016; Ramier et al., 2004) the joints between pavers [7] (Flöter, 2006; Wessolek, 2001; Wessolek, Kluge, Nehls and Kocher, 2009), from free standing water in filled depressions [12] (Mansell and Rollet, 2009; Mansell and Wang, 2010; Nehls et al., 2015) and through cracks [10].

Only a small portion of the water infiltrating through the joints will be held against gravity by the material and subsequently evaporate [7] (Flöter, 2006). Once the topmost few centimetres of the seam material have dried, its hydraulic conductivity is reduced significantly. This leads to almost no upward transportation of water through the joints, which effectively inhibits evaporation from the sublayers through the joints [8] (Flöter, 2006; Wessolek, 2001). The same concept might apply for evaporation through cracks [10]. However, pavers themselves can play a significant role in evaporation processes, sometimes even surpassing the evaporation from joints (Flöter, 2006).

Depending on the material, asphalt pavements can have an extensive network of air voids which are very similar to well-studied soil structures, so that the same principles of water movement in saturated and unsaturated soils can be applied (Garcia, Hassn, Chiarelli and Dawson, 2015; Hassn et al., 2016). Under a constant energy source, evaporation of water stored in the pore network of asphalt [4] follows three stages (Garcia, Hassn, Chiarelli and Dawson, 2015). In the first stage, water evaporates directly from the pores to the atmosphere, during which temperature and heat flux through the asphalt increase. Next, the evaporation rate increases until it reaches its peak, absorbing latent heat and reducing the temperature of the asphalt. During this stage, the surface of the asphalt already appears to be dry, as the waterfront is lower in the asphalt and water moves upward by diffusion. In the last stage, the evaporation rate decreases until the asphalt is dry and no more water is available, leading to increasing surface temperature.

In general, only the topmost layer, consisting of the pavement material and joints, is considered to evaporate, with water that infiltrated to the sublayer being shielded from evaporation [6] (Berthier et al., 2006; Flöter, 2006; Wessolek, 2001; Wiles and Sharp, 2008).

Determined by temperature gradients, water vapour will move downward in summer, when the upper layers are warmer than the lower ones, and upward in winter when the lower levels are warmer [19] (Flöter, 2006). However, this water will not evaporate through the pavement layer but condense at the pavement underside, increasing the water content of the soil directly beneath the pavers, making the pavement an evaporation barrier (Flöter, 2006; Wessolek, 2001). This process together with different hydraulic conductivities between the sublayer and paver indicate that no evaporation from water in the sublayer through the paver [6] will take place.

2.3 Hydrological balance

Investigations of pavement water storage and fluxes gained popularity after studies suggested that some general concepts do not fit observations. For example, groundwater recharge in urban areas was considered to have been declining as an effect of increased soil sealing, preventing infiltration (Berlekamp, 1987; Jacobson, 2011; Scalenghe and Marsan, 2009). However, some studies showed that urban groundwater tables were increasing instead of decreasing (Hibbs and Sharp, 2012; Lerner, 2002). This effect has been attributed to leakage from water supply networks (Fletcher et al., 2013; Lerner, 2002; Wiles and Sharp, 2008), altered flow regimes of semi-permeable pavements (CPPs) allowing (reduced) infiltration while decreasing evaporation (Nehls et al., 2008), or storm water remediation practices involving localised infiltration of runoff (Göbel, Coldewey, Dierkes, Kories, Meßer and Meißner, 2007). Today, it is well established that pavement, including asphalt, is not truly impervious. In the following, studies providing measurements of urban hydrological balance are introduced. All studies except for one were conducted in Europe under moist mid-latitude (Cfb) climate, which is characterised as warm temperate, fully humid, and with warm summers (Kottek et al., 2006). One study by Dreelin et al. (2006) was conducted in Georgia, USA, under Cfa (warm temperate, fully humid, with hot summers) climate.

In order to measure the urban hydrological balance (infiltration, runoff and evaporation), different methods are applied. Most commonly, the well-known application of lysimeters for natural surfaces is transferred to paved ones. These lysimeters mostly consider only a small area and can consist of only the paving material (e.g. Mansell and Rollet, 2006; Ramier et al., 2004) or also include a soil sublayer (e.g. Flöter, 2006; Rim, 2011). One might also determine the runoff for a certain area by measuring the flow in the connected drainage system, and combine this with precipitation measurements and soil moisture profiles for monitoring infiltration processes (Ragab et al., 2003). The resulting hydrological balances of studies that measured at least two of the three processes over

Study	Location & climate zone	Pavement	SD	Annual			Summer			Winter					
				P mm (%)	I mm (%)	RO mm (%)	E mm (%)	P mm (%)	I mm (%)	RO mm (%)	E mm (%)	P mm (%)	I mm (%)	RO mm (%)	E mm (%)
Wessolek 2001	Berlin, Germany; Cfb	Road (asphalt)	IV	610 (100)	50 (8)	441 (72)	119 (20)	325 (100)	25 (8)	226 (69)	74 (23)	285 (100)	25 (9)	215 (75)	45 (16)
		Sidewalk (concrete and cobblestones)	n.a.	610 (100)	233 (38)	191 (31)	186 (31)	325 (100)	110 (34)	77 (24)	138 (42)	285 (100)	123 (43)	114 (40)	48 (17)
Diestel & Schmidt 2001*	Berlin, Germany; Cfb	Small granite stones	II	575 (100)	426 (74)	40 (7)	109 (19)	391 (67)	35 (9)	52 (12)	138 (24)	385 (67)	52 (12)	69 (12)	17 (3)
		Small cobblestones	II	575 (100)	385 (67)	52 (9)	138 (24)	391 (67)	35 (9)	52 (12)	138 (24)	385 (67)	52 (12)	69 (12)	17 (3)
Ragab et al. 2003	Crowmarsh Gifford, UK; Cfb	Interlocking concrete pavers	II	575 (100)	449 (78)	57 (10)	69 (12)	437 (76)	57 (10)	81 (14)	110 (22)	351 (70)	40 (8)	351 (70)	110 (22)
		Rubber pavers	II	575 (100)	495 (86)	63 (11)	17 (3)	391 (68)	35 (6)	149 (26)	575 (100)	437 (76)	57 (10)	81 (14)	110 (22)
Flöter 2006	Hamburg, Germany; Cfb	Grass pavers	I	575 (100)	391 (68)	35 (6)	149 (26)	391 (100)	177 (44)	25 (8)	226 (69)	74 (23)	391 (100)	177 (44)	25 (8)
		Brick pavers	II	575 (100)	437 (76)	57 (10)	81 (14)	437 (76)	57 (10)	81 (14)	110 (22)	351 (70)	40 (8)	351 (70)	110 (22)
Rim 2011	Berlin, Germany; Cfb	Asphalt car park	IV	501 (100)	40 (8)	351 (70)	110 (22)	501 (100)	30 (6)	351 (70)	120 (24)	391 (100)	266 (68)	71 (18)	54 (14)
		Asphalt car park	IV	501 (100)	40 (8)	351 (70)	110 (22)	501 (100)	30 (6)	351 (70)	120 (24)	391 (100)	266 (68)	71 (18)	54 (14)
Flöter 2006	Hamburg, Germany; Cfb	Block paving car park (concrete sublayer)	IV	501 (100)	30 (6)	351 (70)	120 (24)	501 (100)	30 (6)	351 (70)	120 (24)	391 (100)	177 (44)	25 (8)	226 (69)
		Asphalt road	IV	501 (100)	30 (6)	351 (70)	120 (24)	501 (100)	30 (6)	351 (70)	120 (24)	391 (100)	177 (44)	25 (8)	226 (69)
Rim 2011	Berlin, Germany; Cfb	Small concrete pavers road	II	852 (100)	670 (79)	111 (13)	71 (8)	852 (100)	447 (53)	55 (7)	221 (26)	391 (100)	266 (68)	71 (18)	54 (14)
		Large concrete pavers sidewalk	III	852 (100)	447 (53)	360 (42)	45 (5)	852 (100)	447 (53)	360 (42)	45 (5)	221 (26)	391 (100)	177 (44)	25 (8)
Rim 2011	Berlin, Germany; Cfb	Gravel parking lot	I	852 (100)	573 (67)	55 (7)	221 (26)	852 (100)	447 (53)	360 (42)	45 (5)	221 (26)	391 (100)	177 (44)	25 (8)
		Small cobblestones	II	552 (100)	383 (70)	85 (15)	15 (15)	552 (100)	348 (64)	145 (26)	10 (10)	56 (10)	302 (100)	163 (54)	106 (35)
		Large concrete pavers	III	549 (100)	348 (64)	145 (26)	10 (10)	549 (100)	348 (64)	145 (26)	10 (10)	302 (100)	163 (54)	106 (35)	33 (11)

* selected materials (without barrier layer)

Table 2.3: Observed annual hydrological balances of paved surfaces as absolute values and with percentage of precipitation in brackets; SD = sealing degree (see table 2.5); Cfb = warm temperate, fully humid with warm summer

Study	Location & climate zone	Pavement	SD	P mm (%)	I mm (%)	RO mm (%)	E mm (%)	Measurement Period & Remarks
Ramier et al., 2004	Nantes, France; Cfb	Old asphalt concrete	IV	433 (100)	9 (2)	316 (73)	108 (25)	03/09/2002 to 06/01/2003
		New asphalt concrete	IV	252 (100)	8 (3)	186 (74)	58 (23)	08/01/2002 to 16/05/2002
		Porous asphalt	II	197 (100)	114 (58)	32 (16)	51 (26)	06/09/2001 to 08/01/2002
								lysimeter, no soil
Mansell & Rollet, 2006	Paisley, UK; Cfb	Flat concrete slabs	III	n.a. (100)	n.a. (1)	n.a. (69)	n.a. (30)	9 weeks in winter lysimeter, no soil
		Inclined concrete slabs	III	n.a. (100)	n.a. (2)	n.a. (93)	n.a. (5)	
		Hot-rolled asphalt	IV	n.a. (100)	n.a. (0)	n.a. (56)	n.a. (44)	
		Dense Bitumen Macadam	IV	n.a. (100)	n.a. (0)	n.a. (36)	n.a. (64)	
		Bricks	II	n.a. (100)	n.a. (54)	n.a. (9)	n.a. (37)	
		Asphalt	IV	46 (100)		33 (72)		9 storm events between February and April 2003
		Grass pavers	I	46 (100)		5 (1)		
Hollis & Ovenden, 1988b	Redbourn, UK; Cfb	Bitumen Mac., 1-2.4 % slope	IV	392 (100)		11658 (3-8)		1 year (1983) storm events
		Bitumen Mac., 3.6-3.9 % slope	IV	392 (100)		16 (4)		(57% of annual rain) catchment size
		Bitumen Mac., 4-5.4 % slope	IV	392 (100)		16-106 (4-27)		100-3500 m ² gully buckets
		Hot-rolled asphalt	IV	392 (100)		71 (18)		& rain gauges
		Asphalt road	IV	2141 (100)		1606 (75)		3 years catchment size
		Asphalt road	IV	2315 (100)		1458 (63)		300-500 m ² gully buckets & rain gauges

Table 2.4: Short period or single component observations of hydrological balances of paved surfaces; precipitation (P), infiltration (I), runoff (RO) and evaporation (E) as absolute values and with percentage of precipitation in brackets; SD = sealing degree ranging from low (I) to severe (IV) (see table 5); climate zones after Kottke et al. (2006): Cfb = warm temperate, fully humid with warm summer, Cfa = warm temperate, fully humid with hot summer

a period of at least a year are summarised in table 2.3. To our best knowledge, there are only five studies providing this long-term information. Studies that measured only one component and used models to derive the other two, or only offer data for shorter periods, are not considered but may be found in table 2.4.

While asphalt materials (LPPs) exhibit very similar results, with high runoff values (70-72 %), low infiltration (6-9 %) and moderate evaporation (20-24 %), CPP materials such as concrete pavers are showing a wide spread, with lower runoff values (7-42 %), higher infiltration (38-86 %) and low to moderate evaporation (3-24 %). Only one long-term measurement for a DPP material is available from Diestel and Schmidt (2001), where grass pavers show low runoff (6 %), high infiltration (68 %) and high evaporation (26 %). For porous asphalt (DPP), data is available from Ramier et al. (2004) of a four month measurement campaign in winter, which yielded low runoff (16 %), medium infiltration (58 %) and high evaporation (26 %). Nevertheless, this winter measurement cannot be transferred to an annual hydrological balance, as there are distinct seasonal differences between summer and winter periods. Figure 2.3 compares the hydrological balances of five materials for summer and winter graphically. As can be seen, the proportion of infiltration is higher during winter, rising from 44-68 % in summer to 59-89 % in winter. The difference is highest for gravel, where the proportion of infiltration in winter is almost double that in summer. Evaporation and runoff tend to be higher in summer, increasing from 2-12 % to 9-50% and 6-39 % to 6-44 %, respectively. Again, the difference in evaporation is most distinct for gravel, which is more than six times larger in summer. The highest increase in runoff has been observed for small cobblestones, which triples from 7 % in winter to 22 % in summer. This increase of runoff and evaporation and decrease of infiltration from winter to summer can be attributed to different precipitation patterns and other climatic conditions, such as the amount of available energy. Despite these general trends, it also becomes apparent that there are very large variations between different materials.

While few studies provide annual observations for all hydrological balance components, some only offer data for shorter periods or for one component (table 2.4). For example, the rainfall-runoff relationship of urban catchments covered in paving material has been measured using gully buckets and rain gauges (e.g. Hollis and Ovenden, 1988*b*; Ramier et al., 2006). Some insights into evaporation processes of paved surfaces have been won by using a tunnel evaporation gauge to study evaporation independent of the other hydrological balance components (Göbel et al., 2008; Starke et al., 2010). These studies compare evaporation rates of a CPP consisting of concrete pavers and a DPP made of pervious concrete. Göbel et al. (2008) concluded that in summer, the CPP results in higher evaporation rates than the DPP for dry days, but the relationship is reversed after precipitation events, for which the DPP exhibits higher evaporation rates. In winter, the DPP has higher evaporation rates. Additionally, the pattern of evaporation differs. While the CPP are characterised by short and high evaporation rates directly following precipitation events, the DPP continued to evaporate even after four

days of dry and sunny weather after a precipitation event (Starke et al., 2010). These results support the concept of significant losses due to infiltration and evaporation. Furthermore, they again illustrate the diverse behaviour of very similar materials. This might be influenced by rainfall intensity and distribution (Rim, 2011).

Hydrological balance of paved surfaces in summer & winter

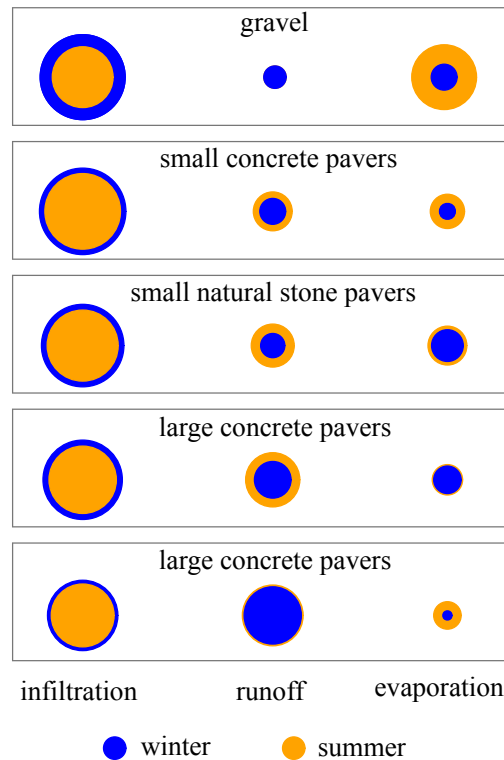


Figure 2.3: Hydrological balances for summer and winter for different paved surfaces after data from Flöter (2006) and Rim (2011). The area of the circle reflects the percentage of the component (infiltration, runoff or evaporation) of the total precipitation during the period. For gravel, percentage of runoff for summer and winter is equal, leading to overlapping circles

2.4 Application

Many methods have been developed to assess the urban hydrological balance. Depending on their intended application, they range from rather rough estimations to complex and detailed numerical models. They are useful tools that allow classification and evaluation of different urban developments. In the following, a few of these methods are introduced. In case of the sealing degree approach, an adapted classification based on the previously presented hydrological balance measurements is proposed.

2.4.1 Sealing degree (SD)

Most models assessing the overall hydrological balance focus on annual or monthly estimations and utilize easy to use parameters and readily available data, such as the sealing degree (SD), which represents the degree of imperviousness and is provided for many cities (e.g. Berlekamp, 1987; Glugla et al., 1987; Haase, 2009; Jacqueminet et al., 2013; Montzka et al., 2008). To that end, certain paving materials or land uses are combined in classes for which the SD ranges from low (open concrete stones with grass in between) to severe (asphalt street) (Glugla et al., 1999). The SD attributed to the same land use can vary significantly depending on the process used, e.g. ranging from 40 to 100 % for streets and 20 to 50 % for single-family houses (Wessolek, 2001). An adapted classification of SDs based on surface cover and the resulting hydrological balance is presented in table 2.5.

There are some empirical, user-friendly models allowing for more or less rough estimations of urban hydrological balances depending on the SD. For example, Wessolek et al. (2008) proposed the Hydro-Pedo-Transfer-Functions (HPTFs) to predict annual percolation rates for numerous surface covers, including urban areas. In this model, infiltration coefficients for predicting infiltration and runoff in summer and winter are provided for four different SDs. Furthermore, they introduce an empirical method for estimating the annual actual evaporation of (partially) sealed surfaces that adjusts the annual potential evapotranspiration as described by Allen et al. (1994) by introducing a reduction coefficient based on lysimeter measurements.

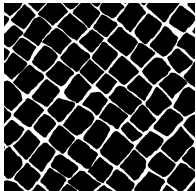
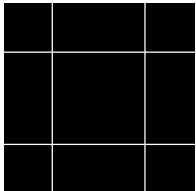
Sealing Degree	I – low < 70 %	II – medium 70 – 94 %	III – high 94 – 98 %	IV – severe > 98 %
Surface cover				
Examples	Grass pavers, gravel	Small pavers of stone/concrete/brick	Large concrete pavers	Asphalt
Properties	Focus on joints and vegetation	Many narrow to wide joints, vegetation possible	Very few and narrow joints, very little vegetation	No joints or vegetation, cracks caused by damage
Hydrological balance:				
Runoff	None 0 – 7 %	Low 3 – 15 %	Medium 16 – 42 %	High 70 – 72 %
Evaporation	High 26 %	Low to high 8 – 35 %	Low to medium 8 – 22 %	Medium 20 – 24 %
Infiltration	Medium to high 58 – 68 %	High 63 – 79 %	Medium 53 – 64 %	Low 6 – 9 %

Table 2.5: Sealing degrees of paved surfaces based on different cover and observed hydrological balance (annual means, not applicable for heavy rainfall events). Table has been altered compared to published version to include results from own conducted measurements as detailed in chapters 3 & 4

2.4.2 Runoff coefficient (RC)

In urban hydrology, runoff coefficients (RC) are used to describe how much of the precipitation reaching a (partially) sealed urban surface will turn into surface runoff and leave the area. Many models use one RC describing any kind of sealed surface that is often set to 1.0 (e.g. Pistocchi et al., 2015). Still other models distinguish between materials or application (e.g. Angrill et al., 2017) and might differentiate summer and winter RC (Hollis and Ovenden, 1988*b*; Ragab et al., 2003). For the typical sealing materials asphalt and concrete, annual RC of 0.4 to 0.9 have been reported (Angrill et al., 2017; Eckley and Branfireun, 2009; Ramier et al., 2006). The percentages of runoff provided for different materials in tables 2.3 and 2.4 can be translated into annual and seasonal RCs. Other factors such as climate and slope may further affect the RC (Grodek et al., 2011). Recently, studies have suggested that individual rainfall events have to be analysed in order to get specific RCs related to the rainfall-intensity (e.g. Diestel and Schmidt, 2001; Dreelin et al., 2006; Gilbert and Clausen, 2006; Rim, 2011). While RC are widely used, not least due to their practicability and simplicity, they are also viewed critically as they do not consider all relevant processes determining the hydrological behaviour of paved surfaces (e.g. Ramier et al., 2011). Hence, some studies additionally consider the micro-topography of sealed surfaces, which may include depressions which reroute and store water and have to overflow to form runoff (e.g. Mansell and Rollet, 2009; Mitchell et al., 2001; Nehls et al., 2015).

2.4.3 Numerical models

Urban water and vapour transport processes are simulated with numerical models by many different disciplines on various scales, with different components and outcomes. One might include water supply and drainage infrastructure to assess the overall water cycle (Bach et al., 2014; Delleur, 2003; García, Barreiro-Gomez, Escobar, Téllez, Quijano and Ocampo-Martinez, 2015; Mitchell et al., 2001; Niemczynowicz, 1999), simulate the generation of storm water flows and their impact on urban rivers and lakes, as well as flooding events (Miller et al., 2014; Revitt et al., 2014; Zoppou, 2001), or estimate urban evapotranspiration (Berthier et al., 2006; Grimmond and Oke, 1991).

In general, the majority of studies and models focus solely on storm water events and neglect smaller rainfall events. As Zoppou (2001) shows, there are hundreds of storm water models developed by academic institutions, regulatory authorities, government departments and engineering consultants, which range from simple conceptual to complex hydraulic models. Commonly used models might not be applicable to sealed areas, as they have not been designed for this purpose. For example, Kodešová et al. (2014) simulated water and heat transfer in soils with different surface covers like grass, gravel and concrete, using the widely applied hydrological model software HYDRUS-1D (Šimůnek et al., 2016). While they achieved a good fit for most surfaces, soil water contents below concrete paving could not be simulated in a satisfactory way, which was attributed by the

authors to the 3D water flows under the pavers. Additionally, it has been pointed out, that water and heat transport processes in urban areas are influenced by more extreme temperature variations, in which case commonly neglected vapour transport processes have to be considered when modelling such areas (Kodešová et al., 2014).

Urban hydrological balance models also often use ‘tank’-systems, in which the different surfaces and their underlying soil layers are seen as tanks with different storage capacities from which the water is redistributed (e.g. Mansell and Wang, 2010; Mitchell et al., 2001). There are only few models estimating evaporation from (partially) sealed surfaces, a lack that has been pointed out over the last 20 years in the field of hydrology (Grimmond and Oke, 1991; Mansell and Wang, 2010). Existing models may be based on the calculation of available water storage and the filling level of that tank. For example, the model AQUACYCLE by Mitchell et al. (2001) considers surface depressions of impervious surfaces (including paving) as water storage. Any precipitation higher than the volume of the depression will form runoff, while the remaining water will completely evaporate without any infiltration. Other models originate from urban climatology; they usually consider larger urban sites with grass as well as paved surfaces, and are based on interception and surface energy balances (e.g. Grimmond and Oke, 1991; Ward et al., 2016).

2.4.4 Data generation

Readily available data and maps of urban areas often contain land-use, area covered by road networks, or SDs of larger areas, but do not standardly provide information on paving material. While images obtained via remote sensing can be used to gain insight into built-up area and different land-uses such as industrial, housing and infrastructure (García and Pérez, 2016; Morabito et al., 2016; Smith et al., 2010), their resolution is too low to distinguish different paving materials.

Detailed information about paving material might be obtained from OpenStreetMap (OSM) (Open Street Map Contributors, 2017) which provides free geographical information collected by local contributors. One attribute assigned to road and sidewalk areas is the surface, which by default is considered to be paved. The term paved is seen as non-specific and includes all types of paving materials including asphalt, sett stones, and wood. However, the surface cover can be further specified with a wide range of materials (e.g. asphalt, sett, paving stones, cobblestones, grass pavers, gravel) allowing for detailed pavement surface data (Open Street Map Wiki Contributors, 2017). Data availability and level of detail depend on the amount of contributors in the area. For the city of Tehran, Forghani and Delavar (2014) compared road maps from OSM and official (municipally produced) maps and found considerably varying quality of OSM maps. They point out that heterogeneity of completeness of OSM data compared to the reference map is the main factor influencing the quality. If the paving material is specified, OSM provides high-detail data that is not easily available from other sources.

Another possibility is the usage of Google Street View (GSV) images (Google, 2017) to replace or support field surveys. GSV is used in research for numerous applications, e.g. the estimation of urban tree canopy cover (Richards and Edwards, 2017; Seiferling et al., 2017) and assessment of urban space quality (Chiang et al., 2017). Similarly, GSV can be used to determine the paving material of streets and sidewalks that are available in the data base.

2.5 Conclusion

Pavement, as a soil-atmosphere interface of urban surfaces, is more than a runoff generator. For nearly all paving materials, infiltration and evaporation takes place, significantly reducing runoff volume. Infiltration takes place through the porous system of the paving material, joints of pavers and cracks. Evaporation occurs from the total surface storage capacity of paver and seam material and from water standing in depressions. While these processes take place for all materials, their extent and interactions vary considerably. The range of paving materials is too large to provide empirical measurements for all of them, especially concerning the complex interaction of many different conditions (e.g. age of material, slope and climatic conditions). For now, the presented studies allow a rough estimation of the hydrological balance of different paved surfaces based on their sealing degree.

The drastic differences between materials, the importance of their condition (e.g. frost damage, cracks) and surface micro topography indicate that in order to accurately simulate the hydrological balance of urban areas, it is crucial to assess a much smaller scale than the commonly used parameterisation over large areas. New data sources, such as Google Street View and OpenStreetMap, can provide detailed, small-scale information about paving material used in a study area.

Overall, a better understanding of the hydrological processes of pavements is essential to improve our model concepts and planning choices, making cities more resilient against the impacts of rapid urbanisation, climate change, and its manifold effects on urban residents.

3 Material & Methods

The aim of this study is to measure the hydrological balance of two different kinds of paved surfaces, as well as underlying processes of heat and water transport. Over a measurement period of one year, a combination of weighable lysimeters and built-in temperature and soil water content sensors are used to achieve this. After noise filtering, data aggregation and combination, hourly and daily results could be obtained. The following sections offer detailed information about the lysimeter station and data processing.

3.1 Lysimeter studies

Lysimeters are a well established and widely used method to study water movement across a soil boundary (Howell et al., 1991), the soil-atmosphere interface. They are used to measure actual evapotranspiration, rainfall and drainage (Meissner et al., 2010). In 2004, Lanthaler (2004) conducted a survey on European lysimeters and found 117 institutions operating lysimeters or sewage water samples at over 178 sites. According to the survey, there were 2440 lysimeters of which 84 % were non-weighable. Two thirds of all lysimeters were used to research arable land, one fourth for grassland and 1 % for forests. As of 2010, there were more than 1700 publications using lysimeters, with a gradual increase in more recent years (Meissner et al., 2010). Despite being cost and maintenance intensive, fixed to a site and requiring extensive data processing (Hannes et al., 2015; Rana and Katerji, 2000), lysimeters are a popular and valuable method to study hydrological processes.

There are two basic types of lysimeters: weighable and non-weighable. While weighable lysimeters are a direct measurement approach using the mass balance of the system, non-weighable lysimeters are indirect and rely on the volume balance (Hirschi et al., 2017; Howell et al., 1991). Non-weighable lysimeters are suitable for long-term (annual) water balances for which the change in soil water storage (ΔS), which is only measured by weighable lysimeters, can be neglected (DVWK, 1996). Precision weighing lysimeters (Unold and Fank, 2007) allow highly precise measurements of these processes, as well as dewfall (Meissner et al., 2007). Due to their improved temporal resolution, newer weighable lysimeter installations can be used to develop and test models of soil hydrological processes (Meissner et al., 2010).

Both types of lysimeter make use of the general water balance (DVWK, 1996):

$$0 = P + E(T) + RO + \Delta S \quad (3.1)$$

P	Precipitation [mm]
$E(T)$	Evapo(transpi)ration [mm]
RO	Runoff [mm]
ΔS	Change in soil water storage [mm]

Using this general water balance equation and assuming that precipitation and evapo(transpi)ration do not take place at the same time, the mass balance used for weighable lysimeters, both vegetated and paved, can be written as (based on Schrader et al. (2013); Peters et al. (2014)):

$$M = \begin{cases} M_{lys} + M_{out} & \text{if vegetated} \\ M_{lys} + M_{out} + M_{ro} & \text{if paved} \end{cases} \quad (3.2)$$

$$\Delta P = \begin{cases} \Delta M & \text{for } \Delta M > 0 \\ 0 & \text{for } \Delta M \leq 0 \end{cases} \quad (3.3)$$

$$\Delta E(T) = \begin{cases} \Delta M & \text{for } \Delta M < 0 \\ 0 & \text{for } \Delta M \geq 0 \end{cases} \quad (3.4)$$

where

M	Total mass of system [kg]
M_{lys}	Mass of lysimeter [kg]
M_{out}	Mass of outflow (infiltration water) [kg]
M_{ro}	Mass of runoff [kg]
ΔM	Change in total mass of system [kg]
ΔP	Precipitation [kg]
$\Delta E(T)$	Evaporation (paved) or evapotranspiration (vegetated) [kg]

Figure 3.1 illustrates the water movement processes and measurement principle of weighable lysimeters. The difference between vegetated and paved lysimeters is the additional collection and weighing of runoff water generated by most paved surfaces. This additional runoff water has to be considered when determining the precipitation volume. For vegetated lysimeters, a common measurement error of up to 20% results from the difference in vegetative area and the inner dimensions of the container when determining the evaporating area (Rana and Katerji, 2000). This source of error does not apply to the sealed lysimeters used in this study, as the evaporating area consisting of pavers and joint material is more fixed and corresponds to the inner dimensions of the container.

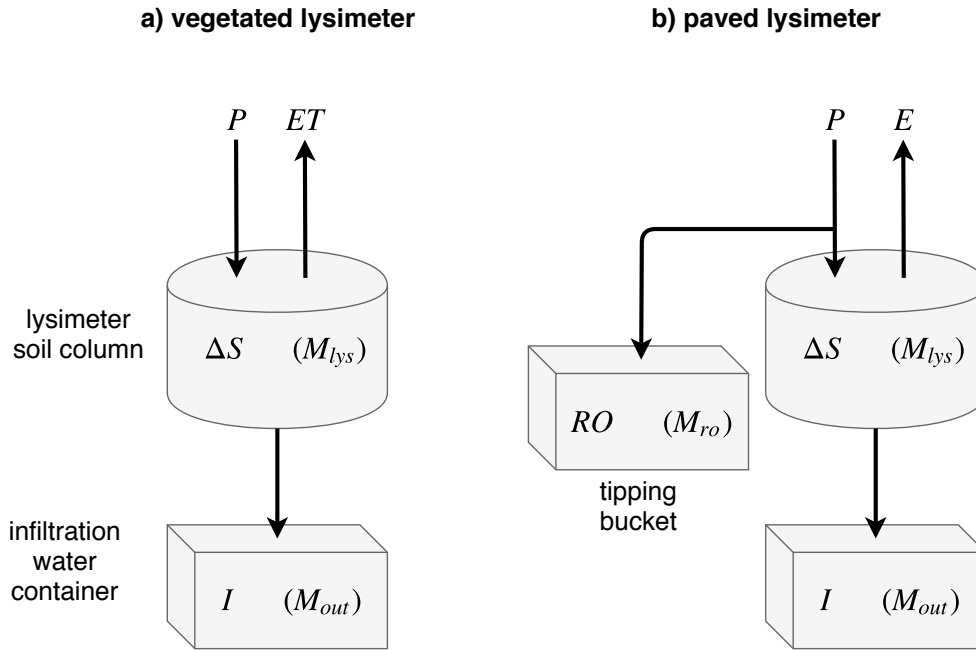


Figure 3.1: Basic principle of vegetated and paved weighable lysimeters. ΔS = change of water storage, P = precipitation, I = infiltration, ET = evapotranspiration, E = evaporation, RO = runoff. Weighted components are M_{lys} = mass of lysimeter, M_{out} = mass of outflow (infiltration), and M_{ro} = mass of runoff

3.2 Lysimeter station

All measurements were conducted on the southern outskirts of Berlin, Germany. There, the two lysimeters used in this study are situated as part of a lysimeter station operated jointly by the Federal Environmental Agency (Umweltbundesamt) and the Technical University Berlin (N 52.3967°, E 13.3673°, climate zone: Cfb; warm temperate, fully humid). The overall station consists of twelve lysimeters and a climate station situated next to the lysimeters. Figure 3.2 shows the two lysimeters with paved surfaces, two grass-reference lysimeters used in other studies, and the climate station.

3.2.1 Surface types

The two lysimeters used in this study are covered in two pavement sealing types commonly used for sidewalks in Berlin (Fig 3.3). The first one (type “cobblestones”) uses “Bernburger Mosaic” paving which consists of second hand cobblestones of different sizes. It is characterised by large a joint area (joints are 20 % of total surface area) and is often used at the edges of pavements to better include trees, rain pipes, drainage holes and other structures that have to be circumvented. The other one (type “concrete slabs”) uses concrete slabs ($30 \times 30 \times 4.4$ cm), resulting in narrow joints (joints are 6 % of total surface area). While both surfaces can be classified as classic permeable pavements (CPPs), their sealing degree (table 2.5 differs. Due to the large joint area, cobblestones

belong to the sealing degree II (medium) and concrete slabs to sealing degree III (high). Both pavings are installed with a slight slope to prevent the formation of puddles. The immediate surrounding is covered in the same concrete slabs to prevent island effects. Both material types have been used in previous studies (Rim, 2011), resulting in slightly weathered surfaces.



Figure 3.2: Research site – lysimeter station at Berlin-Marienfelde



Figure 3.3: Lysimeter surfaces: left – cobblestones, right – concrete slabs

3.2.2 Lysimeter set-up

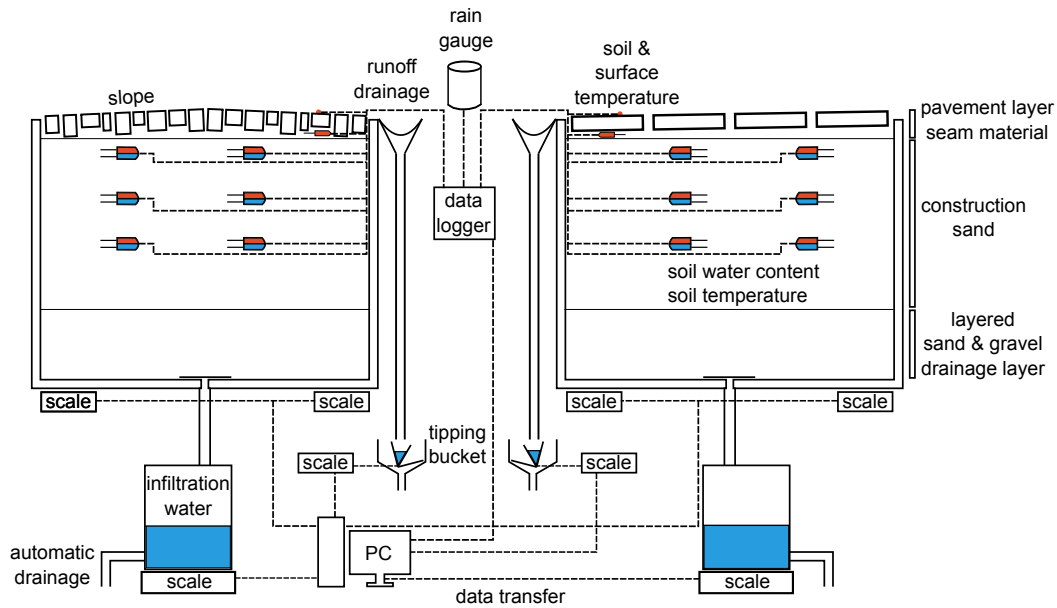


Figure 3.4: Scheme of lysimeter set-up

A schematic set-up of the lysimeters is illustrated in Fig 3.4. They have a circular surface area of 1 m^2 and a depth of 50 cm. The surface layer is 4 to 8 cm deep consists of the paving material and fine sand seam material. Beneath, the soil layer consists of common construction sand. The last 10 cm are a drainage layer consisting of gravel and very coarse sand whose grain size increases towards the bottom. Substrate properties can be found in table 3.1. The drainage layer ensures the transport of infiltrated water to the bottom of the lysimeter where it drains into a mesh-covered pipe. The infiltrating water is collected in a canister standing on top of a scale (resolution $0.1 \text{ g} = 0.0001 \text{ mm}$). In order to reduce maintenance effort, the canister collecting infiltration water is emptied automatically using pumps once a high degree of filling is reached. The lysimeters themselves are weighted using three weighing cells each (resolution $10 \text{ g} = 0.01 \text{ mm}$). A covered drain surrounding the surface area collects runoff and empties it into a weighable tipping bucket based on the device introduced by Nehls et al. (2011). When runoff takes place, a first tipping bucket fills up gradually until the maximum volume of the bucket is reached, resulting in a tipping which drains the bucket and positions the second bucket to be filled up. This one will then tip over in the other direction when full, bringing the first bucket back in position, and so forth. Normally, only the event of buckets tipping is recorded, so that events not resulting in a tipping leads to difficulties in aligning runoff volumes and the corresponding time periods. Additionally, runoff collected in a bucket may evaporate if no tipping occurred, which leads to an underestimation of the overall runoff volume. In this study, the weight of the tipping buckets is logged (resolution

0.1 g = 0.0001 mm) to enable the registration of even small amounts which would not result in a tipping and evaporate before the next rainfall event leading to runoff. Data from all scales is logged simultaneously; lysimeter weight and infiltration water at 1-minute, runoff at 1-second intervals. Maintenance consists of regular removal of weeds growing in the seems and leaves from the runoff drain, replacement of logger batteries, and general check ups.

3.2.3 Built-in sensors

Supplementing the more traditional lysimeter measurements, sensors were installed in each of the lysimeters to measure:

- surface temperature (T_{surf}) [$^{\circ}\text{C}$]
- temperature below paver (T_{pav}) [$^{\circ}\text{C}$]
- soil temperature (T_{soil}) at 5, 15, and 25 cm below the underside of the paver [$^{\circ}\text{C}$]
- volumetric water content (θ) at 5, 15, and 25 cm below the underside of the paver [%]

Soil temperature and θ are measured simultaneously by the same sensors (sensor type 5TM by Decagon), which make use of the time-domain reflectometry principle. These sensors are installed at 5, 15, and 25 cm below the underside of the paver, with two sensors at each of these depths. The distance between lysimeter wall and sensors is roughly 25 – 35 cm, the distance between the sensor pair is approximately 50 cm (Figure 3.5). In order to prevent cables running directly over another sensor, which would affect the water flow and hence θ , sensors at the three different depths are shifted slightly so that they do not align vertically. For each lysimeter, two temperature sensors (one on the surface, another directly below a paver) are installed. Additionally, a rain gauge on ground level between the two lysimeters provides precipitation data. All data is logged at 5-minute intervals.

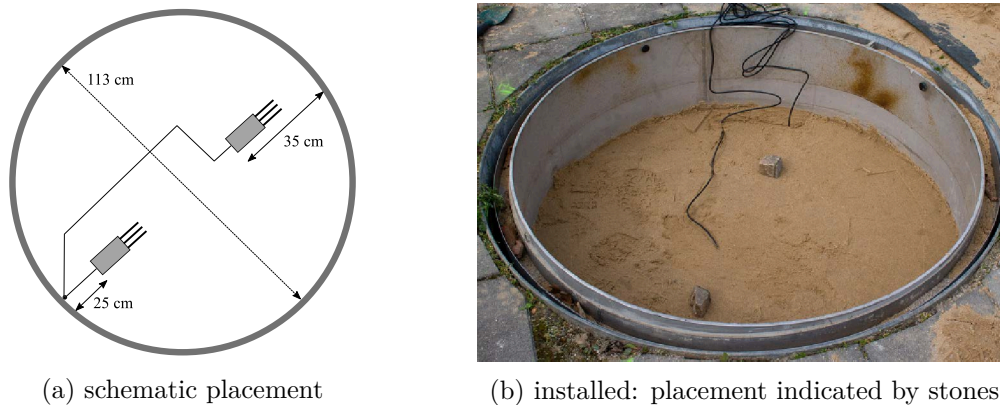


Figure 3.5: Horizontal placement of the build-in sensors

	Cobblestones	Concrete slabs
Paving layer		
Paver material	Natural stone	Concrete
Paver dimension [cm]	2 – 6 × 4 – 6 × 4 – 8	30 × 30 × 4.4
Seam share [%]	20	6
Paver porosity [Vol-%]*	3.9	5.1
Field capacity [Vol-%]*	< 0.5	1
Surface storage capacity [mm]*	0.4	0.8
Seam material		
Depth [cm]	0 – 8	0 – 5
Soil type	Sand	
Dry bulk density ρ_b [g cm ⁻³] [†]	1.15 – 1.67	
<i>Particle size distribution</i>		
Clay [%]	0.8	
Silt [%]	2.3	
Fine sand [%]	20.4	
Medium sand [%]	70.6	
Coarse sand [%]	6.0	
Sublayer material		
Depth [cm]	8 – 40	5 – 40
Soil type	Sand	
Dry bulk density ρ_b [g cm ⁻³]	1.59	
<i>Particle size distribution</i>		
Clay [%]	0.4	
Silt [%]	1.2	
Fine sand [%]	9.7	
Medium sand [%]	76.3	
Coarse sand [%]	12.4	
<i>Van Genuchten parameters</i>		
Scale parameter α [cm ⁻¹]	0.0496	
Saturated water content θ_s [cm ³ cm ⁻³]	0.287	
Residual water content θ_r [cm ³ cm ⁻³]	0.037	
Shape parameter n [–]	5.518	
Drainage layer		
Particle size [mm] at depth 40 – 42 [cm]	1.00 – 2.00	
Particle size [mm] at depth 42 – 43 [cm]	2.00 – 3.15	
Particle size [mm] at depth 43 – 46 [cm]	3.00 – 5.00	
Particle size [mm] at depth 46 – 50 [cm]	5.60 – 8.00	

* (Wessolek and Facklam, 1997)

† (Nehls et al., 2006)

Table 3.1: Properties of lysimeter soils and paving materials. Particle size distribution determined using DIN/ISO 11277

3.2.4 Climate station

The climate station which is situated right next to the two paved lysimeters is operated by the Federal Environmental Agency (Umweltbundesamt) and provides hourly and daily data of:

- precipitation (P) [mm]
- air temperature (T_{air}) [°C]
- wind speed (u) [m s^{-1}]
- relative humidity (RH) [%]
- dew temperature (T_{dew}) [°C]
- solar radiation (R_s) [W m^{-2}]
- daily sunshine hours (N) [h]

3.3 Surface wetting-drying experiment



Figure 3.6: Example of surface wetting

In order to further research the paved layer as urban soil-atmosphere interface, a wetting-drying experiment was undertaken. Its focus was the interaction of surface temperature and surface water storage for the two paved surfaces used in the lysimeter study.

The experiment was carried out at the lysimeter site on July, 25th, 2016, which was characterised by very high air temperatures and low cloud cover, offering optimal conditions for evaporation (mean $T_{air} = 23.87^\circ\text{C}$, daily $R_s = 270 \text{ W m}^{-2}$).

A thermal camera (IR-TCM 384 IR – Jenoptik, resolution 384×288 pixel and $< 0.05 \text{ K}$) was temporarily installed above the lysimeter using a mobile tripod. It was set up to take an individual picture every 4 seconds, using the *IRBIS[®] remote 3 software*

(InfraTec, 2012). After starting the automatic image taking, the surface was watered using a hand pump pressure sprayer with low pressure setting (figure 3.6). This allowed to produce an even water layer completely covering the lysimeter surface. This wetting process took 2 minutes. After that, the entire drying process (until no visible water left on surface) was recorded. The thermal recording took place in the early afternoon, when T_{air} reached its daily maximum of 30 – 31 °C, R_s was high (670 – 763 W m⁻² h⁻¹), RH was low (33 – 35 %), and wind speed was moderate with 1.7 m s⁻¹.

Before thermal pictures were taken, the tripod was used to record the wetting-drying process with a regular camera (Olympus E-510, resolution 3648 × 2736 pixels at 314 dpi). Pictures were taken automatically every 10 seconds.

3.4 Data processing

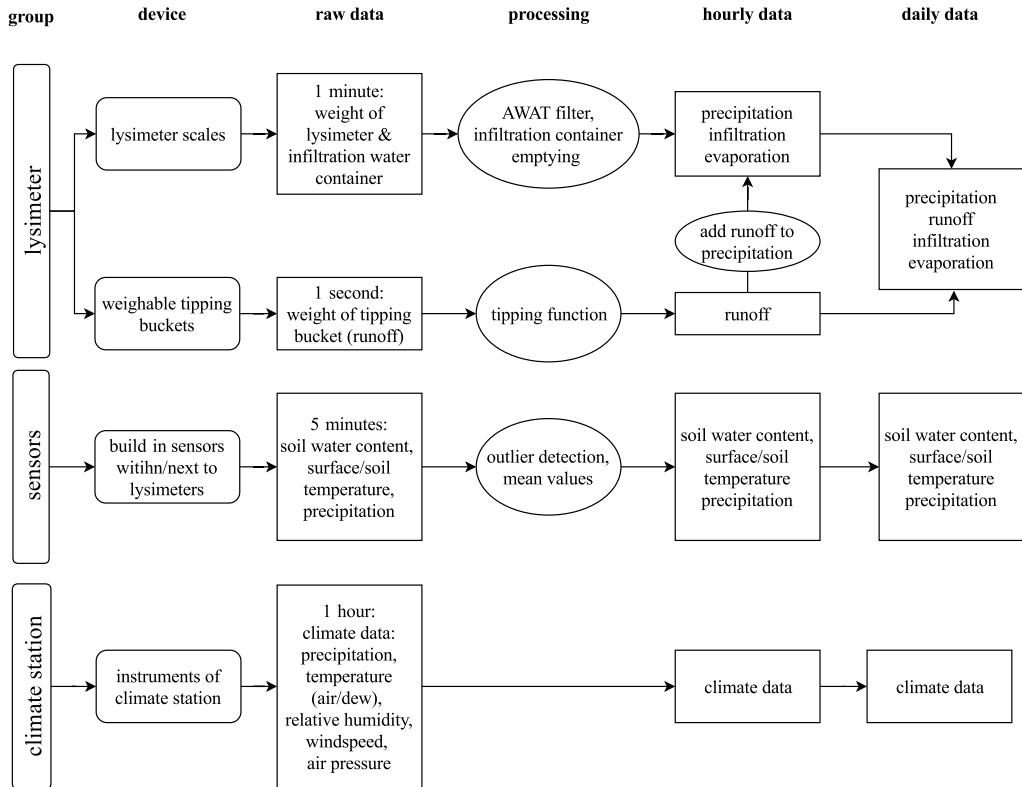


Figure 3.7: Overview of origin and processing of data

Measurement period in this study started on June 3rd, 2016 and ended June 2nd, 2017. Within this period, data is available for 333 out of 365 days (91 %). Data gaps resulted from conducting additional experiments (e.g. wetting-drying experiment) resulting in artificial data ($n = 4$) and from technical disruptions such as power shortage or logging problems ($n = 28$). A larger gap resulted from a power shortage on site from October 4th to October 20th 2016. Raw data was logged at different time-intervals ranging from

1-second (runoff) to 1-hour (climate). After data processing, the highest temporal resolution is 1-hour. This results from data availability and requirements of used filters. An overview of data processing can be found in figure 3.7 and details can be found in the following sections. All data has been converted to CET without daylight saving.

3.4.1 Tools

Thermal pictures obtained during the wetting-drying experiment were processed using the *Infrared Thermography Software IRBIS®3 Professional* (InfraTec, 2008). For application of the AWAT filter routine software was provided by Andre Peters. Non-linear regression was conducted using the Datafit 9.1.32 software by Oakdale Engineering (Oakdale Engineering, 2014). All other data processing was done using R version 3.3.1 (R Core Team, 2016). Apart from packages included in the standard edition of R, the following additional packages have been used for data processing and visualisation:

- data.table (Dowle and Srinivasan, 2017)
- ggcorrplot (Kassambara, 2016)
- ggplot2 (Wickham, 2009)
- lubridate (Grolemund and Wickham, 2011)
- padr (Thoen, 2017)
- plyr (Wickham, 2011)
- zoo (Zeileis and Grothendieck, 2005)

For selection of accessible (colour-blind safe and photocopy friendly) colours for the plots, the Color Brewer tool at colorbrewer2.org (Brewer et al., 2013) has been used.

3.4.2 Lysimeter data

Raw lysimeter data contains the measured weight of the lysimeters (1-minute interval), the weight of the infiltration water container (1-minute interval) and the weight of runoff tipping bucket (1-second interval). This section provides details on how this raw data is processed to obtain hourly results.

3.4.2.1 Runoff

Runoff is recorded by measuring the weight of the tipping buckets in which the runoff water is collected at 1-second intervals. Once a certain amount of water is reached, the tipping device will tilt, emptying the collected water and collecting water in the second bucket. Depending on the runoff rate, this tipping process occurs at a weight of 480 – 500 g. For heavy rainfall, tipping can occur in quick succession, so that a high

temporal resolution of 1-second is necessary to record weight changes before a tipping occurs. If a tipping occurs, the tipping bucket will sometimes sway from side to side before coming to rest after 4 – 5 seconds. Figure 3.8 contains one month of raw runoff data for concrete slab surface. As can be seen, runoff may occur between tipping events (bucket filling period between two tipping events). Weighing of the tipping buckets allows for better temporal assignment of events. The figure also illustrates evaporation from the buckets, which would result in reduced runoff if only tipping events were recorded.

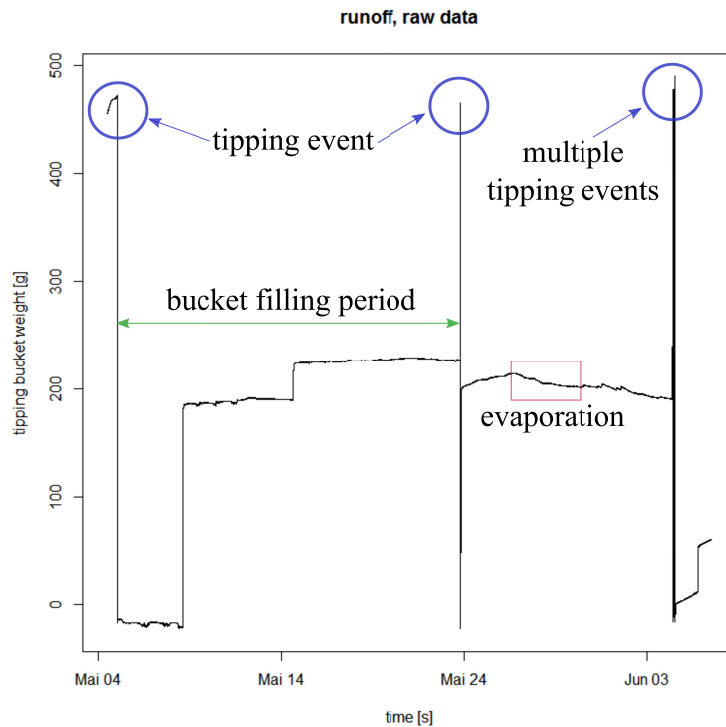


Figure 3.8: Example of raw runoff data (concrete slabs surface)

In order to process and evaluate the runoff data, these tipping events have to be adjusted. At 1-second- resolution, a value of $RO_s < -1$ g is used as tipping indicator, as neither noise nor evaporation would cause this change of weight. Since the bucket needs 4 – 5 seconds to come to rest, the next five data points after a tipping was triggered are considered invalid as well. At 1-second-resolution, the runoff rate can be assumed stable for small periods of time. Hence, the six values associated with a tipping event are replaced by the mean runoff rate immediately before and after the event. The tipping event function used to adjust the 1-second-resolution raw runoff data is:

if $\Delta RO_i < -1$ g:

$$\Delta RO_i, \Delta RO_{i+1}, \dots, \Delta RO_{i+5} = \frac{\Delta RO_{i-1} + \Delta RO_{i+6}}{2} \quad (3.5)$$

where

ΔRO Recorded change of weight (runoff) at 1-second-resolution [g].

Once the data series has been adjusted for tipping events, the 1-second-resolution data is aggregated to 1-minute values. At this resolution, the overall change of weight in case of runoff is larger than the recorded noise of the scale. The 1-minute values include evaporation processes which lead to a decrease of weight ($RO \leq 0 \text{ mm min}^{-1}$). Only values $RO > 0 \text{ mm min}^{-1}$ are used to obtain hourly runoff data, so that:

$$RO_m = \begin{cases} RO_m & \text{if } RO_m > 0 \\ 0 & \text{if } RO_m \leq 0 \end{cases} \quad (3.6)$$

where

RO_m Runoff at 1-minute-resolution [mm min^{-1}].

3.4.2.2 Precipitation, Evaporation & Infiltration

Lysimeter measurements are affected by numerous disturbances resulting in noise, which has to be filtered from the data in order to successfully separate and quantify the individual fluxes (Hannes et al., 2015; Schrader et al., 2013). In this study, lysimeter mass (M_{lys}) and infiltration mass (M_{out}) are processed using the improved Adaptive Window and Adaptive Threshold (AWAT) filter routine (Peters et al., 2016) resulting in hourly values of precipitation, evaporation and infiltration. In order to use the AWAT routine, which does not include runoff in its balance, for paved surfaces, hourly runoff sums are added to the precipitation values produced by AWAT.

The AWAT filter routine

The AWAT filter routine was developed to process raw lysimeter data and receive improved separation of precipitation and evaporation from noise (Peters et al., 2014). It tackles the problem of compromising between too strong and too weak filtering caused by varying atmospheric conditions (e.g. strong wind) producing varying levels of noise and requiring different filter set-ups (Peters et al., 2014). Three benchmark events (smooth evaporation, heavy precipitation, and strong wind) that were used to evaluate the AWAT filter routine are shown in figure 3.9. The AWAT filter routine combines a smoothing routine over a certain averaging window with a threshold value to separate noise from significant weight changes (Peters et al., 2014). The innovation of this routine is the variation of both, the averaging window width and the threshold value, depending on the characteristics of the measured data (Peters et al., 2016). First results indicated that the routine was able to increase overall accuracy and fulfil the requirements set by the three differing benchmark events (Peters et al., 2014). Since then, it has been successfully utilised in other studies (Peters et al., 2016). In 2016, an improved version

has been published (Peters et al., 2016). While the original AWAT filter routine (Peters et al., 2014) used stepwise interpolation, the improved version uses linear and spline interpolations in order to better reflect the smooth and continuous evapotranspiration processes and enable a higher temporal resolution of the output data (Peters et al., 2016). Figure 3.9 illustrates the changes between the original filter (denoted as ‘Steps’) and the improved version (denoted as ‘Linear’ and ‘Spline’). In this study, the improved routine has been utilised to process raw lysimeter data.

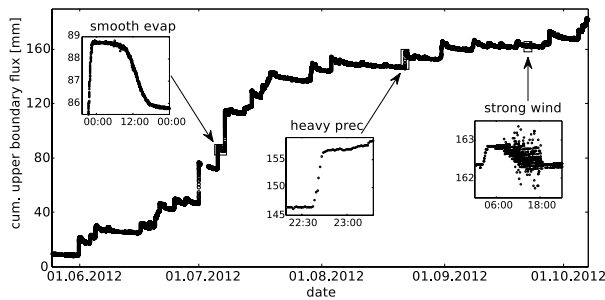


Fig. 1. Raw data for cumulative upper boundary flux of the lysimeter. The three subplots with zoomed data depict three different representative benchmark events (6 July, 21 August and 23 September 2012) that have to be met by the filter routine. Note that the time and flux intervals for the three cases are different.

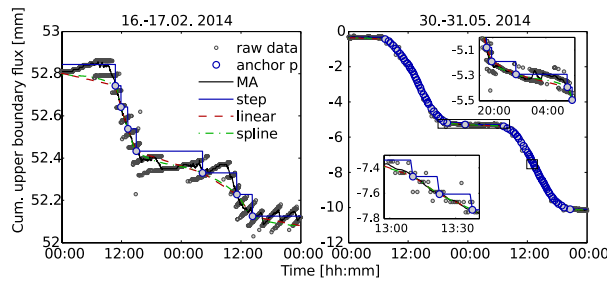


Figure 2 Raw data of two evapotranspiration events, filtered with the original AWAT filter (steps) and linear as well as spline interpolation schemes. Left: low evapotranspiration on 16-17 February 2014; right: high evapotranspiration rates on 30-31 May 2014.

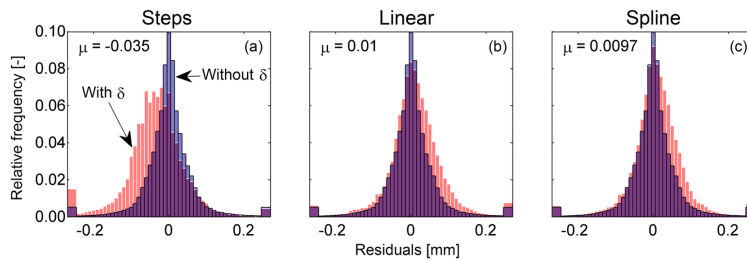


Figure 5 Relative residual frequency distribution for the complete data set and the different interpolation schemes. Blue bars indicate residuals between original and filtered data for the cases with mere smoothing, omitting the threshold values; red bars indicate cases with threshold values and subsequent interpolation. The broad bars at plot edges comprise all residuals greater than 0.25 or smaller than -0.25. Steps: original step interpolation scheme; linear: linear interpolation scheme; spline: cubic Hermitian spline interpolation scheme.

Figure 3.9: Principle of AWAT filter routine. Top: different types of events to be evaluated (Peters et al., 2014); middle and bottom: difference between original and improved filter routine (Peters et al., 2016)

Data preparation In order to use this routine, the automatic drainage of the infiltration water container has to be corrected beforehand to obtain the required input format.

Beneath each lysimeter, a container collects infiltration water leaving the lysimeter at

the bottom. The weight of this container is continuously measured at 1-minute intervals using scales with a resolution of 0.1 g. If infiltration takes place, the weight will increase as the container fills up. If no infiltration takes place, the weight may decrease slowly as small amounts of water evaporate from the container. The sum of weight positive changes in weight is the amount of water passing the lysimeter body as infiltration.

A level sensor monitors the water level within the container and triggers automatic draining to prevent overflowing and reduce manual maintenance input. Depending on the infiltration rate, this process takes 3 – 4 minutes. If one container triggers the drainage, both containers are drained simultaneously.

During processing, drainage of the container is detected automatically by monitoring the change of weight. A threshold difference of -500 g min^{-1} , which is high enough to not be triggered by evaporation processes, initiates a function to replace values recorded during the drainage process.

When a drainage process is detected, the original value that triggered the routine, as well as the next 4 values (enabling a 5 minute time window for drainage) are first removed from the data and then replaced by the value immediately following the drainage process, preserving the overall increase in weight occurring within the 5-minute interval of drainage.

The drainage event function used to adjust the 1-minute-resolution infiltration water data is:

if $\Delta M_{out_i} < -500\text{g}$:

$$\Delta M_{out_i}, \Delta M_{out_{i+1}}, \dots, \Delta M_{out_{i+4}} = \Delta M_{out_{i+5}} \quad (3.7)$$

where

ΔM_{out} Recorded change of weight (infiltration) at 1-minute-resolution [g].

After these corrections, the lysimeter weight and infiltration water weight data have been converted to the required input data file formats and run through the AWAT filter which provides hourly data of precipitation, infiltration and evaporation.

Control As a control, precipitation values produced by both lysimeters have been compared, which resulted in a very good fit of 0.98 and 0.99 for hourly and daily values, respectively (figure 3.10).

precipitation comparisons

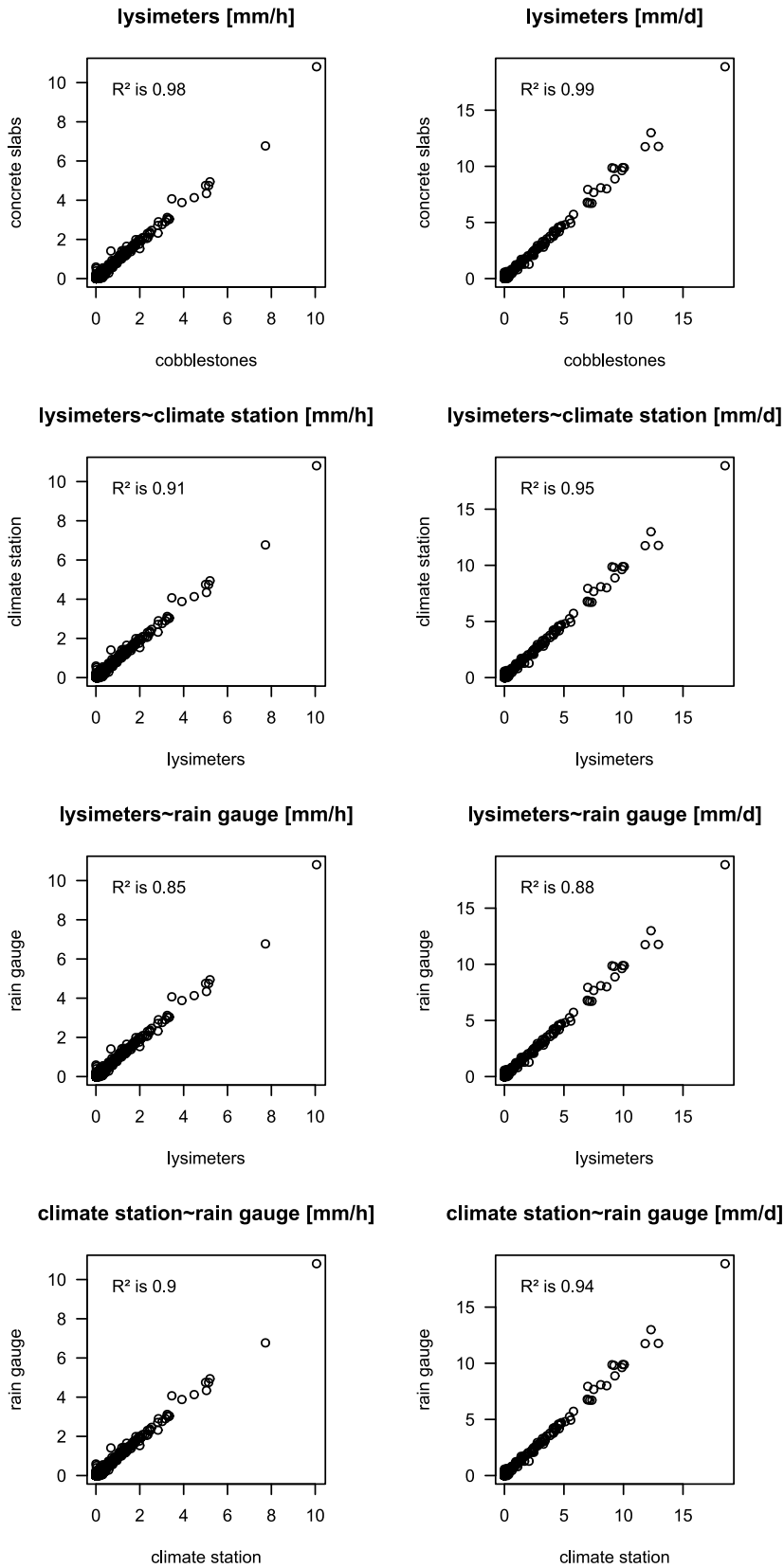


Figure 3.10: Comparison between measured precipitation (hourly and daily) from lysimeters, climate station (1.5 m height) and rain gauge at ground level

3.4.3 Sensor data

Volumetric water content (θ) and soil temperature (T_{soil}) are measured simultaneously by the built-in sensors (Decagon 5TM). To measure θ , the sensors make use of time domain reflectometry, which has to be calibrated using the soil temperature (Ledieu et al., 1986). The following equation by Stoffregen (1998) (based on Ledieu et al., 1986) was used to calibrate measured θ :

$$\theta_{corrected} = \theta_{measured} \times \left(1 + \frac{T_{soil} - 20}{400}\right) \quad (3.8)$$

Both, VWC and T_{soil} are measured at 5-minute intervals. For each depth (5, 15 & 25 cm below paver underside), two sensors were used for measurement in order to generate a mean value for each depth. While the continuous measurement worked well in general, individual sensors were prone to drop out for single values or longer periods. One sensor (lysimeter with concrete slabs at 25 cm depth) proved unreliable and data produced by this sensor has been removed completely. This results in only one measurement being available for this particular depth. The sensors used to measure T_{surf} and T_{pav} proved to be very reliable with mostly continuous measurement. Some additional data gaps affecting all sensor measurements resulted from power shortage of the logger or other logging problems.

Data processing of the available sensor data consisted of:

1. Noise removal (for θ)
2. Mean value calculation for sensor pairs (for θ and T_{soil})
3. Hourly mean value calculation
4. Daily mean value calculation

First, rare cases in which individual data points of θ are wrong had to be filtered out as noise. To achieve this, a threshold of 1% change in θ within the 5-minute resolution was set. If the change of θ exceeded this threshold, the data point was removed. After this exclusion of noise, mean values of θ and T_{soil} were produced for each sensor pair. If one sensor of the pair did not provide data, the value of the corresponding other sensor was used. Finally, these mean values and the values of T_{surf} and T_{pav} , for which only one data point per lysimeter was available, were used to produce hourly mean values. To ensure that enough data points were recorded to accurately assign an hourly mean value, only hours in which at least 6 out of the maximum 12 data points were available had mean values assigned to them. If less than 6 values were available, the hourly mean value was set to *NA*. The resulting hourly data was then aggregated to mean daily values.

4 Results

4.1 Lysimeter study

4.1.1 Climatological conditions

Table 4.1 compares the climatological conditions recorded at the lysimeter site during the measurement period to values of Berlin during the World Meteorological Organization (WMO) reference period spanning from 1981 to 2010 (DWD, 2018*a,d*). Within the measurement period of one year, a total of about 397 mm precipitation was measured by the lysimeters. This does not include 17 days in October and individual other days for which lysimeter data is unavailable. As shown in figure 3.10, daily precipitation data of the lysimeters and the climate station installed in close vicinity to the lysimeters (see figure 3.2) are not identical but in general fit well ($R^2 = 0.95$). Replacing missing precipitation data from the lysimeters with values recorded by the climate station yields a total of 476 mm a⁻¹. Based on reference period, the annual mean precipitation of Berlin is 590 mm a⁻¹ (DWD, 2018*d*). The annual precipitation during the measurement period was 79.3 % of the reference mean value, indicating a rather dry period.

Apart from the total amount, the intensity of rainfall events plays an important role for hydrological processes, especially for paved surfaces. Figure 4.1 illustrates hourly intensities of precipitation events as measured by the two lysimeters. The highest intensity recorded was 10.06 mm h⁻¹, but only 19 out of 2196 hours with rainfall exceeded 2.5 mm h⁻¹. As can be seen in figure 4.1, nearly all hours with rainfall had light intensities below 0.5 mm h⁻¹. The classification of rainfall intensities into light, moderate, or heavy can differ significantly. Comparing two European classifications, light rainfall can range from under 0.5 (MetOffice, 2012) to under 2.5 mm h⁻¹ (DWD, 2018*e*). Depending

	1981 – 2010	Measurement period
Annual mean air temperature (T_{air}) [°C]	9.7	10.1
Coldest month: Mean T_{air} [°C]	JAN: 0.6	JAN: -1.2
Warmest month: Mean T_{air} [°C]	JUL: 19.5	JUL: 19.8
Precipitation (P) [mm a ⁻¹]	590	476
Sunshine hours (n) [h a ⁻¹]	1706	2426
Annual global radiation (R_s) [kW h m ⁻²]	1021–1040	1088

Table 4.1: Climatological conditions at the site during the measurement period (2016-06-03 to 2017-06-02) compared to the long-term climatological mean values of the WMO reference period 1981 – 2010 for Berlin (DWD, 2018*a,d*)

on which classification is used, light rainfall intensities can account for 30 – 80 % of the annual precipitation amount in the measurement period. Heavy rainfall accounted for 3 – 11 %.

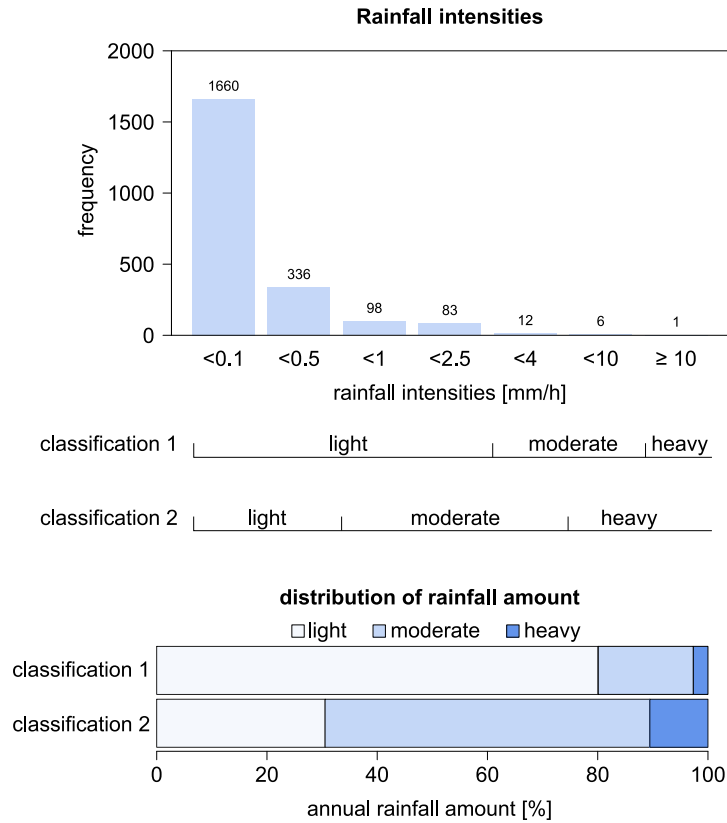


Figure 4.1: Rainfall intensities measured by lysimeters (mean value) from June 2016 to June 2017. Only events with precipitation $> 0 \text{ mm h}^{-1}$ considered. Top: frequency of rainfall intensities; middle: classification of rainfall intensities after 1) DWD (2018e) and 2) MetOffice (2012); bottom: contribution of rainfall intensities to annual sum of rainfall

4.1.2 Hydrological balance & water transport

4.1.2.1 Hydrological balance

Annual and seasonal (summer and winter) hydrological balances of the two paved lysimeters are illustrated in figure 4.2, with detailed values in table 4.2. Infiltration is equal for both surfaces with 61.9 – 62.5 % of the sum of infiltration, evaporation and runoff. Both have higher infiltration in winter, with 67 – 70 % of the total amount of infiltration being recorded between November and April. In contrast, evaporation and runoff differ significantly for the two surfaces. Runoff amounts to 2.6 – 16.0 % annually, with summer runoff being twice as high as in winter. Concrete slabs produced more than five times more runoff than the cobblestones. In winter, both surfaces evaporate the same amount of water. In summer, cobblestones evaporate twice as much as concrete slabs, so that

annually cobblestones evaporate 65 % more.

Hydrological balance of partially sealed surfaces

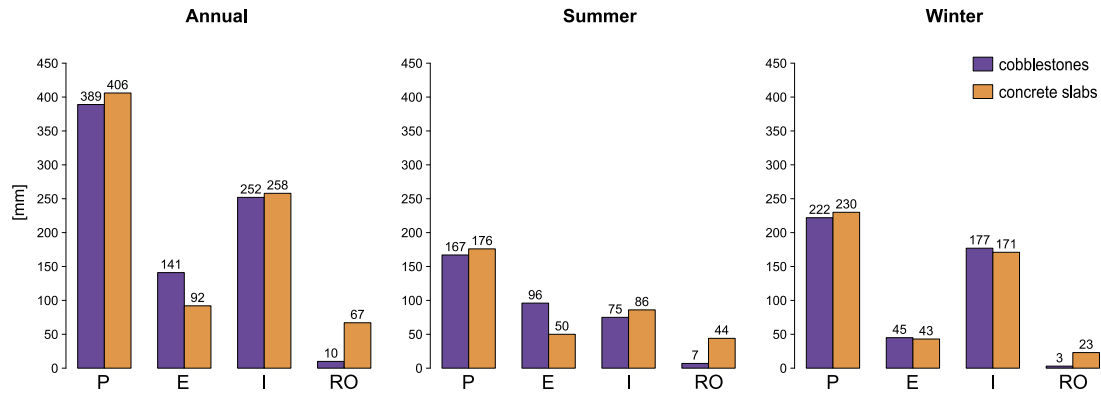


Figure 4.2: Hydrological balance of paved surfaces (annual, winter and summer) as measured June 2016 to June 2017 in Berlin. Hydrological summer May to October, hydrological winter November to April

Runoff generation depends on on the rainfall intensity and duration. Figure 4.3 shows the cumulative hydrological balance based on daily values. For cobblestones, 44% of all runoff was generated on just two days with high intensity precipitation events. On June 17th, 2016, precipitation of 18.70 mm d^{-1} or $0.4 - 3.9 \text{ mm h}^{-1}$ led to runoff of 1.07 and 5.76 mm d^{-1} for cobblestones and concrete slabs, respectively. The highest hourly precipitation and runoff rates were recorded on September 17th, 2016. While daily precipitation rates were lower than in the previous example (12.36 mm d^{-1}), a high hourly rate of 10.44 mm h^{-1} results in high runoff of 3.46 and 8.37 mm d^{-1} and 3.46 and 8.25 mm h^{-1} for cobblestones and concrete slabs, respectively. Both of these days lie within the example periods for hourly hydrological balances illustrated in figure 4.6. The cumulative hydrological balances further show seasonal trends. While for cobblestones, evaporation increases in warm months and comes to a halt in cold periods, concrete slabs have a slow but steady increase of evaporation throughout the year. For both surfaces, infiltration increases sharply between November and April, when precipitation is high whereas temperature and evaporation are relatively low.

	Cobblestones				Concrete Slabs			
	P mm	I mm (%)	RO mm (%)	E mm (%)	P mm	I mm (%)	RO mm (%)	E mm (%)
Annual	389.16	251.89 (62.5)	10.30 (2.6)	140.55 (34.9)	405.65	257.77 (61.9)	66.71 (16.0)	92.24 (22.1)
Summer	166.94	74.71 (42.1)	7.14 (4.0)	95.80 (53.9)	175.94	86.32 (48.0)	44.12 (24.5)	49.50 (27.5)
Winter	222.22	177.18 (78.7)	3.16 (1.4)	44.75 (19.9)	229.71	171.45 (72.4)	22.59 (9.5)	42.74 (18.1)
June*	48.18	28.57 (51.3)	1.29 (2.3)	25.89 (46.4)	50.97	27.93 (50.1)	12.26 (22.0)	15.51 (27.9)
July	39.56	13.43 (37.6)	1.51 (4.2)	20.77 (58.2)	40.49	16.23 (41.1)	12.79 (32.4)	10.46 (26.5)
August	23.94	15.59 (51.9)	0.67 (2.2)	13.81 (45.9)	25.28	13.66 (48.6)	6.74 (24.0)	7.71 (27.4)
September	16.97	3.74 (20.0)	3.48 (18.7)	11.42 (61.3)	19.16	4.22 (22.4)	9.66 (51.2)	4.98 (26.4)
October†	19.41	10.97 (81.9)	0.01 (0.1)	2.41 (18.0)	18.51	10.35 (72.1)	1.86 (12.9)	2.15 (15.0)
November	37.51	30.96 (90.8)	0.47 (1.4)	2.65 (7.8)	37.76	24.43 (67.3)	5.19 (14.3)	6.67 (18.4)
December	37.39	34.32 (86.6)	0.84 (2.1)	4.48 (11.3)	38.45	30.12 (67.0)	4.83 (10.8)	9.98 (22.2)
January	47.63	40.66 (89.1)	0.99 (2.2)	3.97 (8.7)	49.95	37.28 (80.00)	4.59 (9.8)	4.74 (10.2)
February	32.41	28.37 (82.3)	0.24 (0.7)	5.84 (17.0)	34.81	28.71 (75.5)	2.70 (7.1)	6.64 (17.4)
March	46.10	32.66 (70.4)	0.34 (0.7)	13.41 (28.9)	46.83	34.39 (73.4)	3.71 (7.9)	8.78 (18.7)
April	21.18	10.21 (41.0)	0.28 (1.1)	14.40 (57.9)	21.91	16.52 (68.8)	1.57 (6.5)	5.93 (24.7)
May	18.88	2.41 (10.0)	0.18 (0.8)	21.50 (89.2)	21.53	13.93 (59.4)	0.81 (3.5)	8.69 (37.1)

* Sum of values from June 3rd to June 30th 2016 and June 1st to June 2nd 2017

† No data available for 17 out of 31 days in October 2016

Table 4.2: Results from the lysimeter study: hydrological balance (annual, winter, summer, monthly) with absolute values [mm] and share of components [%] related to sum of infiltration, evaporation and runoff. Hydrological summer May to October, hydrological winter November to April

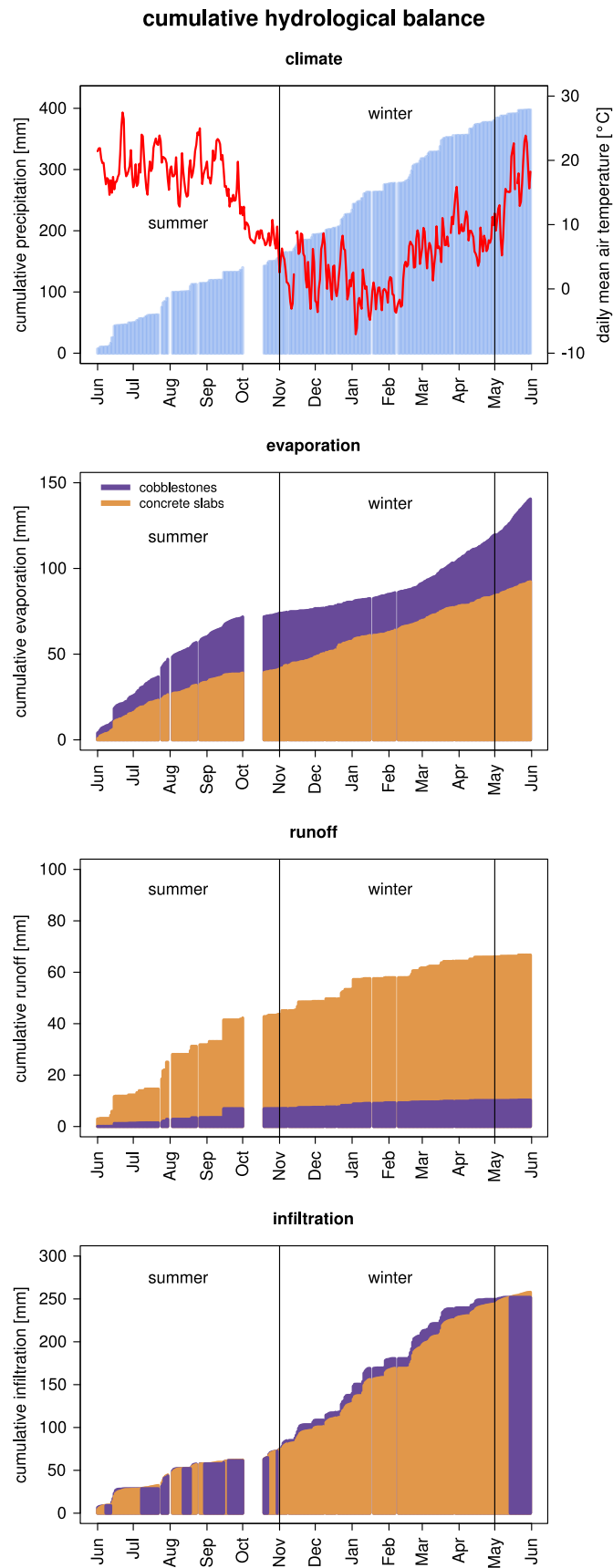


Figure 4.3: Cumulative daily hydrological balance as measured June 2016 to June 2017 in Berlin. Hydrological summer May to October, hydrological winter November to April

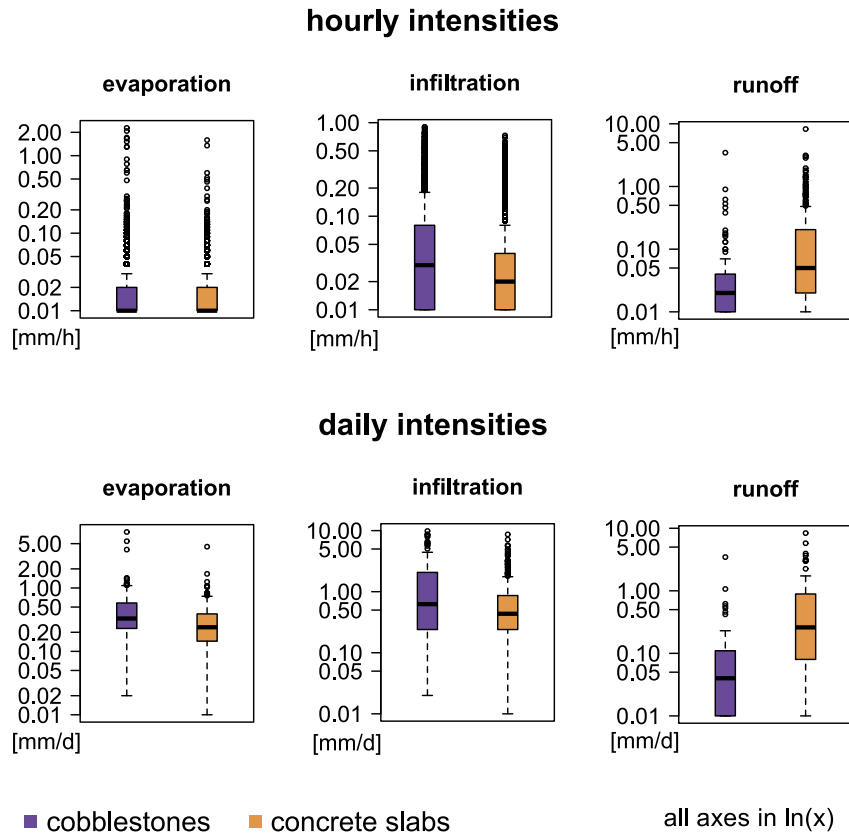


Figure 4.4: Hourly and daily intensities of evaporation, runoff and infiltration events (only values $> 0 \text{ mm d}^{-1}$ or mm h^{-1} considered), axes in $\ln(x)$

Figure 4.4 offers a more detailed view at intensities of evaporation, infiltration and runoff events. It considers only values > 0 , to show the possible extent of intensities. The occurrence of days without any evaporation, infiltration or runoff is shown in table 4.3. On an hourly basis, evaporation events tend to have a very low rate with a median value of 0.01 mm h^{-1} . The highest hourly evaporation rates are 2.28 and 1.59 mm h^{-1} for cobblestones and concrete slabs, respectively. On a daily basis, the median rate for evaporation events are 0.33 mm d^{-1} (cobblestones) and 0.24 mm d^{-1} (concrete slabs). Again, cobblestones reach a higher maximum of 7.64 compared to 4.48 mm d^{-1} . Additionally, the minimal evaporation rate for $ET > 0 \text{ mm d}^{-1}$ is higher for cobblestones. Including days without evaporation, the daily median values are 0.30 mm d^{-1} (cobblestones) and 0.22 mm d^{-1} (concrete slabs). Infiltration events have higher rates than evaporation, with a median of 0.03 mm h^{-1} or 0.63 mm d^{-1} (cobblestones) and 0.02 mm h^{-1} or 0.44 mm d^{-1} (concrete slabs). The maximum values were 0.90 mm h^{-1} or 9.85 mm d^{-1} (cobblestones) and 0.73 mm h^{-1} or 8.66 mm d^{-1} (concrete slabs). While cobblestones tend to higher infiltration rates, nearly 50% of the days registered no infiltration for this surface (see table 4.3). Contrary to that, concrete slabs had more consistent infiltration with only 9% of all days without infiltration. Including days without any infiltration, the median rates are 0.02 mm d^{-1} (cobblestones) and 0.38 mm d^{-1} (concrete slabs). Runoff

occurred very rarely for both surfaces, with 76 – 80 % of all days without runoff. If runoff takes place, concrete slabs exhibit significantly higher rates with a median of 0.05 mm h^{-1} or 0.26 mm d^{-1} compared to 0.02 mm h^{-1} or 0.04 mm d^{-1} for cobblestones. The maximum values were 3.46 mm h^{-1} or 3.46 mm d^{-1} (cobblestones) and 8.25 mm h^{-1} or 8.37 mm d^{-1} (concrete slabs). In both cases, the highest daily runoff rate can be attributed to a high-intensity rainfall event taking place within a single hour.

Days without process	Cobblestones			Concrete slabs		
	<i>E</i>	<i>I</i>	<i>RO</i>	<i>E</i>	<i>I</i>	<i>RO</i>
number of days	31	165	267	42	29	252
% of total days	9.3	49.6	80.2	12.6	8.8	75.7

Table 4.3: Number and percentage of days for which no evaporation (*E*), infiltration (*I*), or runoff (*RO*) was recorded. Total number of days = 333

Apart from intensities, a closer and simultaneous look at the processes over time is necessary to assess interactions. Figure 4.5 and 4.6 depict the hourly hydrological balance and soil water movement for two periods of four days each.

The first period (Fig. 4.5) spans from June 15th to June 19th, 2016. It contains numerous precipitation events with daily intensities of 9.08, 0.08, 18.70 and 0.97 mm d^{-1} . The four days were warm with mean daily air temperatures (T_{air}) of $14.96 - 17.43 \text{ }^\circ\text{C}$, with higher values on the two drier days. On the two days with high precipitation, daily solar radiation (R_s) was relatively low with about 104 W m^{-2} compared to about 264 W m^{-2} on the 16th and 18th of June, when there was no to very little precipitation. Consequently, surface temperature (T_{surf}) decreased, with a daily mean T_{surf} drop of 2 – 4 K on rainy days.

These climatological conditions resulted in the highest hourly and daily evaporation rates recorded during the measurement period. On June 17th, 2016, surfaces evaporated 7.64 mm d^{-1} (cobblestones) and 4.48 mm d^{-1} (concrete slabs). Hourly, evaporation rates reached up to 2.28 mm h^{-1} (cobblestones) and 1.59 mm h^{-1} (concrete slabs). As the hourly hydrological balance shows, evaporation takes place on all four days. On June 16th, 2016, when there was very little precipitation (0.08 mm d^{-1}), both surfaces evaporated more than on the previous day which had higher rainfall intensities, as well as 6 to 10 times as much as the water available from rainfall on that day. Soil water content (θ) measurements show that this additionally evaporated water originated from the underlying soil column. Both lysimeters show increasing θ in 5 and 15 cm depth for June 16th, 2016. Since evaporation exceeded the income of rain water on that day, this increase could not be caused by incoming water. With 0.08 mm provided by rain water, the remaining 0.72 (cobblestones) and 0.41 (concrete slabs) mm of evaporation occurring on that day has to have been provided by the soil layers. The same effect was observed in the second period depicted in figure 4.6, which spans from September 16th to September 20th, 2016. This period features a high-intensity rainfall event on September 17th, 2016, with 12.65 mm d^{-1} , of which 10.44 mm occurred in a single hour. The

previous and the two following days had no precipitation. Again, daily mean T_{air} was relatively high with $15.88 - 20.82^\circ\text{C}$ and reduced R_s on the rainy day (80 W m^{-2} compared to about 165 W m^{-2}). In this case, the precipitation event increased the overall soil water content in all layers. In the two following days, no rainfall provided water but upward water transport resulted in 0.98 mm d^{-1} (cobblestones) and 0.3 mm d^{-1} (concrete slabs) on September 18th, 2016, followed by 0.52 mm d^{-1} (cobblestones) and 0.12 mm d^{-1} (concrete slabs) on September 19th, 2016. This pattern of slightly decreasing daily evaporation rates on the following days shows that upward water transport is especially effective on days following and between precipitation events. It is highly dependent on precipitation filling up the soil layers. Both periods show that upward water transport is responsible for evaporation processes.

Both surfaces led to infiltration on all four days with daily rates of $3.21 - 6.06 \text{ mm d}^{-1}$ (cobblestones) and $1.08 - 5.72 \text{ mm d}^{-1}$ (concrete slabs).

4.1.2.2 Water transport processes

The combination of lysimeter data revealing water transport processes leaving the system and sensor data recording the water movement within the system offered new insights into processes and their interactions. Tables 4.4 and A.1* summarise measured soil water content (θ) at a monthly, seasonal and annual scale. On all of these scales, water tended to accumulate towards the bottom of the lysimeter, with highest hourly θ at 25 cm depth and lowest at 5 cm. Throughout the year, cobblestone paving resulted in slightly higher θ compared to concrete slabs. In winter, the difference between the two surfaces is larger than in summer. While mean hourly θ at 25 cm is mostly stable throughout the year, larger seasonal fluctuation can be observed at 5 cm depth. Over the whole year, hourly θ in all depths reached their minimum in winter and their maximum in summer ($\theta_{25_{COB}}$ has its maximum in winter but nearly the same value in summer with a difference of 0.08 Vol.-%). A closer look at monthly mean values of θ (excluding October 2016 because of a lack of data in that period) shows that the two surfaces have different patterns. At the top (θ_5), both lysimeters had the highest value in June 2016, the month with the highest P in the period, which then gradually decreased towards winter and then increased again starting February/March. The difference between highest and lowest θ_5 is 1.71 Vol.-% (cobblestones, June–November) and 3.44 Vol.-% (concrete slabs, June–January). In the month with lowest θ_5 , the lysimeters recorded high infiltration, high precipitation, and low evaporation.

For this upper layer, the months June, January and March are most interesting. These are the three months with the highest and similar P . For cobblestones, the net precipitation ($P^* = P - RO$) is very similar for these months, ranging from 45.76 to 46.89 mm. Hence, they received roughly the same water input. However, evaporation amounts varied significantly. June recorded the highest E_{COB} (25.89 mm), January

*Figures and tables with indices A are found in the appendices

hourly hydrological balance period with highest evaporation

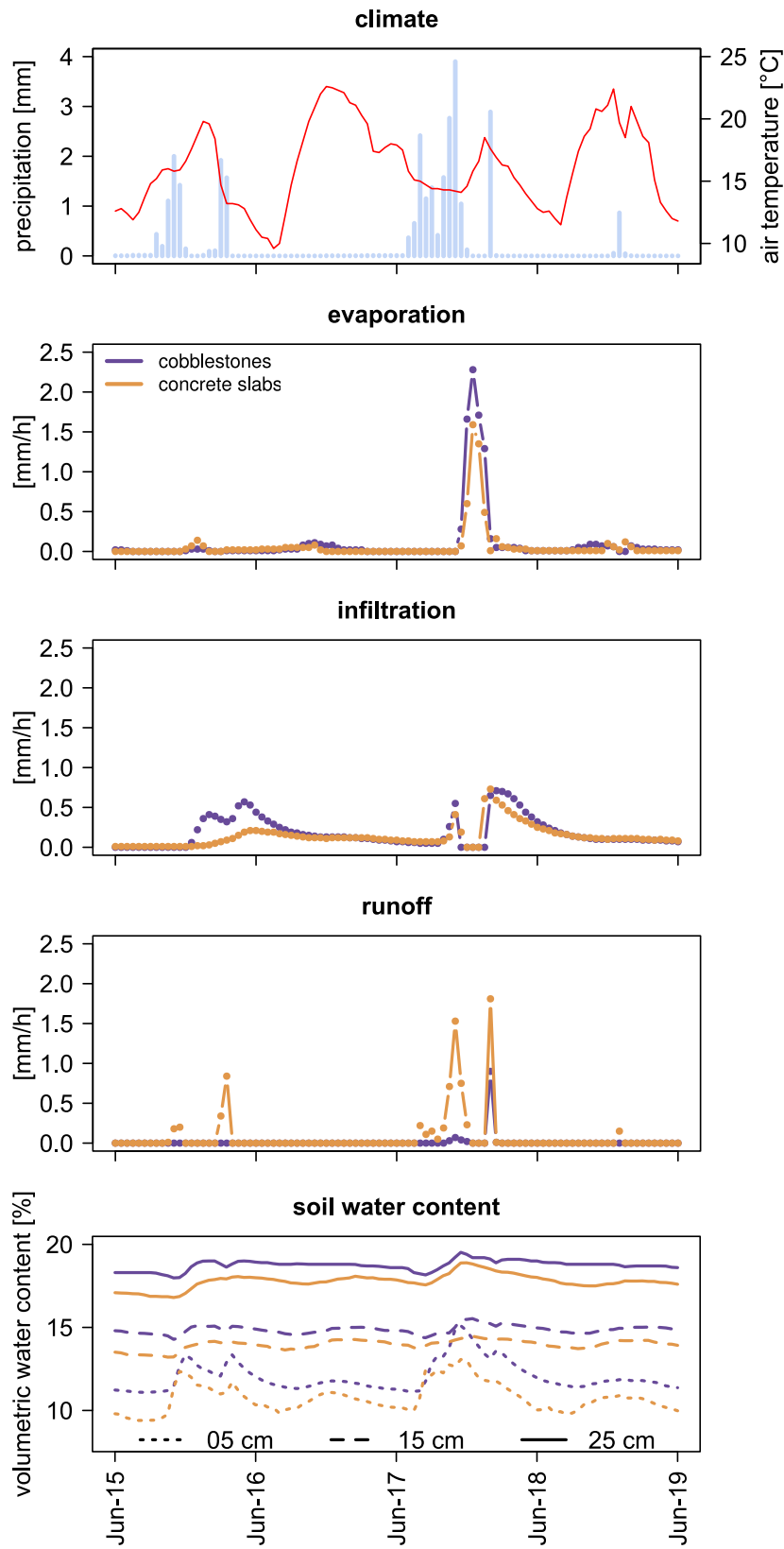


Figure 4.5: Hourly hydrological balances and soil water movement for four days in June 2016, period with highest hourly and daily evaporation event

hourly hydrological balance period with highest precipitation

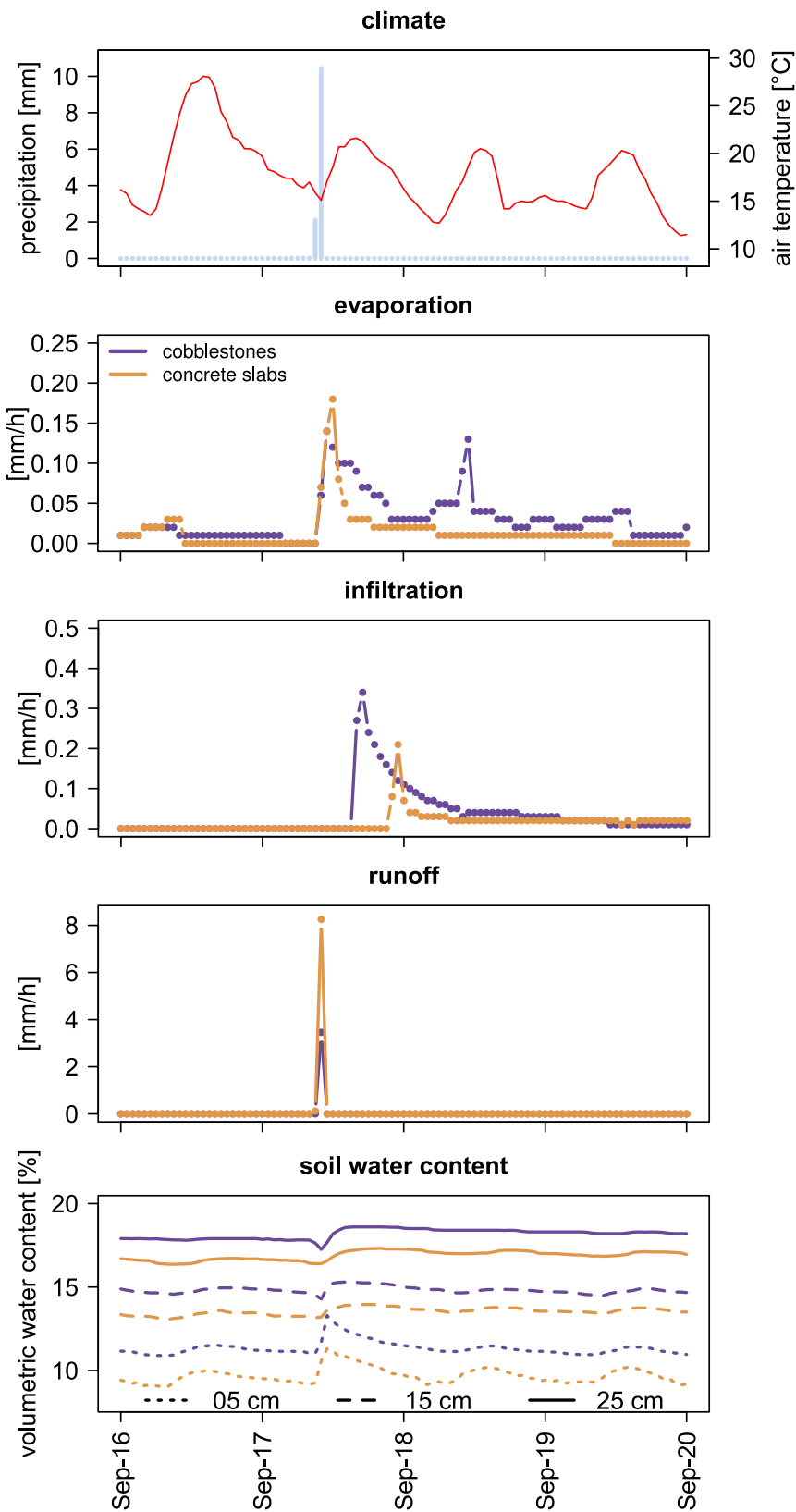


Figure 4.6: Hourly hydrological balances and soil water movement for four days in September 2016, period with highest rainfall intensity event

was among the lowest three months (3.97 mm), and March showed a medium value (13.41 mm). At the same time, all three months had high infiltration amounts. In January, the highest monthly I_{COB} was recorded (40.66 mm), and March and June had similar infiltration (28.57 – 32.66 mm). Combining these observations, it becomes again clear that large amounts of water are transported upwards in the cobblestone lysimeter. In June, water infiltrating through the pavement-interface to the upper soil layer will mostly evaporate, which decreases θ_5 . Yet, June has the highest mean θ_5 , which shows that water is transported upward through capillary rise, increasing the amount of water available for evaporation. This is further supported by θ_{15} being high and θ_{25} being comparatively low. June and March have very similar P^*_{COB} and I_{COB} , but E_{COB} in March is just half of that in June. The distribution of θ_{COB} shows a shift towards the lower layers, with the overall highest θ_{25COB} being recorded in March, indicating less upward water transport which fits the lower evaporation rate. With the same P^* , January has the highest I_{COB} and very low E_{COB} . In this month, most of the water passing the pavement-interface will pass through the lysimeter and result in infiltration without or with very little upward water transport. Hence, θ_{5COB} and θ_{15COB} reach their minimum values. Another example for upward water transport can be found in May 2017. With very low P_{COB} and P^*_{COB} , E_{COB} was very high and exceeded incoming precipitation. Again, θ_{5COB} was relatively high. At the same time, θ_{25COB} and I_{COB} reached their minimum in May. Assuming that incoming precipitation is reduced by runoff and infiltration leaving the system, 5.21 mm were supplied for evaporation by upward water transport, corresponding to 24 % of the overall evaporation of the month.

In June, January and March, concrete slabs, for which runoff has a higher influence, resulted in $P^*_{CON} = 38.71 - 45.36$ mm. In June, about a fifth of monthly rainfall left the system as runoff. The remaining water evaporated from the surface storage or passed the paved layer, increasing θ_{CON} throughout the soil column, leading to the maximum monthly values for all layers. These high values of θ_{CON} occur simultaneously with the highest monthly amount of E_{CON} , which indicates soil layers and upward water transport playing an active role in evaporation processes. In January, less of the similar amount of rainfall leaves the concrete slab surface as runoff and evaporation reaches its lowest monthly value. Hence, water passes into the soil column. This time, low temperatures lead to less upward water transport and the water passes the soil column more quickly. This fast downward water transport is also reflected by the lowest monthly values of θ_{CON} for all layers, despite high precipitation and the highest value of I_{CON} . In March, the processes of the concrete slab surface are very similar to those of cobblestones. The main difference is the amount of RO affecting how much water is available in the system, leading to less E . Again, May is another interesting month worth a closer look. Compared to the three previously described months, P was low (yet three times as much as the lowest value), with the lowest monthly amount and percentage of RO for this surface ($RO_{CON} = 0.81$ mm, 3.5 %). With less of the rainfall leaving the system as runoff, the soil water content increased, with all three depths reaching the second highest

Depth below paver [cm]	Cobblestones			Concrete slabs		
	5	15	25	5	15	25
<i>Annual</i>						
Min θ [Vol.-%]	4.05	11.36	16.00	3.20	7.69	14.00
Mean θ [Vol.-%]	10.70	14.02	18.18	8.79	13.12	16.64
Median θ [Vol.-%]	10.84	14.00	18.20	9.03	13.15	16.70
Max θ [Vol.-%]	15.83	16.75	19.60	13.95	14.65	18.89
<i>Summer</i>						
Min θ [Vol.-%]	10.09	13.05	16.62	8.03	12.70	16.00
Mean θ [Vol.-%]	11.19	14.53	18.00	9.68	13.48	16.96
Median θ [Vol.-%]	11.13	14.57	18.00	9.64	13.44	16.92
Max θ [Vol.-%]	15.83	16.75	19.52	13.95	14.65	18.89
<i>Winter</i>						
Min θ [Vol.-%]	4.05	11.36	16.00	3.20	7.69	14.00
Mean θ [Vol.-%]	10.22	13.53	18.36	7.94	12.78	16.33
Median θ [Vol.-%]	10.55	13.65	18.50	8.33	12.85	16.38
Max θ [Vol.-%]	13.33	14.70	19.60	10.97	14.00	18.02

Table 4.4: Hourly soil water content θ measured within the lysimeter soil column. Hydrological summer May to October, hydrological winter November to April

monthly values of θ_{CON} recorded. This differs from θ_{COB} , which increased for upper layers but decreased for a depth of 25 cm. For cobblestones, high amounts of water were transported upwards and evaporated, leading to high E and very low I . Under concrete slabs, upward water transport resulted in a medium amount E but the highest monthly percentage of E relative to P ($E_{CON} = 37.1\%$). Still, most water that reached the soil layers left the system as infiltration rather than evaporation. Given that for this month, the temperature difference between the two surfaces reached its maximum for all layers with concrete slabs leading to higher values (figure 4.10), the difference in E can not be solely assigned to energy available for evaporating processes. Instead, the effect of pavers acting as evaporation barrier with upward transported water condensing on the underside of the paver and travelling back downward (Flöter, 2006; Wessolek, 2001) is likely to occur for concrete slabs. However, the extent of this effect is lower than previously assumed, as it does not prevent any kind of upward water transport resulting in evaporation. The high percentage of evaporation in May is more likely to result mainly from water evaporating from the surface storage, as low relative RO indicates low precipitation rates, which gradually and often fill the surface storage.

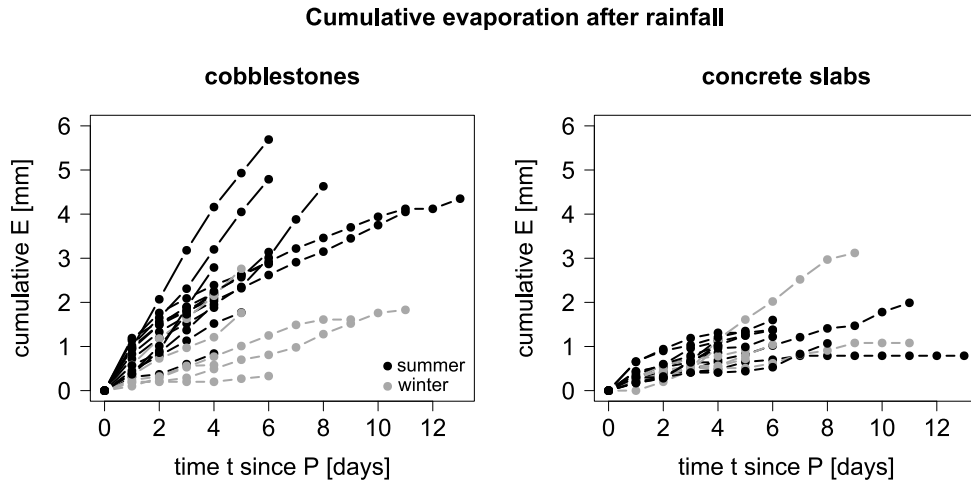


Figure 4.7: Cumulative evaporation during dry periods following days with rainfall. Only periods of at least four days considered

The upward water transport from underlying soil layers resulting in evaporating can be further analysed by studying evaporation on consecutive dry days following days with rainfall. Figure 4.7 illustrates cumulative evaporation during dry periods (of at least four days length) following precipitation. Within the measurement period, there were 19 such periods, of which 13 lay in summer. The longest dry period lasted 13 days in September 2016. Concurrent to previous observations, cobblestones tend to higher evaporation rates. Generally, the daily evaporation is highest on the first dry and gradually decreases with each further day. For both surfaces, there are periods for which the daily evaporation rate is nearly constant or may even increase slightly with progressing time. For cobblestones, there is a distinct differentiation between summer and winter periods, which can not be observed for concrete slabs. Additionally, the cumulative evaporation rates are mostly constant for concrete slabs but vary for cobblestones. This again reflects the differences between the two surfaces functioning as active interfaces between the soil and the atmosphere.

These examples show the interaction between the overall hydrological balance and the water flow direction, as well as the importance of upward water transport.

In order to quantify how relevant upward water transport resulting in evaporation is, table 4.5 summarises how much of the measured evaporation takes place on days with and without precipitation. Annually, 13.23 % (concrete slabs) to 47.23 % (cobblestones) of evaporation is recorded on days without precipitation. In winter, more evaporation is attributed to days without precipitation than in summer. The table only considers days without any rainfall. When including cases as described for June 16th, 2016, 62.72 % (cobblestones) and 46.65 % (concrete slabs) of the overall evaporation can be attributed to days on which rainfall did not provide all of the water evaporating ($E [\text{mm d}^{-1}] > P [\text{mm d}^{-1}]$).

	Evaporation cobblestones		Evaporation concrete slabs	
	$P > 0 \text{ mm d}^{-1}$	$P = 0 \text{ mm d}^{-1}$	$P > 0 \text{ mm d}^{-1}$	$P = 0 \text{ mm d}^{-1}$
Annual	52.75 %	47.23 %	86.77 %	13.23 %
Summer	54.30 %	45.70 %	89.25 %	10.75 %
Winter	49.43 %	50.57 %	83.90 %	16.10 %

Table 4.5: Percentage of total amount of evaporation (annual, summer, or winter) measured on days with ($P > 0 \text{ mm d}^{-1}$) and without ($P = 0 \text{ mm d}^{-1}$) precipitation

4.1.3 Heat balance & transport

Temperatures were measured in both lysimeters and at their surfaces, with sensors on the surface (T_{surf}), directly below the pavers (T_{pav}) and at 5, 15, and 25 cm below the paver underside (T_5, T_{15}, T_{25}). For both surfaces, mean temperatures are highest within the soil column and lowest at the underside of pavers, with surface temperatures in between (figure 4.8). With otherwise small differences, there is a large temperature gradient between T_{pav} and T_5 . Concrete slabs lead to higher mean temperatures in all depths, with the highest difference for surface temperatures. In general, the upper layers, especially surface and paver, are most exposed and hence influenced by atmospheric conditions. Temperature fluctuations are highest at the surface and decrease with depth. Independent of surface, T_{surf} reached the highest and lowest hourly temperatures and T_{25} had the smallest maximum and highest minimum values of hourly temperatures (see table A.2).

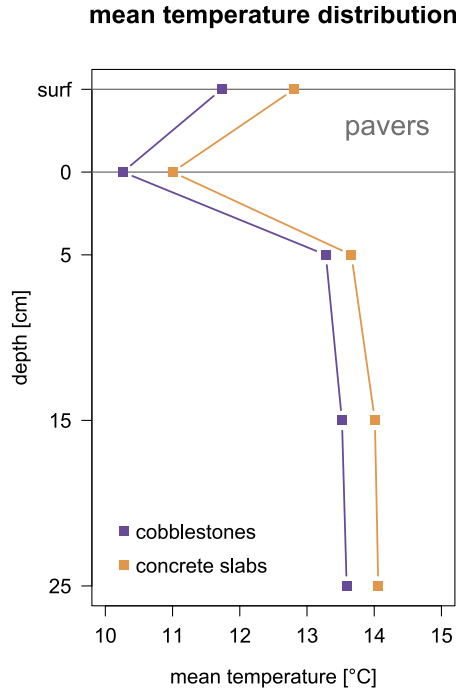


Figure 4.8: Comparison of annual mean temperature profiles

temperature profiles

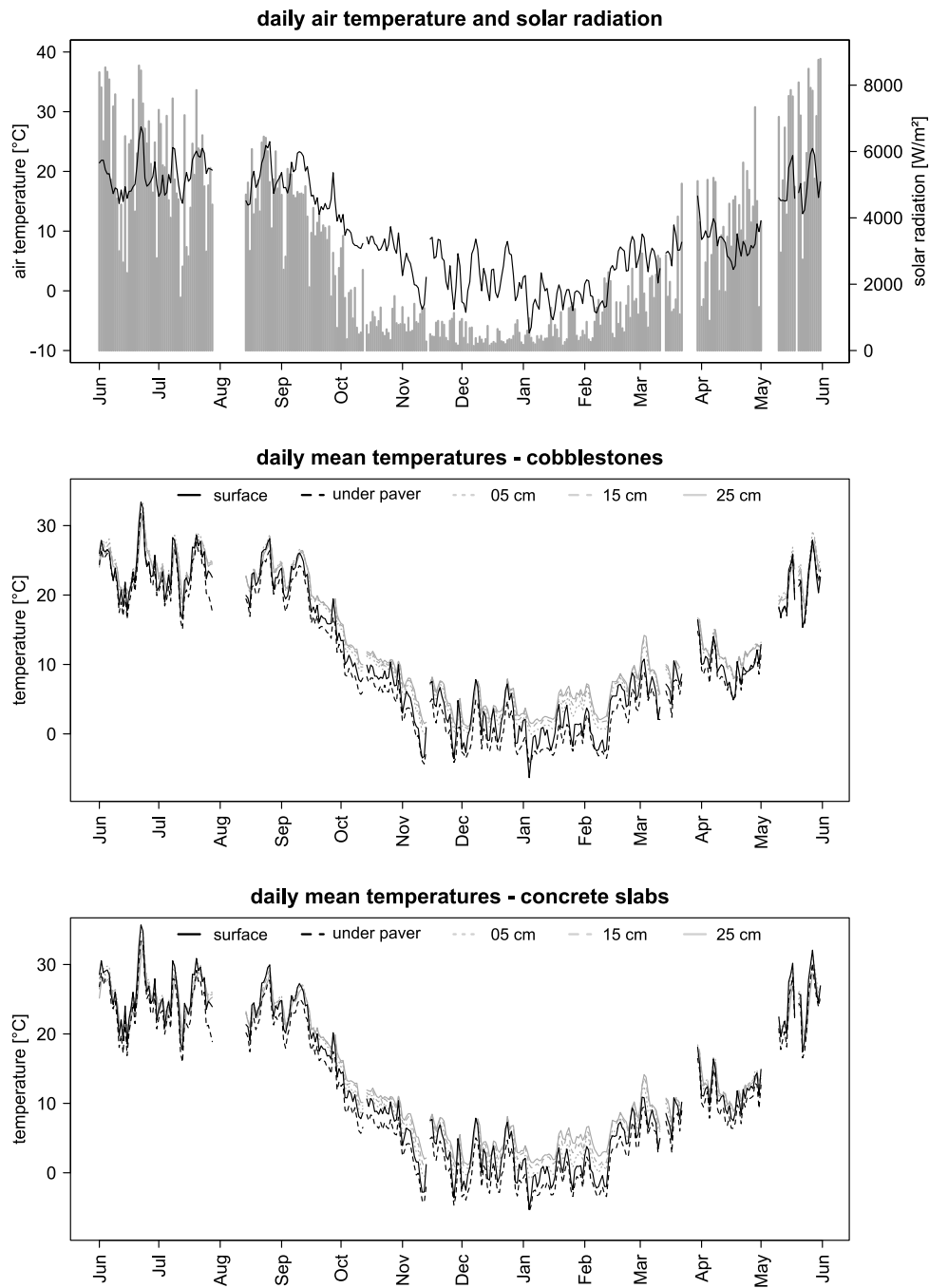


Figure 4.9: Daily solar radiation & mean temperatures (air, surface, below paver, at 5, 15 & 25 cm) during measurement period

Monthly mean temperatures for all depths and T_{air} can be found in table A.3. For all layers, highest mean temperatures were recorded in June 2016, which resulted in high evaporation. Lowest overall temperatures in all depths were recorded in January 2017, a month with very little water evaporating and very high infiltration. During warm

months (June to September 2016), mean temperatures were highest at 5 cm depth. With less incoming energy from above, the highest temperatures are found in the lowest layer at 25 cm in the cold months (October 2016 to March 2017). Starting April 2017, the upper layers start heating up again and by May 2017 T_5 has again the highest mean temperatures. At a higher temporal resolution, figure 4.9 depicts daily mean values for all layers, as well as T_{air} and R_s . It shows how closely daily mean surface and soil temperatures follow daily T_{air} and R_s . In summer months, all layers have very similar mean T , with larger temperature gradients in colder months.

Largest differences between daily mean values of T_{25} and T_{surf} were in January to mid-February 2017. The figure shows that the overall response to T_{air} and R_s changes is very similar between the two lysimeters. As has been shown, concrete slabs generally lead to higher temperatures in all layers. The difference between the two surfaces differs depending on layer and time (figure 4.10). Most of the time, concrete slabs result in higher temperatures, with the highest difference to cobblestones in May 2017. T_{surf} generally differs most between the two surfaces. From October to March, T_5 is slightly higher under cobblestones and in January, cobblestones reach higher temperatures in all layers, with the largest difference for T_5 . Overall, the temperature differences range from 1 to 3 K.

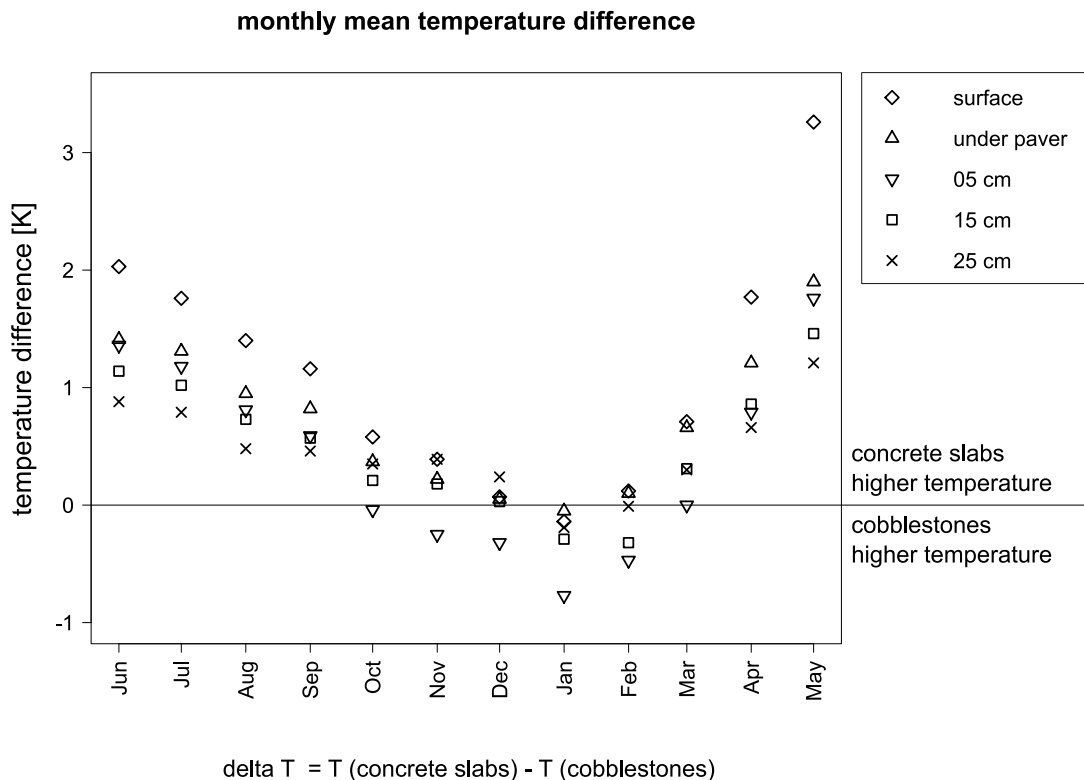


Figure 4.10: Differences in monthly mean temperatures between the two surfaces for all measurement depths

hourly air, surface and soil temperatures

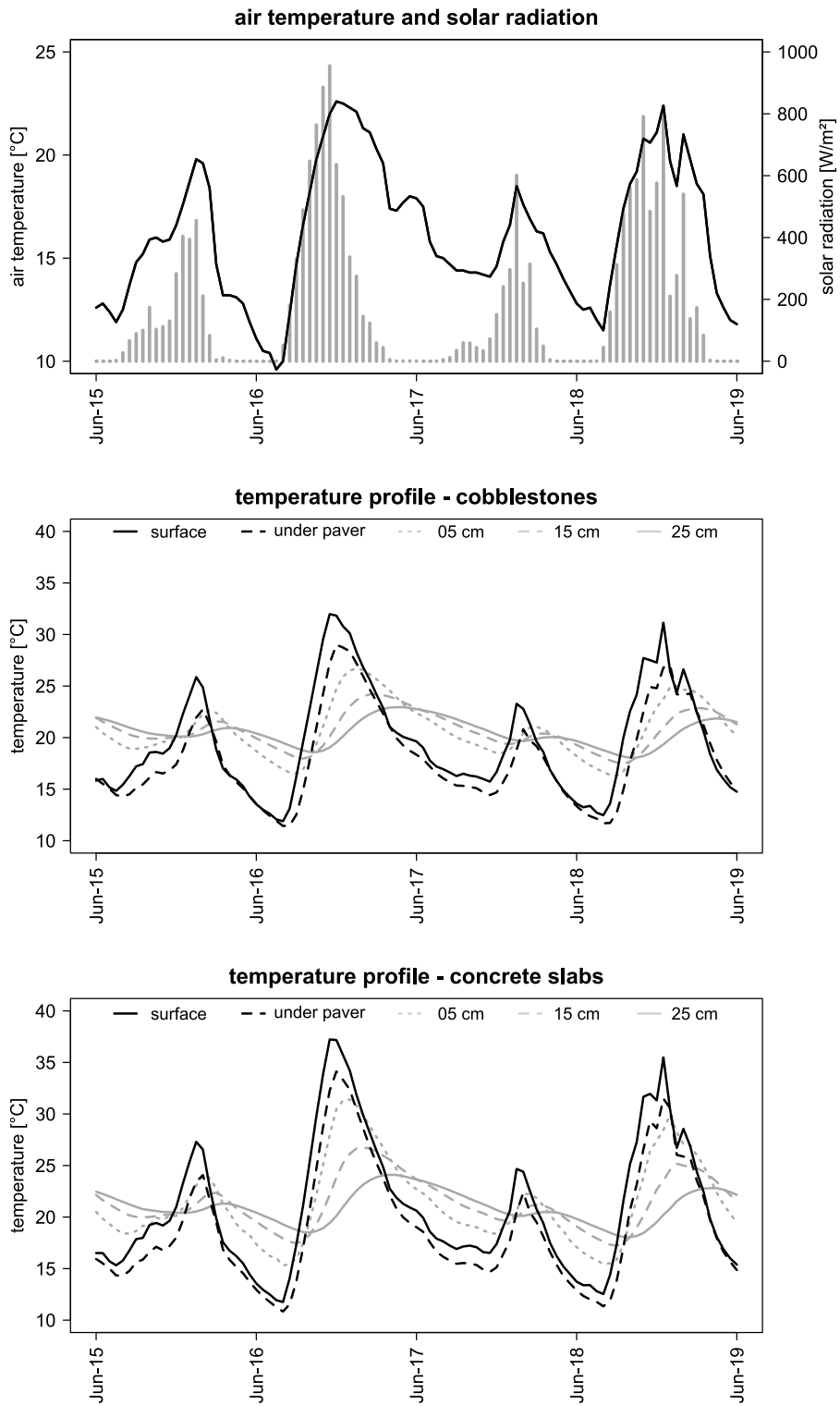


Figure 4.11: Hourly air, surface & soil temperatures – period with highest evaporation from June 15th to June 19th, 2016

Corresponding to figures 4.5 and 4.6, hourly temperature data is illustrated for two example periods of four days each in figures 4.11 and A.1. The hourly data supports previous observations. For both periods, the two surfaces responded very similarly but concrete slabs surface leads to higher temperatures and fluctuations than cobblestones. At this scale, diurnal cycles become apparent. During night, temperature drops in all layers. With a sharp decrease at the upper layers, which are more exposed to atmospheric conditions, and smaller changes at lower levels, highest T is recorded at the lowest level and increases towards the surface. Towards noon and early afternoon, T increases again and the higher levels heat up rapidly. During most of the cycle, T_{pav} is smaller than T_{surf} . When T_{surf} starts cooling down in the evening, T_{surf} responds more rapidly, which can result in times for which $T_{surf} = T_{pav}$. In general, a lag of response time can be observed, with a shift of diurnal cycles between the layers. For example, on June 16th, 2016, T_{surf} reaches its daily maximum at 11:00, followed one hour later by T_{pav} and nine hours later by T_{25} . This lag is present throughout the diurnal cycle. In this study, no temperature measurements for other surface covers are available. However, data is available for bare soils (DWD, 2018c) and forests (Trinks, 2010) from studies carried out in Berlin with measurements at a common depth of 5 cm (T_5). Since one of those studies provided data on a monthly basis, figure 4.12 compares the relationship between monthly T_{air} and T_5 . For the two paved surfaces, the relationship is nearly identical, with slightly higher values of T_{5CON} except for very cold months, as previously described. Both pavements led to T_5 exceeding T_{air} , with less difference in colder months. This is also the case for bare soil, which still exceeds T_{air} but led to lower T_5 than the two paved surfaces. While these three are very similar, forest cover creates a different pattern. Here, T_5 exceeds T_{air} in cold months and decreases in warmer months. This is likely to be caused by forest trees reducing solar radiation which contributes to heating up the bare and paved surfaces and hence, the layers beneath, as well as evapotranspiration processes leading to cooling. A similar comparison can be found in Wu et al. (2014), in which daily soil temperature measurements up to 300 cm below the surface were carried out for bare soil, grass and concrete cover in both urban and rural settings. They too observed increased soil temperature beneath concrete compared to bare soil or grass in all depths, with larger differences in warmer months. In their study, bare soil and grass led to very similar soil temperatures.

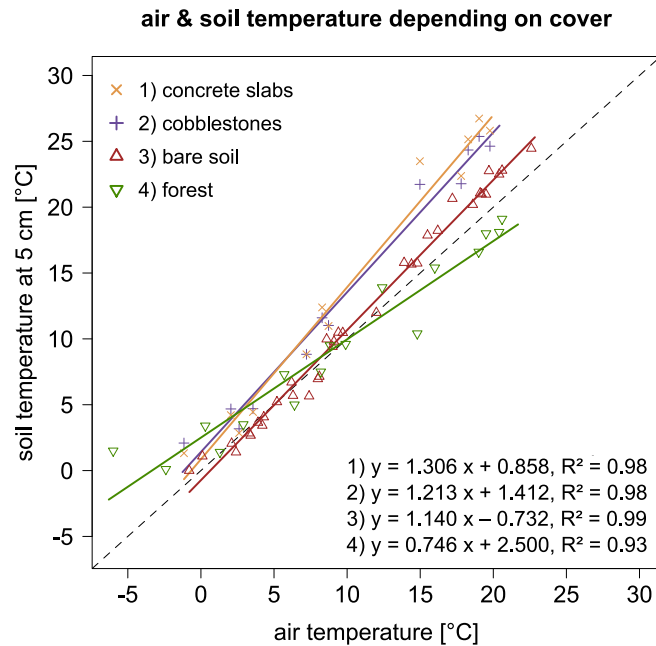


Figure 4.12: Monthly air & soil temperatures for different surface covers. Bare soil measurements in Berlin for the years 2015–2017 (DWD, 2018c), forest measurements in Berlin between June 2008 and January 2010 (Trinks, 2010). All soil temperature measurements taken at 5 cm below surface cover

4.2 Process interactions

Hydrological processes are closely linked between individual processes, as well as to atmospheric conditions. For paved surfaces, these interactions are focussed at the pavement layer as the soil-atmosphere interface. Depending on the properties of the pavement, their response to hydrological and atmospheric conditions differs greatly. In the next section, a closer look at the coupled heat and water transport offers insight into how different the two studied surfaces react to these conditions. After that, all measured hourly and daily data is paired up to analyse process interactions based on their correlations. Both sections illustrate how complex and varied paved surfaces react to and impact their surroundings.

4.2.1 Coupled heat and water transport

Water and heat transport within soils are closely coupled and influence the water and energy exchange at the soil-atmosphere interface (Bachmann and van der Ploeg, 2002; Heitman et al., 2008; Lakshmi et al., 2003; Menziani et al., 2003; Schrödter, 1985). Soil moisture (VWC) plays a key role in how much of the incoming energy will be turned into latent or sensible heat flux (Lakshmi et al., 2003). Latent heat means energy is utilised to transition between phases (e.g. from liquid to gas) and does not lead to a change in temperature. In contrast, sensible heat leads to a change in temperature.

Evaporation, the amount of water transferred from the soil into the atmosphere in the form of vapour, is the latent heat flux (Lakshmi et al., 2003; Schrödter, 1985). Energy for evaporation processes is provided by solar radiation and the energy stored at the soil surface and in the soil column (Schrödter, 1985). By affecting evaporation processes from the surface and the soil, changes in T_{surf} impact the soil moisture, which in turn affect the temperature (Lakshmi et al., 2003). As Heitman et al. (2008) point out, evaporation of soil water can be seen as a large heat sink. When energy is being utilised for evaporation processes, it is not available to maintain the sensible heat of the surrounding, which leads to a cooling effect. Sensible heat fluxes in the soil column are driven by temperature gradients (Heitman et al., 2008), which are influenced by evaporation from the surface and underlying soil.

Figure 4.13 illustrates hourly observations of volumetric water content (θ) and temperature at 5, 15 and 25 cm depth for the example period in September 2016 (see also figures 4.6 & A.1). On September 17th, a high precipitation event occurred at noon,

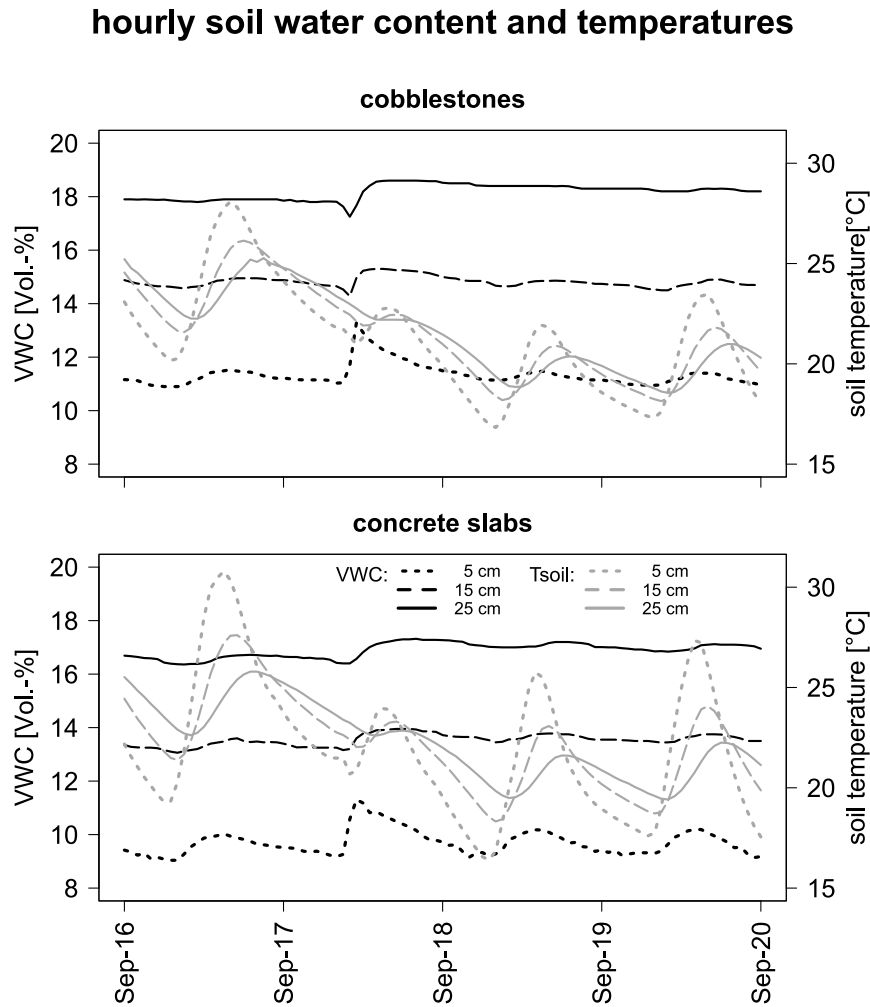


Figure 4.13: Example of hourly soil water content and temperatures at 5, 15, and 25 cm below the paver underside

followed by an increase of θ for all three depths as water infiltrates into the soil. At the same time, T_{soil} decreases in all depths with a slight lag with increasing depth. The supplied water starts to evaporate, for which energy is consumed as latent heat. As a result, this energy can not be used as sensible heat and it takes a couple of days for T_{soil} to gradually increase again as the soil dries. This heating up process takes longer for cobblestones, which tend to higher evaporation rates and hence, to more energy being used as latent heat. The figure shows upward water transport in form of evaporation: T_{15} is decreasing at the same time as θ_{15} decreases, followed shortly after by θ_5 increasing. The same can be observed for depth 25 and depth 15 cm. Water at the lower depths uses the energy stored in the soil as heat to evaporate and travels upward, leading to a decrease of θ at the lower layer and an increase above. From the 5 cm, some of the water will pass the paved soil-atmosphere interface and leave the soil, using the energy stored in the upper soil layer and the new incoming energy from the atmosphere. The less water is transported to the upper 5 cm, the less incoming energy is used as latent heat, leading to slowly increasing T_5 in the following days and decreasing evaporation rates (see also figure 4.7). It should be noted that capillary rise of liquid water is another source of upward water transport, which plays an important role at the beginning with water vapour being the dominant source of water as the soil becomes drier. Heitman et al. (2008) carried out spatially high-resolution measurement of soil temperatures at the first 6.6 cm below the surface and showed that soil thermal properties near the surface are affected by wetting and drying processes. In order to analyse this wetting–drying process, an additional experiment was carried out using a thermal camera (see chapter 3.3). On this day, mean air temperature was 23.87°C and daily R_s reached 270 W m^{-2} . The results for one wetter/drying cycle for each surface are illustrated in figures 4.14 (mean temperature time series) and 4.15 (thermal pictures). In the time series, the first value ($t = 0 \text{ s}$) is the initial dry surface. Next, the surface was watered, which is excluded in this figure, followed by the first picture after the surface was completely covered in water ($t = 4 \text{ s}$). For concrete slabs, joints and pavers follow the same pattern, with joints maintaining higher temperatures. Water application leads to a sharp decline in temperature by $1 - 2 \text{ K}$, as the applied water was cooler than the surface temperature in dry conditions. Immediately after, the applied water is heating up, with sensible heat fluxes dominating the process. T_{surf} remains more or less stable with a slight tendency to decrease until $t = 200 \text{ s}$. The fluctuations indicate that both processes, sensible and latent heat flux, take place. At this point, the water film adhering to the surface has been completely evaporated but the concrete slabs were visibly still wet, with the pores storing water. For the next 340 seconds, the surface is first cooling down and then remaining at this low temperature, with the water evaporating from the surface storage and the upper soil layers transforming energy to latent heat. Figure 4.15 shows the surface at $t = 420 \text{ s}$, when it reached its lowest T_{surf} . Overall, it takes 540 seconds until most of the available water has been evaporated and sensible heat fluxes start to dominate, gradually increasing T_{surf} again. Yet, even during this increase, small

Surface temperatures during wetting-drying process

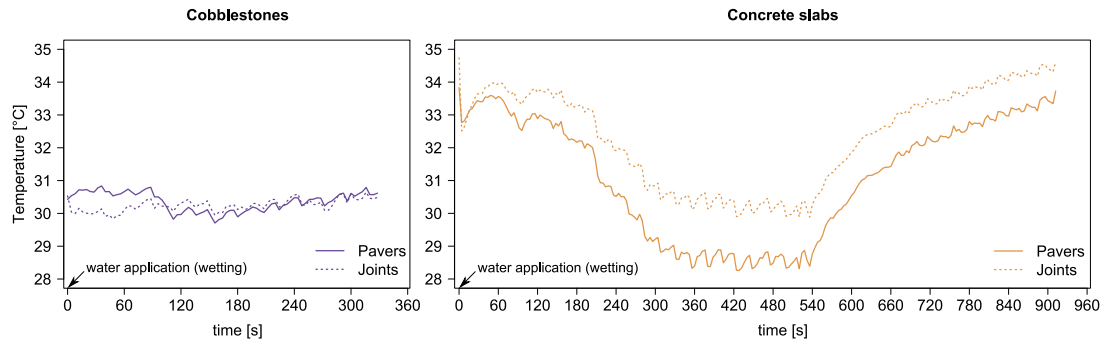


Figure 4.14: Timeseries of T_{surf} during surface wetting and drying process. Based on thermal pictures with 4-second resolution. Wetting process was cut, so that $t = 0$ is initial dry surface and $t = 4$ is surface immediately after water application. Drying process complete after 322 (cobblestones) and 908 (concrete slabs) seconds

fluctuations with decreasing T_{surf} show that latent heat fluxes still take place. After a total of 908 seconds, the surface is mostly dry again with only small amount of pores still visibly containing water and T_{surf} again reaching its initial temperature. Throughout the process, joints has lower temperatures, which can be attributed to higher evaporation rates compared to the pavers due to their utilisation of soil water.

The wetting–drying process differs significantly between the two surfaces. For cobblestones the whole cycle only takes 322 seconds until initial T_{surf} is reached again. Furthermore, the overall decrease in temperature is very small compared to concrete slabs. Both can be attributed to the lower porosity of the pavers, which leads to no or very little water being stored on the pavers. The little amount of water adhering to the paver surfaces follows the same pattern as described for the concrete slabs, with sensible heat dominating as the surface water heats up, followed by latent heat flux as the water evaporated and finally an increase of T_{surf} after most of the water has been evaporated. Figure 4.15 shows that individual pavers may react very differently, depending on material and micro-topography of the surface. Some pavers included small indentations in which water accumulated. Different materials (e.g. granite and sand stone) have varying thermal properties and heat up at different rates. For the cobblestone surface, joints have a high share of the surface area (20 %) and are influences less heavily by the pavers. In the first minute after watering, latent heat fluxes dominate and the joints cool down. After that, joints generally heat up again, but fluctuations again show that both sensible and latent heat fluxes are taking place. For both surfaces, it has to be taken into account that evaporation processes increase the relative humidity of its surrounding, which decreases the evaporation potential. However, since only the two surfaces were watered, the surrounding area was mostly unaffected and supplied dry air to the surfaces through advection. This also means that this experiment represents idealised conditions rather than natural ones. Still, it is useful to observe these underlying processes.

Surface temperature during wetting-drying process

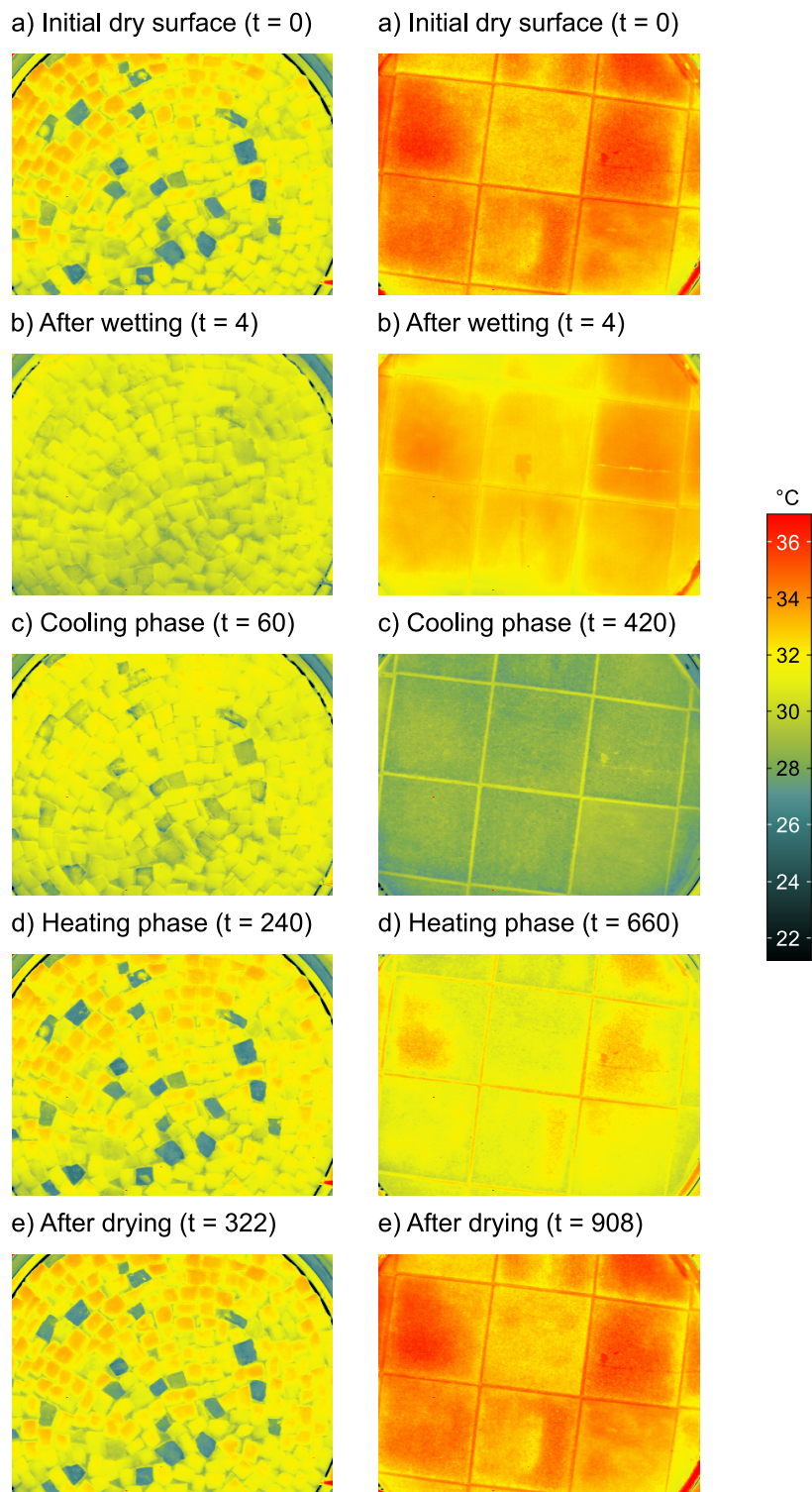


Figure 4.15: Thermal pictures of surface wetting and drying process. Timestamp (t) in seconds

4.2.2 Correlation of processes

Correlation is a measure of relationship and interdependence between processes. In this thesis, the coefficient of determination based on the Pearson correlation coefficient (R^2) is used, to describe if there is a linear fit between two variables. In this section, a more general relationship is analysed, which does not have to be linear. The Spearman correlation (ρ) is another method to determine this relationship. The main difference is, that ρ can also be used for non-linear correlation. Since the analysed data very seldom follows a linear pattern, ρ is used to gain insight into relationships and hence, possible parametrisation of models. The results are summarised in figures 4.16 and 4.17. A value of 0 indicates no correlation and -1 or 1 indicating highly dependent variables. Negative values point to one variable decreasing while another increases. For example, grass-reference evapotranspiration (ET_0 , see chapter 5) is highly dependent on relative humidity (RH) with dry air (low RH) being able to absorb more water vapour, increasing evaporation rates ($\rho(RH, ET_0) = -0.9$). The other way around, high T_{air} provides energy to heat up paved surfaces, so that $\rho(T_{air}, T_{surf}) = 1.0$. For other pairs, correlation can exist but be weakened by other factors or temporal resolution. For example, runoff formation logically is highly dependent on precipitation. Without precipitation, there can be no runoff. The amount of runoff depends on the intensity of the rainfall event, as well as the moisture of surface and soil at the start of the event. For hourly data, ρ of P and RO is 0.2 (cobblestones) or 0.4 (concrete slabs), compared to 0.5 (cobblestones) or 0.7 (concrete slabs) when considering daily data. The relationship is stronger for concrete slabs which tend to form runoff more often and in higher absolute amounts. For both surfaces, ρ is relatively low because hourly or daily precipitation intensities do not reflect the behaviour of the event. The hourly amount could be evenly distributed over one hour, or take place in just a couple of minutes. To accurately describe precipitation and runoff relationships, precipitation events would have to be recorded at a higher temporal resolution (Rim, 2011). The relationship may be stronger for daily data due to possible lags between precipitation and runoff collection. These examples illustrate the interpretation of ρ . While the amount of information contained in the two correlation matrices is too high to examine in detail here, it is included in full to provide data and insights that may be interesting for others. It should be taken into account that a small ρ does not necessarily mean that there is complete independence between two variables. For example, it is possible for a specific combination of variables to correlate with another variable, without all of the individual ones having high values of ρ with the aimed for variable.

Some further observations are noteworthy for this work. As described in the previous section, soil temperature and water content are governed by coupled processes. This is reflected by high values of ρ . E_{COB} is linked to T_{soil} and θ , as well as atmospheric conditions (T_{air}, RS, RH), which is also reflected by its relationship to ET_0 . In contrast, E_{CON} has no or very small correlation to the same variables, but a higher correlation

to precipitation compared to cobblestones. For the next chapter, the relationship between ET_0 , which represents the evapotranspiration of a grass surface with optimum water supply, and E_{COB} and E_{CON} . This relationship is represented by κ , the ratio between E and ET_0 . Figure 4.17 contains daily values of κ , which is the ratio for each day individually. While E_{CON} had low correlation with atmospheric conditions determining ET_0 , κ_{CON} has a relatively high correlation with these variables. In most cases, $\rho(\kappa_{CON}, ET_0)$ is equal or even slightly higher than $\rho(\kappa_{COB}, ET_0)$. This indicates that estimating E_{CON} by first calculating ET_0 and then adjusting it could be more promising than attempting to directly deduce E_{CON} from climatological data. Daily values of κ also show that for concrete slabs, the relationship is weakly correlated to daily precipitation, which does not affect κ_{COB} . This reflects previous observations which showed that 47% of E_{COB} takes place on days without precipitation, compared to 13% for concrete slabs. Therefore, κ_{COB} does not depend on precipitation events as strongly.

Correlation matrix for hourly data

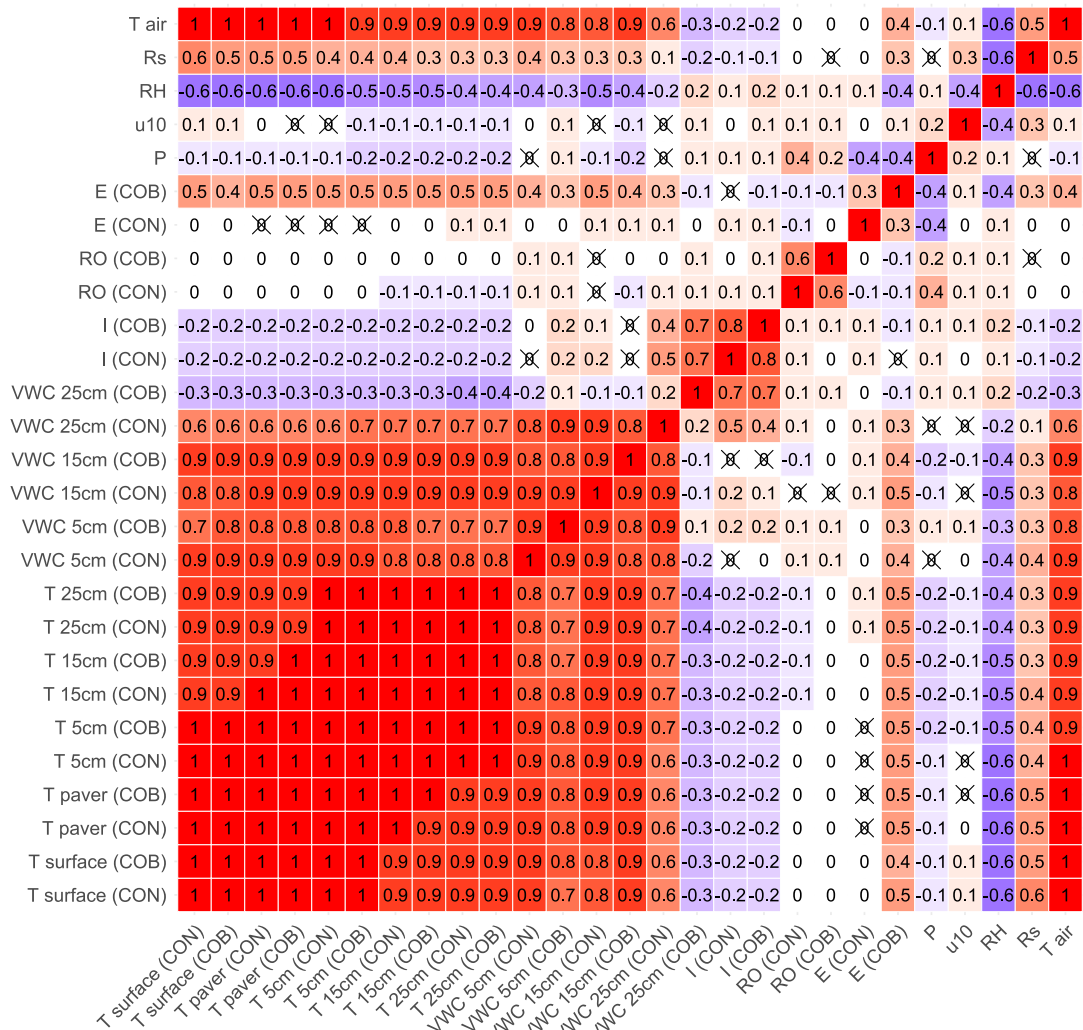


Figure 4.16: Correlation matrix for hourly data (Spearman correlation). All data measured at lysimeter site, P as mean of the two lysimeters. Non-significant values are crossed out

Correlation matrix for daily data

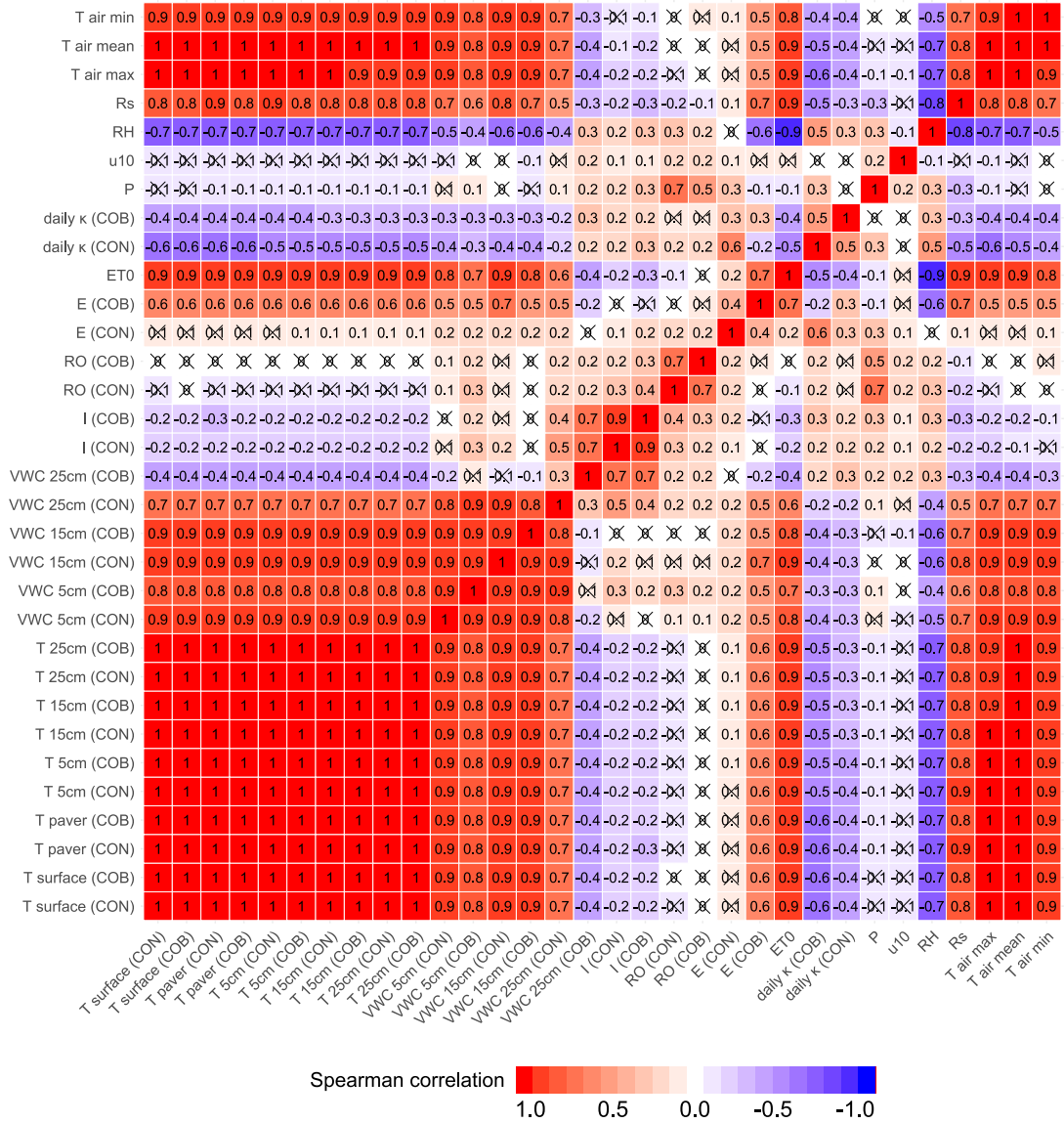


Figure 4.17: Correlation matrix for daily data (Spearman correlation). All data measured at lysimeter site, P as mean of the two lysimeters. Additional data: ET_0 = grass-reference evapotranspiration after Penman-Monteith (Allen et al., 1998; ASCE-EWRI, 2005), κ = relationship between daily measured E and calculated daily ET_0 with $\kappa = \frac{E}{ET_0}$. Non-significant values are crossed out

5 Estimating evaporation of paved surfaces

As shown in the previous chapter, evaporation (E) processes have a cooling effect. Paved surfaces react differently, depending on paver material and sealing degree, leading to varying heat storage capacities and evaporation potentials. Evaporation takes place on wet and dry days. For dry days, evaporation originates mostly from underlying soil layers. On wet days, the surface storage of the paving material and the intensity of precipitation play key roles. Given the function of evapo(transpi)ration ($E(T)$) as heat sink and its potential for countering the Urban Heat Island (UHI) effect, it is essential to assess how different vegetated and paved surfaces impact urban areas. Because of its application in agriculture, evapotranspiration (ET) has been studied for several decades with numerous estimation models and measurements. As Schrödter (1985) points out, estimating actual evaporation is a significant challenge, as it is the result of numerous interdependent physical processes. For vegetated surfaces, there are many models to estimate ET . Combined with a crop coefficient, grass-reference evapotranspiration (ET_0) is used as a standardised model. It has also been used together with a reduction coefficient to estimate evaporation from paved surfaces (Mansell and Wang, 2010; Wessolek et al., 2008). In this chapter, the usage of ET_0 for estimating E from paved surfaces is discussed.

5.1 Grass-reference evapotranspiration ET_0

A commonly used method for evapotranspiration estimations is the physically based FAO Penman-Monteith grass-reference evapotranspiration, which offers high accuracy for various locations (ASCE-EWRI, 2005; Azhar and Perera, 2011; Nandagiri and Kovoov, 2006; Razei and Pereira, 2013; Yoder et al., 2005). It uses the grass reference crop, a hypothetical crop with a uniform height of 0.12 m, an albedo of 0.23 and a surface resistance of 70 s m^{-1} , which is based on the characteristics of extensive grass surface (Allen et al., 1998). It assumes vegetation cover throughout the year with an optimal water supply through capillary rise (ASCE-EWRI, 2005).

The general formula for calculating ET_0 is (ASCE-EWRI, 2005):

$$ET_0 = \frac{0.408 \Delta (R_n - G) + \gamma \frac{C_n}{T_{air} + 273} u_2 (e_s - e_a)}{\Delta + \gamma (1 + C_d u_2)} \quad (5.1)$$

where

ET_0	Standardized reference evapotranspiration [mm d^{-1}]
Δ	Slope of saturation vapour pressure-temperature curve [$\text{kPa } ^\circ\text{C}^{-1}$]
R_n	Net radiation at crop surface [$\text{MJ m}^{-2} \text{d}^{-1}$]
G	Soil heat flux density at soil surface [$\text{MJ m}^{-2} \text{d}^{-1}$]
γ	Psychrometric constant [$\text{kPa } ^\circ\text{C}^{-1}$]
C_n	Constant changing with calculation time step and crop [$\text{K mm s}^3 \text{Mg}^{-1} \text{d}^{-1}$]
T_{air}	Mean daily or hourly air temperature at 1.5 to 2.5 m height [$^\circ\text{C}$]
u_2	Mean daily or hourly wind speed at 2 m height [m s^{-1}]
e_s	Saturation vapour pressure at 1.5 to 2.5 m height [kPa]
e_a	Mean actual vapour pressure at 1.5 to 2.5 m height [kPa]
C_d	Constant changing with calculation time step and reference crop [s m^{-1}].

The 0.408 coefficient is a conversion factor for radiation to gain equivalent evaporation [mm d^{-1}] from [$\text{MJ m}^{-2} \text{d}^{-1}$] and its units are [$\text{m}^2 \text{mm MJ}^{-1}$].

Detailed description of computation can be found in the ASCE-EWRI Task Committee Report and its appendices (ASCE-EWRI, 2005).

The climate station at the lysimeter site Berlin-Marienfelde offers all required input data to compute ET_0 . For three days for which lysimeter measurements were obtained, the climate station did not provide data. For these days, data from the nearby DWD climate station at Berlin-Tempelhof (DWD, 2018b) has been used to compute ET_0 . For the 333 days with lysimeter results, the FAO Penman-Monteith grass-reference evapotranspiration results in $ET_0 = 643 \text{mm}$. This value is used as reference in the following considerations.

5.2 Relationship between E and ET_0 for paved surfaces

ET_0 is based on a hypothetical surface with hypothetical conditions. Hence, it is a representation of the atmospheric potential for evaporation for a specific surface cover. Consequently, it differs from actual evaporation, even for surfaces that closely resemble the hypothetical grass vegetation. For vegetated surfaces, crop coefficients are used to derive ET of different surfaces from ET_0 . This crop coefficient differs throughout the year as vegetation develops (Allen et al., 1998). Additionally, water supply is seldom as optimal as assumed for ET_0 . Hence, water availability as to be considered when estimating $E(T)$ (Allen et al., 1998; Schrödter, 1985). For pavements, surface properties remain the same throughout the year. However, water availability remains a key factor for estimating E . In the following sections, one model for estimating annual E and

possibilities for a higher temporal resolution are introduced.

5.2.1 TUBGR model

For urban areas, the TUBGR model (Wessolek et al., 2008) can be used to estimate the annual hydrological balance based on precipitation and ET_0 . Depending on the sealing degree (SD), different empirical coefficients (table 5.1) have been determined using data from other lysimeter studies (Wessolek and Facklam, 1997; Flöter, 2006). The focus of this chapter is evaporation. For calculation of infiltration and runoff according to this model, the reader is advised to refer to publications of this model (Wessolek et al., 2008; Wessolek, Kaupenjohann and Renger, 2009).

The TUBGR formula for estimating annual evaporation is:

$$E = \kappa \times ET_0 \quad (5.2)$$

with

$$\kappa = \left(\frac{\log(0.6 \times \beta_s \times P_s)}{\log(ET_0)} \right)^4 \quad (5.3)$$

where

E	Evaporation from paved surface [mm a^{-1}]
κ	Reduction coefficient [-]
ET_0	Grass-reference evapotranspiration [mm a^{-1}]
β_s	Summer infiltration coefficient [-]
P_s	Precipitation in summer (April to September) [mm a^{-1}].

It uses ET_0 and introduces a term reflecting water availability based on net precipitation (precipitation minus runoff and infiltration losses). The model has been tested with the data from the two paved lysimeters. For this, mean values of both lysimeters have been used for precipitation. ET_0 was calculated for days with lysimeter data as described in the previous section. Results for all four sealing degrees can be found in table 5.2. Comparing these results to the measured hydrological balance (table 4.2) shows that the annual actual evaporation has a very good fit between model and measurement for the two paved surfaces studied. According to the TUBGR model, cobblestones should have evaporated 141 mm, which corresponds to the measured 140.55 mm. For concrete slabs, there was a small overestimation by about 7% with 99 mm (model) compared to 92.24 mm (lysimeter). While annual evaporation was estimated accurately, the distribution of the remaining water between runoff and infiltration is off. Runoff was significantly overestimated for both surfaces, being 2.5 (concrete slabs) to 6.6 (cobblestones) as high as measured runoff. Contrary to that, infiltration is underestimated. Cobblestones were estimated to infiltrate 188 mm and actually infiltrated 252 mm. The discrepancy is higher for concrete slabs, an estimation of 131 mm compared to measured 258 mm.

Sealing degree	Examples	β_s^\dagger	β_w^\dagger
Class I (low: < 10%)	Grass pavers	0.90	0.95
Class II (medium: 10 – 50%)	Cobblestones	0.80	0.85
Class III (high: 50 – 90%)	Concrete slabs	0.55	0.60
Class IV (severe: > 90%)	Asphalt	0.20	0.25

[†] infiltration coefficient for summer (β_s) and winter (β_w)

Table 5.1: TUBGR model coefficients for paved surfaces (Wessolek et al., 2008)

Sealing degree	Examples	κ	E	RO	I
		[-]	[mm a ⁻¹]	[mm]	[mm a ⁻¹]
Class I (low: < 10%)	Grass pavers	0.24	156	29	213
Class II (medium: 10 – 50%)	Cobblestones	0.22	141	68	188
Class III (high: 50 – 90%)	Concrete slabs	0.15	99	168	131
Class IV (severe: > 90%)	Asphalt	0.05	31	307	59

Table 5.2: Annual hydrological balance estimated for paved surfaces by TUBGR model

In reality both paved surfaces yielded very similar infiltration amounts, yet the model resulted in a rather large difference between the two. It should be noted however, that this comparison between measured and estimated values is not sufficient to evaluate the model. Given annual and seasonal changes in precipitation patterns and other climatological factors, measurement of one year resulting in one data point per paved surface type can be an indicator but not enough to confirm or calibrate a model. However, estimation of annual E is independent of the calculation of RO and I , and therefore, can be considered separately.

Running the TUBGR model for the same time period, the same climate and the same soil type results in evapotranspiration sums of 351 mm (arable land), 321 mm (grassland) and 444 mm (deciduous forest).

5.2.2 Determining the ratio between E and ET_0

In the TUBGR model, the reduction coefficient κ is used to derive annual E from annual ET_0 and summer P . Based on equation 5.2, with measurements of E_{COB} and E_{CON} combined with estimated ET_0 , κ can be calculated from the available data with:

$$\kappa = \frac{E}{ET_0} \quad (5.4)$$

where

- κ Reduction coefficient [-]
- E Evaporation from paved surface [mm a⁻¹]
- ET_0 Grass-reference evapotranspiration [mm a⁻¹].

Relationship evaporation to grass-reference evapotranspiration

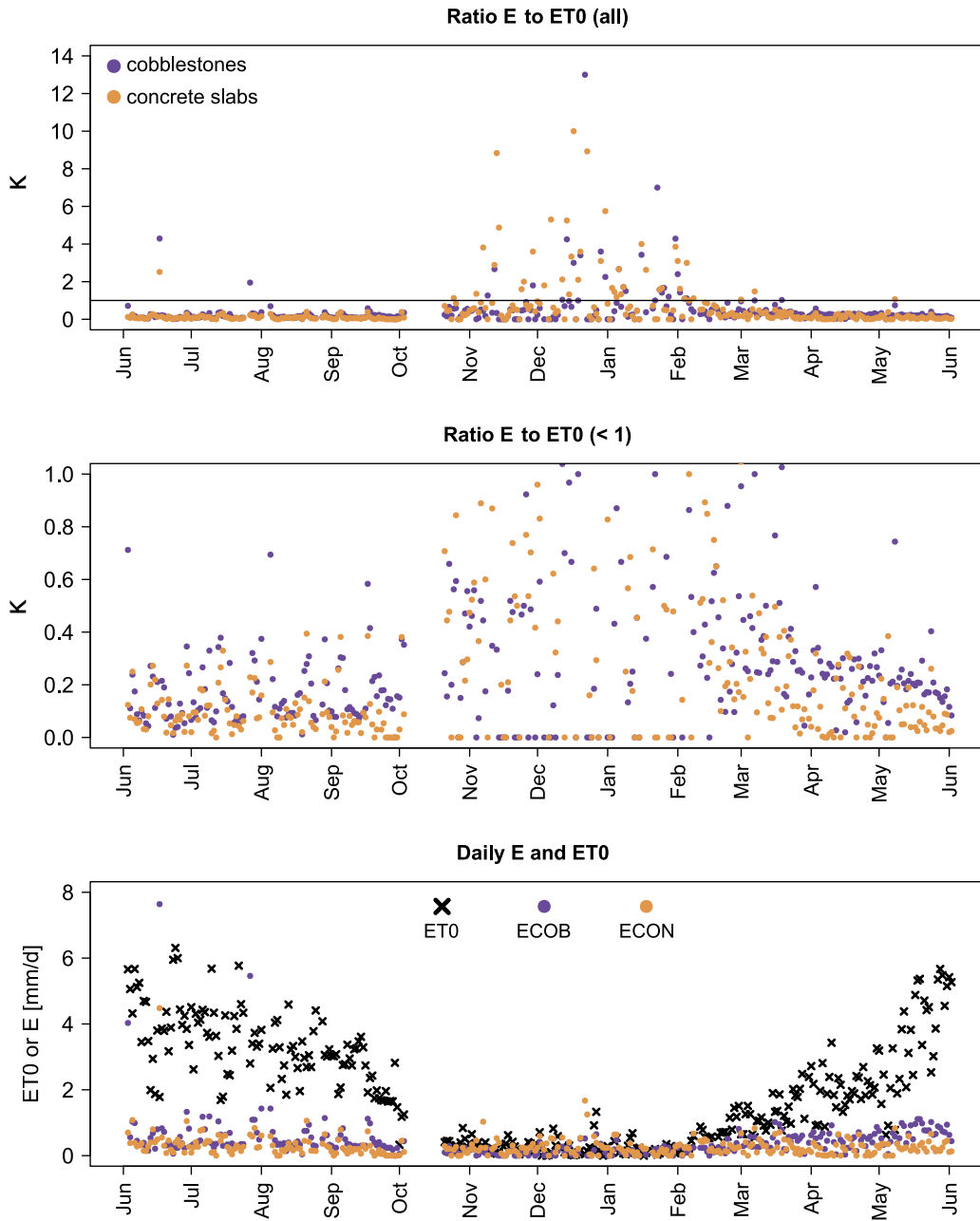


Figure 5.1: Relationship between daily evaporation (E) from paved surfaces and grass-reference evapotranspiration (ET_0)

Calculating κ on a daily basis (ratio daily E and daily ET_0) results in varying values. Figure 5.1 illustrates daily values of κ for both paved surfaces, as well as absolute amounts of daily measured E and calculated ET_0 . Since it is the ratio, values of $\kappa < 1$ indicate a reduced E compared to ET_0 and $\kappa > 1$ means that the paved surfaces evaporated more than a grass surface with optimal water supply. As can be seen, there are some days for which $E > ET_0$. One case is in mid June 2016, which is the day with highest recorded

evaporation from the surfaces, corresponding to figure 4.5. Otherwise, $\kappa > 1$ occurs in winter, mostly between November and February. As the bottom plot illustrates, this is the time for which ET_0 and E_{COB} are low in general, so that even a high κ results in small differences when calculating amounts of E . For concrete slabs, E is more or less stable throughout the year and monthly E_{CON} between November and February can even exceed that of months with high ET_0 (see also table 4.2). For example, E_{CON} reaches its third highest value in December. As shown in figure 4.17, daily κ is weakly to moderately correlated to climatological conditions (RH, Rs, T_{air}) and only κ_{CON} shows a relationship to daily precipitation. However, it does not correlate strongly with a single easily measured variable. A look at median values of daily κ over annual, seasonal, and monthly periods (table A.4) yields insights into general trends. Annual mean values of κ based on measurements are very similar to the annual κ estimated by the TUBGR model. For cobblestones, both methods yield an annual κ_{COB} of 0.22 and concrete slabs differed slightly with $\kappa_{CON} = 0.12$ (measured) compared to 0.15 (TUBGR). However, this annual κ_{CON} as the median of daily κ would lead to an underestimation of E_{CON} . As previously shown, E_{COB} can be attributed to nearly 50% to dry days, with upward water transport providing water to evaporate. Concrete slabs are more dependent on rainfall events and their intensities, as their main evaporative potential stems from water stored in the porous pavers. This is reflected when differentiating between wet and dry days. Table A.4 also contains the median values of daily κ values separated into dry (κ_d) and wet (κ_w) days. While there is very little difference for cobblestones, κ_w is significantly larger than κ_d for concrete slabs. This effect is especially noticeable in summer months. It should be noted that some of the monthly values of κ , especially when separating κ_d and κ_w are based on few data points. Applying these monthly values to obtain daily E_{COB} and E_{CON} did not yield satisfactory results.

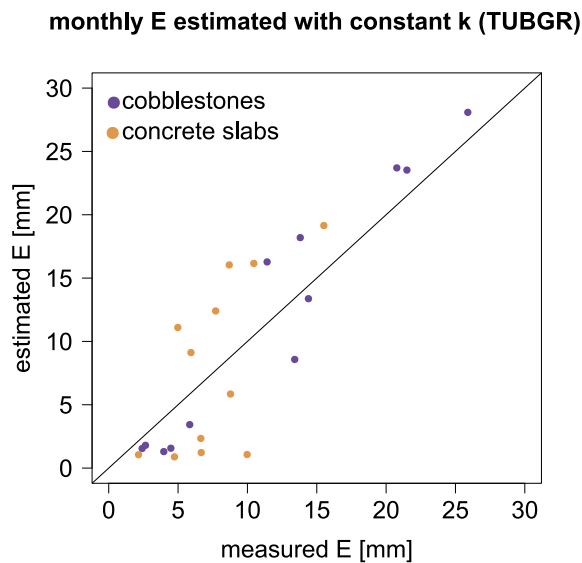


Figure 5.2: Monthly estimation of E with annual constant κ of TUBGR model compared to measured E

So far, the TUBGR model offers good estimation of annual E_{COB} and E_{CON} . Figure 5.2 shows monthly estimations of E when using the constant annual κ estimated by the TUBGR model (equation 5.3) compared to measured values of monthly E . As can be seen, the fit is better for E_{COB} , where the monthly κ do not differ as much and for which wet and dry conditions lead to similar amounts of evaporation. Still, months with small amounts of E tend to be underestimated while those with high E are slightly overestimated. This pattern is the same for concrete slabs, combined with an overall poor fit. Monthly values of measured and estimated E as well as ET_0 can be found in table 5.3. This result is to be expected, as the κ from the TUBGR model is intended for annual estimations, based on ET_0 and P over longer periods.

On a monthly scale, κ (here: ratio monthly E and monthly ET_0) for both surfaces showed moderate to strong correlation with monthly mean T_{air} . Other correlations were tested for deriving κ , including single or combined variables of T_{air} , P , RH , Rs , ET_0 . In the end, the best fit was achieved using monthly mean T_{air} . This relationship is not linear but can be approximated using an exponential function, with higher values of κ for lower temperatures (figure 5.3). The relationship is stronger for cobblestones with rather high deviations for concrete slabs.

Using the results of the non-linear regression, monthly values of κ can be estimated with:

$$\kappa = a \times 0.9^{T_{air}} \quad (5.5)$$

- κ Monthly reduction coefficient[-]
- a Surface type specific constant: 0.6 (COB) or 0.9 (CON)
- T_{air} Monthly mean air temperature at 2 m height [°C].

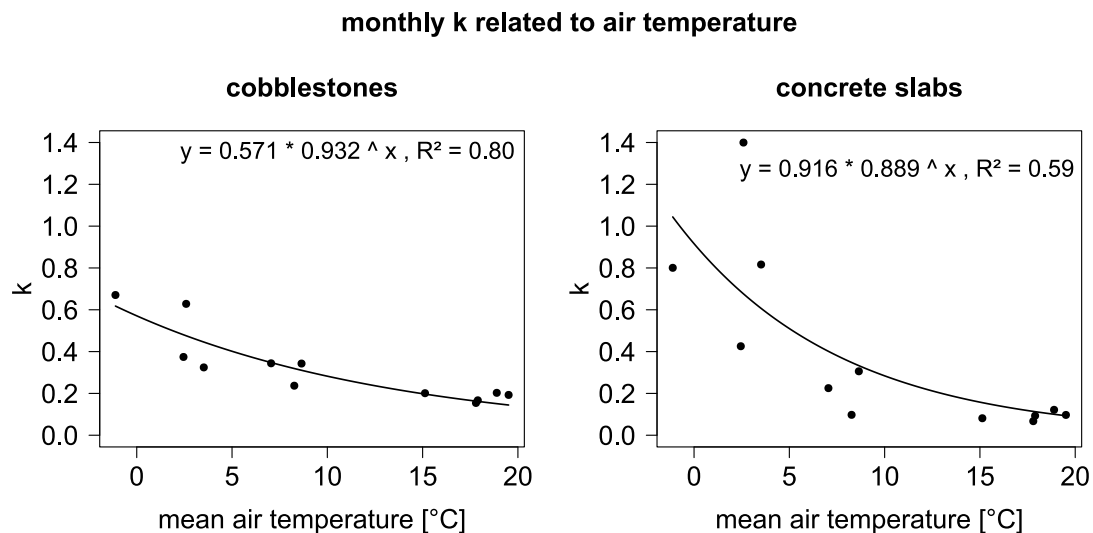


Figure 5.3: Deriving measured monthly reduction coefficient κ from monthly mean T_{air}

Using these monthly values of κ derived from T_{air} , monthly E is estimated. Figure 5.4 compares the fit of estimated and measured E for constant κ (TUBGR model) and monthly κ (derived from T_{air}). Corresponding monthly values and annual sums can be found in table 5.3. For cobblestones, estimating E with κ_{COB} derived from T_{air} generally improves the fit. However, for three months there is a large deviation, leading to an underestimation of annual E_{COB} . Two of these month are June and July, when evaporation potential of the surfaces was high, with the highest daily and hourly evaporation event recorded in June. For concrete slabs, the relationship between κ and T_{air} was weaker, which is conveyed to estimating monthly E_{CON} using these κ_{CON} values. Both, constant and monthly κ did not yield satisfying results on a monthly scale. Using the derived monthly κ improves the fit for months with low E_{CON} , yet leads to some significant overestimations for months with high values, leading to a significant overestimation on an annual scale. For April, this overestimation is especially high with estimated 21.15 mm compared to measured 5.93 mm, which could be caused by long dry periods and transitioning climatological conditions, as reflected in figure 5.1. The fit for concrete slabs could potentially be improved by separating κ_d and κ_w . For this, daily values would be needed as basis. Figure A.2 shows the median values of daily κ_d and κ_w for each month related to monthly mean values of T_{air} (only months with at least 10 days classified as dry or wet were considered). For concrete slabs, this results in a better fit than combined κ , especially for wet days. Applying these monthly values of κ_d and κ_w to daily values of ET_0 improves the fit for concrete slabs slightly compared to using the combined monthly κ as in figure 5.4. While some months still have high deviations, the sum of E_{CON} using monthly values of κ_d and κ_w derived from T_{air} is 96.5 mm, which is close to the measured sum of 92.24 mm.

	ET_0	Cobblestones			Concrete slabs			
		Lys	TUBGR	with κ_T	Lys	TUBGR	with κ_T	with $\kappa_{w,d}$
Jan	5.92	3.97	1.30	3.66	4.74	0.89	6.18	4.33
Feb	15.6	5.84	3.43	7.50	6.64	2.34	10.72	7.90
Mar	38.98	13.14	8.58	13.55	8.78	5.85	15.64	12.12
Apr	60.79	14.40	13.37	19.39	5.93	9.12	21.15	16.44
May	106.94	21.50	23.53	21.04	8.69	16.04	16.67	13.05
Jun	127.66	25.89	28.09	19.28	15.51	19.15	12.80	10.99
Jul	107.72	20.77	18.19	15.57	10.46	16.16	10.04	8.75
Aug	82.70	13.81	18.19	13.39	7.71	12.41	9.32	7.60
Sep	73.98	11.42	16.28	12.06	4.98	11.10	8.43	6.29
Oct	7.03	2.41	1.55	2.18	2.51	1.05	2.34	1.86
Nov	8.17	2.65	1.80	3.64	6.67	1.23	4.96	3.69
Dec	7.13	4.48	1.57	3.39	9.98	1.07	4.82	3.48
Sum	642.62	140.55	141.38	134.65	92.24	96.39	123.08	96.50

Table 5.3: Monthly and annual estimated E_{COB} and E_{CON} based on ET_0 . Lys = measured E , TUBGR = E estimated using constant κ for each month as derived from annual TUBGR model, κ_T = E estimated using monthly κ derived from monthly T_{air} , $\kappa_{w,d}$ = E estimated using monthly median κ_w and κ_d derived from monthly T_{air} applied to daily data depending on wet or dry conditions

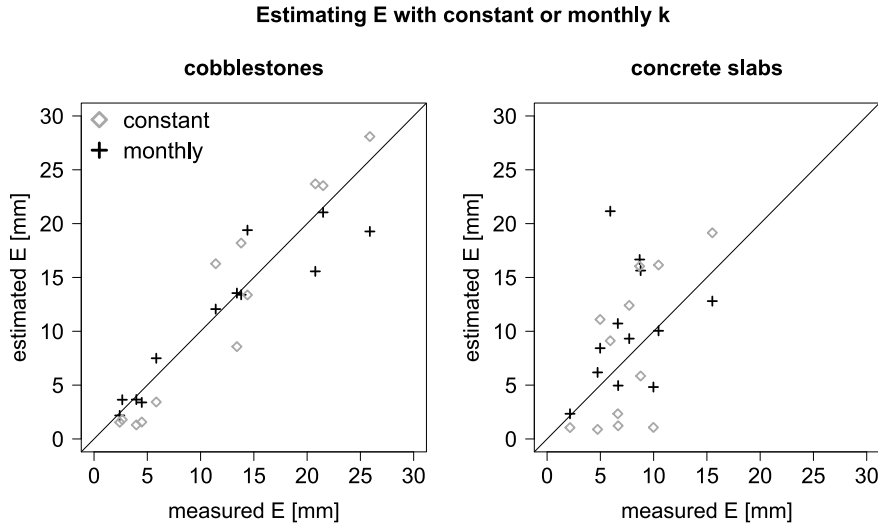


Figure 5.4: Comparison of monthly estimations of E compared to measured E , with annual constant κ of TUBGR model and monthly κ derived from T_{air}

5.2.3 Outlook

For annual estimations, the TUBGR model has yielded very good results in this study as well as previous ones. Overall, monthly E from cobblestones and concrete slabs proved difficult to estimate using ET_0 . For practice, it could be useful to make a general differentiation between summer and winter conditions. In that case, the usage of the seasonal values of κ determined from daily measurements (table A.4) would be feasible. For cobblestones, these are $\kappa = 0.16$ (summer) and $\kappa = 0.30$ (winter). In case of concrete slabs, the seasonal values are $\kappa = 0.08$ (summer) and $\kappa = 0.34$ (winter). If monthly reduction coefficients are required, they may be derived from mean T_{air} . This method seems promising but would require additional data sets of monthly ET_0 , E , and T_{air} , ideally originating from different climate zones. With this additional data, a more universal equation for deriving monthly κ values could be developed. This would be valuable, as the usage of ET_0 includes atmospheric conditions at different sites and deriving κ from T_{air} rather than assigning fixed monthly values would further enable its potential application at different sites. For concrete slabs, water storage on the surface plays an important role, so that a differentiation between wet and dry days could be promising. This would again require data of ET_0 , E , and T_{air} , as well as P , but on a daily basis. Since the available data from this study is limited, the analysis, ideas, and methods presented in this chapter should be seen as conceptual approaches that might contribute to the collective development of an estimation model for evaporation from paved surfaces on an improved temporal scale. Compared to the grass-reference evapotranspiration model, which is the result of decades of research and numerous lysimeter studies providing calibration data, the development of a robust model for paved surfaces is still at its beginning.

6 Conclusion

Paved surfaces are a key element of urban areas. The modified soil-atmosphere interface alters the urban hydrological balance and can lead to significant challenges. With a focus on stormwater management, most existing hydrological models treat all paving materials as the same and assume little or no infiltration and evaporation losses. Few studies providing measurements of the hydrological balance and water transport processes of pavements have been published in the past. They show that the impact of different paving materials varies considerably, and even severe sealing with asphalt exhibited in infiltration and evaporation processes.

In this study, two common pavement types (cobblestones and concrete slabs) were researched. The combination of weighable lysimeters and sensors to measure soil water content and temperature provided insights into their hydrological balance, as well as water and heat transport processes, at a high temporal-resolution. Over the measurement period of one year, the surfaces led to similar infiltration and differed in evaporation and runoff production. Cobblestones, which are characterised by large joint areas, evaporated 25 % and rarely produced runoff (3 %). Concrete slabs, which represent a higher degree of sealing with narrow joint areas, tended to produce more runoff (16 %) and less evaporation (22 %). Both surfaces reacted differently depending on seasonal conditions. Evaporation processes did not occur exclusively on days for which precipitation provided water. Upward water transport from underlying soil layers led to evaporation processes during dry periods. This effect contributed 47 % of evaporation for cobblestones and 13 % for concrete slabs. Previous descriptions of pavements acting as evaporation barrier were not supported by the results. Both surfaces led to increased heat storage in the soil compared to natural surfaces, with concrete slabs tending to slightly higher temperatures. Thermal and water transport processes are closely linked. Compared to cobblestones, evaporation from concrete slabs surfaces relies more on water supply from precipitation events.

Estimating evaporation of paved surfaces by reducing the common parameter of grass-reference evapotranspiration produced mixed results. For annual estimations, the pre-existing TUBGR model provided a good fit. On a higher temporal resolution, the reduction coefficient changes depending on month or season. For concrete slabs, a distinction between wet and dry conditions should be made. Monthly coefficients might be derived from air temperature. The presented modelling ideas and approaches did not yield satisfying results for monthly evaporation estimations.

Overall, it could be shown that pavements, as the urban soil-atmosphere interface,

are highly active systems determining the urban hydrological balance. They are more than runoff generators. Upward water transport is essential when assessing evaporation from pavements. Varying types of paving material and degree of surface cover lead to different impacts on heat and water transport. Understanding and utilising these differences has the potential to improve the design of urban areas.

Bibliography

- Allen, R. G., Pereira, L. S., Raes, D. and Smith, M. (1998), ‘Crop evapotranspiration (guidelines for computing crop water requirements)’, FAO Irrigation and Drainage Paper No. 56. URL: <http://www.kimberly.uidaho.edu/water/fao56/fao56.pdf>, last accessed 2018-06-16.
- Allen, R., Smith, M., Perrier, A. and Pereira, L. (1994), ‘An update of reference evapotranspiration’, *ICID Bulletin*, 43(2), 1–34.
- Andersen, C. T., Foster, I. D. L. and Pratt, C. J. (1999), ‘The role of urban surfaces (permeable pavements) in regulating drainage and evaporation: development of a laboratory simulation experiment’, *Hydrological Processes*, 13(4), 597–609. doi: 10.1002/(sici)1099-1085(199903)13:4<597::aid-hyp756>3.0.co;2-q.
- Angrill, S., Petit-Boix, A., Morales-Pinzón, T., Josa, A., Rieradevall, J. and Gabarrell, X. (2017), ‘Urban rainwater runoff quantity and quality – a potential endogenous resource in cities?’, *Journal of Environmental Management*, 189, 14–21. doi: 10.1016/j.jenvman.2016.12.027.
- ASCE-EWRI (2005), The ASCE standardized reference evapotranspiration equation, Technical report, American Society of Civil Engineers, Environmental & Water Resource Institute. URL: <https://www.kimberly.uidaho.edu/water/asceewri/ascestdetmain2005.pdf>, last accessed 2014-10-10.
- Azhar, A. H. and Perera, B. J. C. (2011), ‘Evaluation of Reference Evapotranspiration Estimation Methods under Southeast Australian Conditions’, *Journal of Irrigation and Drainage Engineering*, 137(5), 268–279. doi: 10.1061/(asce)ir.1943-4774.0000297.
- Bach, P. M., Rauch, W., Mikkelsen, P. S., Mccarthy, D. T. and Deletic, A. (2014), ‘A critical review of integrated urban water modelling – Urban drainage and beyond’, *Environmental Modelling & Software*, 54, 88–107. doi: 10.1016/j.envsoft.2013.12.018.
- Bachmann, J. and van der Ploeg, R. R. (2002), ‘A review on recent developments in soil water retention theory: interfacial tension and temperature effects’, *Journal of Plant Nutrition and Soil Science*, 165(4), 468. doi: 10.1002/1522-2624(200208)165:4<468::AID-JPLN468>3.0.CO;2-G.
- Berlekamp, L. (1987), ‘Bodenversiegelung als Faktor der Grundwasserneubildung (Soil sealing as factor of groundwater recharge)’, *Landschaft + Stadt*, 19(3), 129–136.

- Berthier, E., Dupont, S., Mestayer, P. and Andrieu, H. (2006), ‘Comparison of two evapotranspiration schemes on a sub-urban site’, *Journal of Hydrology*, 328(3-4), 635–646. doi: 10.1016/j.jhydrol.2006.01.007.
- Bhaduri, B., Minner, M., Tatalovich, S. and Harbor, J. (2001), ‘Long-Term Hydrologic Impact of Urbanization: A Tale of Two Models’, *Journal of Water Resources Planning and Management*, 127(1), 13–19. doi: 10.1061/(asce)0733-9496(2001)127:1(13).
- Bonicelli, A., Giustozzi, F. and Crispino, M. (2015), ‘Experimental study on the effects of fine sand addition on differentially compacted pervious concrete’, *Construction and Building Materials*, 91, 102–110. doi: 10.1016/j.conbuildmat.2015.05.012.
- Booth, D. B. and Leavitt, J. (1999), ‘Field Evaluation of Permeable Pavement Systems for Improved Stormwater Management’, *Journal of the American Planning Association*, 65(3), 314–325. doi: 10.1080/01944369908976060.
- Brattebo, B. O. and Booth, D. B. (2003), ‘Long-term stormwater quantity and quality performance of permeable pavement systems’, *Water Research*, 37(18), 4369–4376. doi: 10.1016/s0043-1354(03)00410-x.
- Brewer, C., Harrower, M., Sheesley, B., Woodruff, A. and Heyman, D. (2013), ‘Color Brewer 2.0 – color advice for cartography’. URL: <http://colorbrewer2.org/>, last accessed 2017-06-01.
- Bricker, S., Banks, V., Galik, G., Tapete, D. and Jones, R. (2017), ‘Accounting for groundwater in future city visions’, *Land Use Policy*, 69, 618–630. doi: 10.1016/j.landusepol.2017.09.018.
- Carbone, M., Mancuso, A. and Piro, P. (2014), ‘Porous Pavement Quality Modelling’, *Procedia Engineering*, 89, 758–766. doi: 10.1016/j.proeng.2014.11.504.
- Chatzidimitriou, A. and Yannas, S. (2015), ‘Microclimate development in open urban spaces: The influence of form and materials’, *Energy and Buildings*, 108, 156–174. doi: 10.1016/j.enbuild.2015.08.048.
- Chen, J., Theller, L., Gitau, M. W., Engel, B. A. and Harbor, J. M. (2017), ‘Urbanization impacts on surface runoff of the contiguous United States’, *Journal of Environmental Management*, 187, 470–481. doi: 10.1016/j.jenvman.2016.11.017.
- Chiang, Y., Sullivan, W. and Larsen, L. (2017), ‘Measuring Neighborhood Walkable Environments: A Comparison of Three Approaches’, *International Journal of Environmental Research and Public Health*, 14(6), 593. doi: 10.3390/ijerph14060593.
- Corazza, M. V., Mascio, P. D. and Moretti, L. (2016), ‘Managing sidewalk pavement maintenance: A case study to increase pedestrian safety’, *Journal of Traffic and Transportation Engineering (English Edition)*, 3(3), 203–214. doi: 10.1016/j.jtte.2016.04.001.

- Daniel, M., Lemonsu, A. and Viguié, V. (2018), ‘Role of watering practices in large-scale urban planning strategies to face the heat-wave risk in future climate’, *Urban Climate*, 23, 287–308. doi: 10.1016/j.uclim.2016.11.001.
- Delleur, J. W. (2003), ‘The Evolution of Urban Hydrology: Past, Present, and Future’, *Journal of Hydraulic Engineering*, 129(8), 563–573. doi: 10.1061/(asce)0733-9429(2003)129:8(563).
- Diestel, H. and Schmidt, M. (2001), Untersuchungen an der Lysimeteranlage zur Ermittlung von Versickerungs- und Oberflächenabfluß für unterschiedliche Gehwegbefestigungen (Investigations using lysimeters to determine infiltration and runoff of different pavements). Unpublished Research Report for the water works of Berlin, executed by Technical University Berlin, Berlin - Germany, Department of Architecture, Environment and Society, Institute Landscape and Environmental Planning.
- Dirckx, G., Daele, S. V. and Hellinck, N. (2016), ‘Groundwater Infiltration Potential (GWIP) as an aid to determining the cause of dilution of waste water’, *Journal of Hydrology*, 542, 474–486. doi: 10.1016/j.jhydrol.2016.09.020.
- Dowle, M. and Srinivasan, A. (2017), *data.table: Extension of ‘data.frame’*. URL: <https://CRAN.R-project.org/package=data.table>, last accessed 2018-06-10.
- Dreelin, E. A., Fowler, L. and Carroll, C. R. (2006), ‘A test of porous pavement effectiveness on clay soils during natural storm events’, *Water Research*, 40(4), 799–805. doi: 10.1016/j.watres.2005.12.002.
- Dupont, S., Mestayer, P. G., Guilloteau, E., Berthier, E. and Andrieu, H. (2006), ‘Parameterization of the Urban Water Budget with the Submesoscale Soil Model’, *Journal of Applied Meteorology and Climatology*, 45(4), 624–648. doi: 10.1175/jam2363.1.
- DVWK (1996), Ermittlung der Verdunstung von Land- und Wasserflächen (Determination of evaporation from land and water surfaces), DVWK-Merkblatt (DVWK-Bulletin) 238/1996, Deutscher Verband für Wasserwirtschaft und Kulturbau e.V.
- DWD (2018a), ‘Globalstrahlung in der Bundesrepublik Deutschland. Mittlere Jahressummen, Zeitraum: 1981–2010 (Global radiation in the Federal Republic of Germany, average annual sum, period 1981–2010)’. URL: https://www.dwd.de/DE/leistungen/solarenergie/lstrahlungskarten_mi.html?nn=16102, last accessed 2018-06-08.
- DWD (2018b), ‘Klimadaten Deutschland – Monats- und Tageswerte (Archiv) (Climate data for Germany – monthly and daily data (archive))’. URL: <https://www.dwd.de/DE/leistungen/klimadatendeutschland/klarchivtagmonat.html?nn=16102>, last accessed 2018-06-08.

- DWD (2018c), ‘Klimadaten Deutschland - Stundenwerte (Archiv) (Climate data for Germany – hourly data (archive))’. URL: <https://www.dwd.de/DE/leistungen/klimadatendeutschland/klarchivstunden.html?nn=16102>, last accessed 2018-06-08.
- DWD (2018d), ‘Vieljährige Mittelwerte (Long-term mean values)’. URL: https://www.dwd.de/DE/leistungen/klimadatendeutschland/vielj_mittelwerte.html, last accessed 2018-06-08.
- DWD (2018e), ‘Wetterlexikon – Niederschlagsintensität (Weather Encyclopedia – Precipitation intensities)’. URL: <https://www.dwd.de/DE/service/lexikon/Functions/glossar.html;jsessionid=4B114C00C68DCF3517F3329C67D52136.live21074?lv2=101812&lv3=101906>, last accessed 2018-03-28.
- EC (2012), ‘Soil sealing’, Science for Environment Policy, DG Environment News Alert Service. In-depth report, URL: http://ec.europa.eu/environment/soil/pdf/guidelines/pub/soil_en.pdf, last accessed 2015-11-10.
- Eckley, C. S. and Branfireun, B. (2009), ‘Simulated rain events on an urban roadway to understand the dynamics of mercury mobilization in stormwater runoff’, *Water Research*, 43(15), 3635–3646. doi: 10.1016/j.watres.2009.05.022.
- Fletcher, T., Andrieu, H. and Hamel, P. (2013), ‘Understanding, management and modelling of urban hydrology and its consequences for receiving waters: A state of the art’, *Advances in Water Resources*, 51, 261–279. doi: 10.1016/j.advwatres.2012.09.001.
- Flöter, O. (2006), Wasserhaushalt gepflasterter Straßen und Gehwege. Lysimeterversuche an drei Aufbauten unter praxisnahen Bedingungen unter Hamburger Klima (Water balance of roads and sidewalks. Lysimeter experiments for three surfaces under realistic conditions with Hamburg climate)., in ‘Hamburger Bodenkundliche Arbeiten’, Vol. 58.
- Forghani, M. and Delavar, M. (2014), ‘A Quality Study of the OpenStreetMap Dataset for Tehran’, *ISPRS International Journal of Geo-Information*, 3(2), 750–763. doi: 10.3390/ijgi3020750.
- Fukahori, K. and Kubota, Y. (2003), ‘The role of design elements on the cost-effectiveness of streetscape improvement’, *Landscape and Urban Planning*, 63(2), 75–91. doi: 10.1016/s0169-2046(02)00180-9.
- Garcia, A., Hassn, A., Chiarelli, A. and Dawson, A. (2015), ‘Multivariable analysis of potential evaporation from moist asphalt mixture’, *Construction and Building Materials*, 98, 80–88. doi: 10.1016/j.conbuildmat.2015.08.061.
- García, L., Barreiro-Gomez, J., Escobar, E., Téllez, D., Quijano, N. and Ocampo-Martinez, C. (2015), ‘Modeling and real-time control of urban drainage

- systems: A review', *Advances in Water Resources*, 85, 120–132. doi: 10.1016/j.advwatres.2015.08.007.
- García, P. and Pérez, E. (2016), 'Mapping of soil sealing by vegetation indexes and built-up index: A case study in Madrid (Spain)', *Geoderma*, 268, 100–107. doi: 10.1016/j.geoderma.2016.01.012.
- Göbel, P., Coldewey, W., Dierkes, C., Kories, H., Meßer, J. and Meißner, E. (2007), 'Einfluss von Gründächern und Regenwassernutzungen auf Wasserhaushalt und Grundwasserstand in Siedlungen (Effect of green roofs and usage of rainwater on the water balance and groundwater level of residential areas)', *Grundwasser*, 12(3), 189–200. doi: 10.1007/s00767-007-0032-y.
- Göbel, P., Dierkes, C. and Coldewey, W. (2007), 'Storm water runoff concentration matrix for urban areas', *Journal of Contaminant Hydrology*, 91(1-2), 26–42. doi: 10.1016/j.jconhyd.2006.08.008.
- Göbel, P., Starke, P. and Coldewey, W. G. (2008), Evaporation measurements on enhanced water-permeable paving in urban areas, *in* '11th International Conference on Urban Drainage, Edinburgh, Scotland, UK, 2008'.
- Gessner, M., Hinkelmann, R., Nützmann, G., Jekel, M., Singer, G., Lewandowski, J., Nehls, T. and Barjenbruch, M. (2014), 'Urban water interfaces', *Journal of Hydrology*, 514, 226–232. doi: 10.1016/j.jhydrol.2014.04.021.
- Gilbert, J. K. and Clausen, J. C. (2006), 'Stormwater runoff quality and quantity from asphalt, paver, and crushed stone driveways in Connecticut', *Water Research*, 40(4), 826–832. doi: 10.1016/j.watres.2005.12.006.
- Glugla, G., Eyrich, A., König, B. and Fürtig, G. (1987), 'Wasserhaushaltsuntersuchungen im Raum Berlin (Investigating the water balance of Berlin)', *Wasserwirtschaft Wassertechnik*, 5, 113–116.
- Glugla, G., Goedecke, M., Wessolek, G. and Fürtig, G. (1999), 'Langjährige Abflussbildung und Wasserhaushalt im urbanen Gebiet Berlin (Long-term formation of runoff and water balance of the urban area Berlin)', *Wasserwirtschaft*, 89, 34–42.
- Gogate, N. G., Kalbar, P. P. and Raval, P. M. (2017), 'Assessment of stormwater management options in urban contexts using Multiple Attribute Decision-Making', *Journal of Cleaner Production*, 142(4), 2046–2059. doi: 10.1016/j.jclepro.2016.11.079.
- Google (2017), 'Google street view'. URL: <https://www.google.com/streetview/>, last accessed 2017-11-21.
- Grimmond, C. S. B. and Oke, T. R. (1991), 'An evapotranspiration-interception model for urban areas', *Water Resources Research*, 27(7), 1739–1755. doi: 10.1029/91wr00557.

- Grodek, T., Lange, J., Lekach, J. and Husary, S. (2011), ‘Urban hydrology in mountainous middle eastern cities’, *Hydrology and Earth System Sciences*, 15(3), 953–966. doi: 10.5194/hess-15-953-2011.
- Grolemund, G. and Wickham, H. (2011), ‘Dates and Times Made Easy with lubridate’, *Journal of Statistical Software*, 40(3), 1–25.
- Haase, D. (2009), ‘Effects of urbanisation on the water balance – A long-term trajectory’, *Environmental Impact Assessment Review*, 29(4), 211–219. doi: 10.1016/j.eiar.2009.01.002.
- Hannes, M., Wollschläger, U., Schrader, F., Durner, W., Gebler, S., Pütz, T., Fank, J., Unold, G. V. and j. Vogel, H. (2015), ‘A comprehensive filtering scheme for high-resolution estimation of the water balance components from high-precision lysimeters’, *Hydrology and Earth System Sciences*, 19(8), 3405–3418. doi: 10.5194/hess-19-3405-2015.
- Haselbach, L. M., Valavala, S. and Montes, F. (2006), ‘Permeability predictions for sand-clogged Portland cement pervious concrete pavement systems’, *Journal of Environmental Management*, 81(1), 42–49. doi: 10.1016/j.jenvman.2005.09.019.
- Hassn, A., Chiarelli, A., Dawson, A. and Garcia, A. (2016), ‘Thermal properties of asphalt pavements under dry and wet conditions’, *Materials & Design*, 91, 432–439. doi: 10.1016/j.matdes.2015.11.116.
- Heitman, J. L., Horton, R., Sauer, T. J. and DeSutter, T. M. (2008), ‘Sensible Heat Observations Reveal Soil-Water Evaporation Dynamics’, *Journal of Hydrometeorology*, 9(1), 165–171. doi: 10.1175/2007JHM963.1.
- Hendel, M., Gutierrez, P., Colombert, M., Diab, Y. and Royon, L. (2016), ‘Measuring the effects of urban heat island mitigation techniques in the field: Application to the case of pavement-watering in paris’, *Urban Climate*, 16, 43–58. doi: 10.1016/j.uclim.2016.02.003.
- Hibbs, B. J. and Sharp, J. M. (2012), ‘Hydrogeological Impacts of Urbanization’, *Environmental & Engineering Geoscience*, 18(1), 3–24. doi: 10.2113/gsegeosci.18.1.3.
- Hirschi, M., Michel, D., Lehner, I. and Seneviratne, S. I. (2017), ‘A site-level comparison of lysimeter and eddy covariance flux measurements of evapotranspiration’, *Hydrology and Earth System Sciences*, 21. doi: 10.5194/hess-21-1809-2017.
- Hollis, G. E. and Ovenden, J. C. (1988a), ‘One year irrigation experiment to assess losses and runoff volume relationships for a residential road in Hertfordshire, England’, *Hydrological Processes*, 2(1), 61–74. doi: 10.1002/hyp.3360020106.

- Hollis, G. E. and Owendon, J. C. (1988*b*), ‘The quantity of stormwater runoff from ten stretches of road, a car park and eight roofs in Hertfordshire, England during 1983’, *Hydrological Processes*, 2(3), 227–243. doi: 10.1002/hyp.3360020304.
- Howell, T., Schneider, A. and Jensen, M. (1991), History of Lysimeter Design and Use for Evapotranspiration Measurements, *in* ‘Proceedings of the International Symposium on Lysimetry, Honolulu’, pp. 1–9.
- InfraTec (2008), *IRBIS 3 Infrared Thermography Software – User Manual*.
- InfraTec (2012), *VarioCAM hr head incl. IRBIS remote 3.0 software description – User Manual*.
- Jacobson, C. R. (2011), ‘Identification and quantification of the hydrological impacts of imperviousness in urban catchments: A review’, *Journal of Environmental Management*, 92(6), 1438–1448. doi: 10.1016/j.jenvman.2011.01.018.
- Jacqueminet, C., Kermadi, S., Michel, K., Béal, D., Gagnage, M., Branger, F., Jankowsky, S. and Braud, I. (2013), ‘Land cover mapping using aerial and VHR satellite images for distributed hydrological modelling of periurban catchments: Application to the Yzeron catchment (Lyon, France)’, *Journal of Hydrology*, 485, 68–83. doi: 10.1016/j.jhydrol.2013.01.028.
- Jung, H., young Lee, S., Kim, H. S. and Lee, J. S. (2017), ‘Does improving the physical street environment create satisfactory and active streets? evidence from seoul’s design street project’, *Transportation Research Part D: Transport and Environment*, 50, 269–279. doi: 10.1016/j.trd.2016.11.013.
- Kakar, M. R., Hamzah, M. O. and Valentin, J. (2015), ‘A review on moisture damages of hot and warm mix asphalt and related investigations’, *Journal of Cleaner Production*, 99, 39–58. doi: 10.1016/j.jclepro.2015.03.028.
- Kaparias, I., Bell, M., Biagioli, T., Bellezza, L. and Mount, B. (2015), ‘Behavioural analysis of interactions between pedestrians and vehicles in street designs with elements of shared space’, *Transportation Research Part F: Traffic Psychology and Behaviour*, 30, 115–127. doi: 10.1016/j.trf.2015.02.009.
- Kardos, A. J. and Durham, S. A. (2015), ‘Strength, durability, and environmental properties of concrete utilizing recycled tire particles for pavement applications’, *Construction and Building Materials*, 98, 832–845. doi: 10.1016/j.conbuildmat.2015.08.065.
- Kassambara, A. (2016), *ggcorrplot: Visualization of a Correlation Matrix using ‘ggplot2’*. URL: <https://CRAN.R-project.org/package=ggcorrplot>, last accessed 2018-06-10.
- Kayhanian, M., Anderson, D., Harvey, J. T., Jones, D. and Muhunthan, B. (2012), ‘Permeability measurement and scan imaging to assess clogging of pervious concrete

- pavements in parking lots', *Journal of Environmental Management*, 95(1), 114–123. doi: 10.1016/j.jenvman.2011.09.021.
- Kelly, G., Delaney, D., Chai, G. and Mohamed, S. (2016), 'Optimising local council's return on investment from annual pavement rehabilitation budgets through targeting of the average pavement condition index', *Journal of Traffic and Transportation Engineering (English Edition)*, 3(5), 465–474. doi: 10.1016/j.jtte.2016.09.008.
- Kodešová, R., Fér, M., Klement, A., Nikodem, A., Teplá, D., Neuberger, P. and Bureš, P. (2014), 'Impact of various surface covers on water and thermal regime of Technosol', *Journal of Hydrology*, 519, 2272–2288. doi: 10.1016/j.jhydrol.2014.10.035.
- Kotteck, M., Grieser, J., Beck, C., Rudolf, B. and Rubel, F. (2006), 'World Map of the Köppen-Geiger climate classification updated', *Meteorologische Zeitschrift*, 15(3), 259–263. doi: 10.1127/0941-2948/2006/0130.
- Lakshmi, V., Jackson, T. J. and Zehrhuhs, D. (2003), 'Soil moisture-temperature relationships: results from two field experiments', *Hydrological Processes*, 17(15), 3041–3057. doi: 10.1002/hyp.1275.
- Lanthaler, C. (2004), Lysimeter Stations and Soil Hydrology Measuring Sites in Europe – Purpose, Equipment, Research Results, Future Developments, Master's thesis. URL: http://www.lysimeter.at/HP_EuLP/reports/THESIS_LYSIMETERS.pdf, last accessed 2018-06-03.
- Ledieu, J., Ridder, P. D., Clerck, P. D. and Dautrebande, S. (1986), 'A method of measuring soil moisture by time-domain reflectometry', *Journal of Hydrology*, 88(3-4), 319–328. doi: 10.1016/0022-1694(86)90097-1.
- Lehmann, A. and Stahr, K. (2007), 'Nature and significance of anthropogenic urban soils', *Journal of Soils and Sediments*, 7(4), 247–260. doi: 10.1065/jss2007.06.235.
- Lerner, D. N. (2002), 'Identifying and quantifying urban recharge: a review', *Hydrogeology Journal*, 10(1), 143–152. doi: 10.1007/s10040-001-0177-1.
- Liu, Z. and Hansen, W. (2016a), 'Effect of hydrophobic surface treatment on freeze-thaw durability of concrete', *Cement and Concrete Composites*, 69, 49–60. doi: 10.1016/j.cemconcomp.2016.03.001.
- Liu, Z. and Hansen, W. (2016b), 'Freeze-thaw durability of high strength concrete under deicer salt exposure', *Construction and Building Materials*, 102(1), 478–485. doi: 10.1016/j.conbuildmat.2015.10.194.
- López-Montero, T. and Miró, R. (2016), 'Differences in cracking resistance of asphalt mixtures due to ageing and moisture damage', *Construction and Building Materials*, 112, 299–306. doi: 10.1016/j.conbuildmat.2016.02.199.

- Mansell, M. and Rollet, F. (2006), ‘Water balance and the behaviour of different paving surfaces’, *Water and Environment Journal*, 20(1), 7–10. doi: 10.1111/j.1747-6593.2005.00015.x.
- Mansell, M. and Rollet, F. (2009), ‘The effect of surface texture on evaporation, infiltration and storage properties of paved surfaces’, *Water Science & Technology*, 60(1), 71. doi: 10.2166/wst.2009.323.
- Mansell, M. and Wang, S. (2010), ‘Water balance modelling in glasgow and beijing’, *Proceedings of the Institution of Civil Engineers - Water Management*, 163(5), 219–226. doi: 10.1680/wama.2010.163.5.219.
- Meissner, R., Prasad, M., Du Laing, G. and Rinklebe, J. (2010), ‘Lysimeter application for measuring the water and solute fluxes with high precision’, *Current Science*, 99(5), 601–607.
- Meissner, R., Seeger, J., Rupp, H., Seyfarth, M. and Borg, H. (2007), ‘Measurement of dew, fog, and rime with a high-precision gravitation lysimeter’, *Journal of Plant Nutrition and Soil Science*, 170(3), 335–344. doi: 10.1002/jpln.200625002.
- Menziani, M., Pugnaghi, S., Vincenzi, S. and Santangelo, R. (2003), ‘Soil moisture monitoring in the Toce valley (Italy)’, *Hydrology and Earth System Sciences*, 7(6), 890–902. doi: 10.5194/hess-7-890-2003.
- MetOffice (2012), ‘National meteorological library and archive fact sheet 3 – water in the atmosphere (version 01)’. URL: https://www.metoffice.gov.uk/binaries/content/assets/mohippo/pdf/f/c/fact_sheet_no._3.pdf, last accessed 2018-06-04.
- Miller, J. D., Kim, H., Kjeldsen, T. R., Packman, J., Grebby, S. and Dearden, R. (2014), ‘Assessing the impact of urbanization on storm runoff in a peri-urban catchment using historical change in impervious cover’, *Journal of Hydrology*, 515, 59–70. doi: 10.1016/j.jhydrol.2014.04.011.
- Mitchell, V., Mein, R. and McMahon, T. (2001), ‘Modelling the urban water cycle’, *Environmental Modelling & Software*, 16(7), 615–629. doi: 10.1016/s1364-8152(01)00029-9.
- Montzka, C., Canty, M., Kunkel, R., Menz, G., Vereecken, H. and Wendland, F. (2008), ‘Modelling the water balance of a mesoscale catchment basin using remotely sensed land cover data’, *Journal of Hydrology*, 353(3-4), 322–334. doi: 10.1016/j.jhydrol.2008.02.018.
- Morabito, M., Crisci, A., Messeri, A., Orlandini, S., Raschi, A., Maracchi, G. and Munafò, M. (2016), ‘The impact of built-up surfaces on land surface temperatures in italian urban areas’, *Science of The Total Environment*, 551-552, 317–326. doi: 10.1016/j.scitotenv.2016.02.029.

- Morel, J. L., Chenu, C. and Lorenz, K. (2014), ‘Ecosystem services provided by soils of urban, industrial, traffic, mining, and military areas (SUITMAs)’, *Journal of Soils and Sediments*, 15(8), 1659–1666. doi: 10.1007/s11368-014-0926-0.
- Nakayama, T. and Fujita, T. (2010), ‘Cooling effect of water-holding pavements made of new materials on water and heat budgets in urban areas’, *Landscape and Urban Planning*, 96(2), 57–67. doi: 10.1016/j.landurbplan.2010.02.003.
- Nandagiri, L. and Kooror, G. M. (2006), ‘Performance Evaluation of Reference Evapotranspiration Equations across a Range of Indian Climates’, *Journal of Irrigation and Drainage Engineering*, 132(3), 238–249. doi: 10.1061/(asce)0733-9437(2006)132:3(238).
- Nehls, T., Jozefaciuk, G., Sokołowska, Z., Hajnos, M. and Wessolek, G. (2006), ‘Pore-system characteristics of pavement seam materials of urban sites’, *Journal of Plant Nutrition and Soil Science*, 169(1), 16–24. doi: 10.1002/jpln.200521724.
- Nehls, T., Jozefaciuk, G., Sokolowska, Z., Hajnos, M. and Wessolek, G. (2008), ‘Filter properties of seam material from paved urban soils’, *Hydrology and Earth System Sciences*, 12(2), 691–702. doi: 10.5194/hess-12-691-2008.
- Nehls, T., Menzel, M. and Wessolek, G. (2015), ‘Depression storage capacities of different ideal pavements as quantified by a terrestrial laser scanning-based method’, *Water Science and Technology*, 71(6), 862–869. doi: 10.2166/wst.2015.025.
- Nehls, T., Rim, Y. N. and Wessolek, G. (2011), ‘Technical note on measuring run-off dynamics from pavements using a new device: the weighable tipping bucket’, *Hydrology and Earth System Sciences*, 15(5), 1379–1386. doi: 10.5194/hess-15-1379-2011.
- Niemczynowicz, J. (1999), ‘Urban hydrology and water management – present and future challenges’, *Urban Water*, 1(1), 1–14. doi: 10.1016/s1462-0758(99)00009-6.
- Oakdale Engineering (2014), ‘DataFit’. URL: <http://www.oakdaleengr.com/datafit.htm>, last accessed 2018-06-19.
- Open Street Map Contributors (2017), ‘Open Street Map’. URL: <https://www.openstreetmap.org>, last accessed 2017-11-17.
- Open Street Map Wiki Contributors (2017), ‘Open Street Map Wiki – Key:surface’. URL: <http://wiki.openstreetmap.org/wiki/Key:surface>, last accessed 2017-11-17.
- Penttala, V. (2006), ‘Surface and internal deterioration of concrete due to saline and non-saline freeze–thaw loads’, *Cement and Concrete Research*, 36(5), 921–928. doi: 10.1016/j.cemconres.2005.10.007.
- Peters, A., Nehls, T., Schonsky, H. and Wessolek, G. (2014), ‘Separating precipitation and evapotranspiration from noise – a new filter routine for high-resolution lysimeter

- data', *Hydrology and Earth System Sciences*, 18(3), 1189–1198. doi: 10.5194/hess-18-1189-2014.
- Peters, A., Nehls, T. and Wessolek, G. (2016), 'Technical note: Improving the AWAT filter with interpolation schemes for advanced processing of high resolution data', *Hydrology and Earth System Sciences*, 20(6), 2309–2315. doi: 10.5194/hess-20-2309-2016.
- Pistocchi, A., Calzolari, C., Malucelli, F. and Ungaro, F. (2015), 'Soil sealing and flood risks in the plains of Emilia-Romagna, Italy', *Journal of Hydrology: Regional Studies*, 4(B), 398–409. doi: 10.1016/j.ejrh.2015.06.021.
- Qin, H., Li, Z. and Fu, G. (2013), 'The effects of low impact development on urban flooding under different rainfall characteristics', *Journal of Environmental Management*, 129, 577–585. doi: 10.1016/j.jenvman.2013.08.026.
- Qin, Y. (2015), 'A review on the development of cool pavements to mitigate urban heat island effect', *Renewable and Sustainable Energy Reviews*, 52, 445–459. doi: 10.1016/j.rser.2015.07.177.
- R Core Team (2016), *R: A Language and Environment for Statistical Computing*, R Foundation for Statistical Computing, Vienna, Austria. URL: <https://www.R-project.org/>, last accessed 2018-06-04.
- Ragab, R., Rosier, P., Dixon, A., Bromley, J. and Cooper, J. D. (2003), 'Experimental study of water fluxes in a residential area: 2. Road infiltration, runoff and evaporation', *Hydrological Processes*, 17(12), 2423–2437. doi: 10.1002/hyp.1251.
- Ramier, D., Berthier, E. and Andrieu, H. (2004), 'An urban lysimeter to assess runoff losses on asphalt concrete plates', *Physics and Chemistry of the Earth, Parts A/B/C*, 29(11-12), 839–847. doi: 10.1016/j.pce.2004.05.011.
- Ramier, D., Berthier, E. and Andrieu, H. (2011), 'The hydrological behaviour of urban streets: long-term observations and modelling of runoff losses and rainfall-runoff transformation', *Hydrological Processes*, 25(14), 2161–2178. doi: 10.1002/hyp.7968.
- Ramier, D., Berthier, E., Dangla, P. and Andrieu, H. (2006), 'Study of the water budget of streets: experimentation and modelling', *Water Science & Technology*, 54(6-7), 41. doi: 10.2166/wst.2006.587.
- Rana, G. and Katerji, N. (2000), 'Measurement and estimation of actual evapotranspiration in the field under Mediterranean climate: a review', *European Journal of Agronomy*, 13(2-3), 125–153. doi: 10.1016/s1161-0301(00)00070-8.
- Raziei, T. and Pereira, L. S. (2013), 'Estimation of ET_0 with Hargreaves–Samani and FAO-PM temperature methods for a wide range of climates in Iran', *Agricultural Water Management*, 121, 1–18. doi: 10.1016/j.agwat.2012.12.019.

- Revitt, D. M., Lundy, L., Coulon, F. and Fairley, M. (2014), ‘The sources, impact and management of car park runoff pollution: A review’, *Journal of Environmental Management*, 146, 552–567. doi: 10.1016/j.jenvman.2014.05.041.
- Richards, D. R. and Edwards, P. J. (2017), ‘Quantifying street tree regulating ecosystem services using Google Street View’, *Ecological Indicators*, 77, 31–40. doi: 10.1016/j.ecolind.2017.01.028.
- Rim, Y. (2011), Analyzing Runoff Dynamics of paved Soil Surface Using Weighable Lysimeters, PhD thesis, Technical University Berlin.
- Rodriguez, F., Andrieu, H. and Morena, F. (2008), ‘A distributed hydrological model for urbanized areas – Model development and application to case studies’, *Journal of Hydrology*, 351(3-4), 268–287. doi: 10.1016/j.jhydrol.2007.12.007.
- Rodríguez, M. C., Dupont-Courtade, L. and Oueslati, W. (2016), ‘Air pollution and urban structure linkages: Evidence from European cities’, *Renewable and Sustainable Energy Reviews*, 53, 1–9. doi: 10.1016/j.rser.2015.07.190.
- Salvadore, E., Bronders, J. and Batelaan, O. (2015), ‘Hydrological modelling of urbanized catchments: A review and future directions’, *Journal of Hydrology*, 529(1), 62–81. doi: 10.1016/j.jhydrol.2015.06.028.
- Scalenghe, R. and Marsan, F. A. (2009), ‘The anthropogenic sealing of soils in urban areas’, *Landscape and Urban Planning*, 90(1-2), 1–10. doi: 10.1016/j.landurbplan.2008.10.011.
- Schrader, F., Durner, W., Fank, J., Gebler, S., Pütz, T., Hannes, M. and Wollschläger, U. (2013), ‘Estimating Precipitation and Actual Evapotranspiration from Precision Lysimeter Measurements’, *Procedia Environmental Sciences*, 19, 543–552. doi: 10.1016/j.proenv.2013.06.061.
- Schrödter, H. (1985), *Verdunstung – Anwendungsorientierte Meßverfahren und Bestimmungsmethoden (Evaporation – Applied methods for measurement and estimation)*, Springer Berlin Heidelberg. doi: 10.1007/978-3-642-70434-5.
- Seiferling, I., Naik, N., Ratti, C. and Proulx, R. (2017), ‘Green streets - Quantifying and mapping urban trees with street-level imagery and computer vision’, *Landscape and Urban Planning*, 165, 93–101. doi: 10.1016/j.landurbplan.2017.05.010.
- Shuster, W. D., Bonta, J., Thurston, H., Warnemuende, E. and Smith, D. R. (2005), ‘Impacts of impervious surface on watershed hydrology: A review’, *Urban Water Journal*, 2(4), 263–275. doi: 10.1080/15730620500386529.
- Šimůnek, J., Genuchten, M. T. V. and Šejna, M. (2016), ‘Recent Developments and Applications of the HYDRUS Computer Software Packages’, *Vadose Zone Journal*, 15(7), 25. doi: 10.2136/vzj2016.04.0033.

- Smith, M. L., Zhou, W., Cadenasso, M., Grove, M. and Band, L. E. (2010), 'Evaluation of the National Land Cover Database for Hydrologic Applications in Urban and Suburban Baltimore, Maryland', *JAWRA Journal of the American Water Resources Association*, 46(2), 429–442. doi: 10.1111/j.1752-1688.2009.00412.x.
- Solpuker, U., Sheets, J., Kim, Y. and Schwartz, F. (2014), 'Leaching potential of pervious concrete and immobilization of Cu, Pb and Zn using pervious concrete', *Journal of Contaminant Hydrology*, 161, 35–48. doi: 10.1016/j.jconhyd.2014.03.002.
- Starke, P., Göbel, P. and Coldewey, W. G. (2010), 'Urban evaporation rates for water-permeable pavements', *Water Science & Technology*, 62(5), 1161. doi: 10.2166/wst.2010.390.
- Starke, P., Göbel, P. and Coldewey, W. G. (2011), 'Effects on evaporation rates from different water-permeable pavement designs', *Water Science & Technology*, 63(11), 2619. doi: 10.2166/wst.2011.168.
- Stoffregen, H. (1998), 'Hydraulische Eigenschaften deponiespezifischer Materialien unter Berücksichtigung von Temperaturveränderungen (Hydraulic properties of landfill materials related to temperature changes)'. Rote Reihe - Bodenökologie und Bodengeneese Heft 32.
- Thoen, E. (2017), *padr: Quickly Get Datetime Data Ready for Analysis*. URL: <https://CRAN.R-project.org/package=padr>, last accessed 2018-06-10.
- Timm, A., Kluge, B. and Wessolek, G. (2018), 'Hydrological balance of paved surfaces in moist mid-latitude climate – a review', *Landscape and Urban Planning*, 175, 80–91. doi: 10.1016/j.landurbplan.2018.03.014.
- Trinks, S. (2010), Einfluss des Wasser- und Wärmehaushaltes von Böden auf den Betrieb erdverlegter Energiekabel (Influence hydrological and heat balance of the soil on operation of underground power cables), PhD thesis, Technical University Berlin.
- UN (2014), World urbanization prospects - 2014 revision, Technical report, United Nations. URL: <https://esa.un.org/unpd/wup/publications/files/wup2014-report.pdf>, last accessed 2018-06-21.
- Unold, G. V. and Fank, J. (2007), 'Modular Design of Field Lysimeters for Specific Application Needs', *Water, Air, & Soil Pollution: Focus*, 8(2), 233–242. doi: 10.1007/s11267-007-9172-4.
- Ward, H., Kotthaus, S., Järv, i. L. and Grimmond, C. (2016), 'Surface Urban Energy and Water Balance Scheme (SUEWS): Development and evaluation at two UK sites', *Urban Climate*, 18, 1–32. doi: 10.1016/j.uclim.2016.05.001.

- Wessolek, G. (1993), Erarbeitung eines Schlüssels zur Einschätzung von Versickerung und Oberflächenabfluß versiegelter Flächen Berlins (Development of a tool to estimate infiltration and runoff of sealed surfaces in Berlin). Unpublished Research Report commissioned by the Federal Agency for Hydrology Germany, executed at Technical University Berlin, Germany.
- Wessolek, G. (1994), Auswertung von Versuchen zur Ermittlung der Abflußverhältnisse unterschiedlich versiegelter und kanalisierter Flächen Berlins (Evaluating experiments investigating drainage from different sealed and canalised areas in Berlin). Unpublished Research Report commissioned by the Federal Agency for Hydrology Germany, executed at Technical University Berlin, Germany.
- Wessolek, G. (2001), ‘Bodenüberformung und -versiegelung (Transformation and sealing of soil)’, *Handbuch der Bodenkunde*. doi: 10.1002/9783527678495.hbbk2001002.
- Wessolek, G., Duijnsveld, W. and Trinks, S. (2008), ‘Hydro-pedotransfer functions (HPTFs) for predicting annual percolation rate on a regional scale’, *Journal of Hydrology*, 356(1-2), 17–27. doi: 10.1016/j.jhydrol.2008.03.007.
- Wessolek, G. and Facklam, M. (1997), ‘Standorteigenschaften und Wasserhaushalt von versiegelten Flächen (Characteristics and water balance of sealed surfaces)’, *Journal of Plant Nutrition and Soil Science*, 160(1), 41–46. doi: 10.1002/jpln.19971600109.
- Wessolek, G., Kaupenjohann, M. and Renger, M. (2009), *Bodenphysikalische Kennwerte und Berechnungsverfahren für die Praxis (Soil physical parameters and calculation methods for use in practice)*, Vol. 40 of *Bodenökologie und Bodengese*, TU Berlin. URL: https://www.boden.tu-berlin.de/fileadmin/fg77/_pdf/Rote_Liste/Rote_Reihe_Heft_40.pdf, last accessed 2018-06-25.
- Wessolek, G., Kluge, B., Nehls, T. and Kocher, B. (2009), ‘Aspekte zum Wasserhaushalt und Stofftransport urbaner Flächen (Aspects of water balance and solute transport of urban surfaces)’, *Korrespondenz Wasserwirtschaft*, 2(4), 205–210. doi: 10.3243/kwe2009.04.001.
- Wickham, H. (2009), *ggplot2: Elegant Graphics for Data Analysis*, Springer-Verlag New York.
- Wickham, H. (2011), ‘The Split-Apply-Combine Strategy for Data Analysis’, *Journal of Statistical Software*, 40(1), 1–29.
- Wiles, T. J. and Sharp, J. M. (2008), ‘The Secondary Permeability of Impervious Cover’, *Environmental and Engineering Geoscience*, 14(4), 251–265. doi: 10.2113/gsee-geosci.14.4.251.

- Willuweit, L. and O'Sullivan, J. J. (2013), 'A decision support tool for sustainable planning of urban water systems: Presenting the Dynamic Urban Water Simulation Model', *Water Research*, 47(20), 7206–7220. doi: 10.1016/j.watres.2013.09.060.
- Wu, J., Tang, C., Shi, B., Gao, L., Jiang, H. and Daniels, J. (2014), 'Effect of Ground Covers on Soil Temperature in Urban and Rural Areas', *Environmental & Engineering Geoscience*, 20(3), 225–237. doi: 10.2113/gsegeosci.20.3.225.
- Xu, H., Guo, W. and Tan, Y. (2016), 'Permeability of asphalt mixtures exposed to freeze–thaw cycles', *Cold Regions Science and Technology*, 123, 99–106. doi: 10.1016/j.coldregions.2015.12.001.
- Yao, L., Wei, W. and Chen, L. (2016), 'How does imperviousness impact the urban rainfall-runoff process under various storm cases?', *Ecological Indicators*, 60, 893–905. doi: 10.1016/j.ecolind.2015.08.041.
- Yoder, R. E., Odhiambo, L. O. and Wright, W. C. (2005), 'Evaluation Of Methods For Estimating Daily Reference Crop Evapotranspiration At A Site In The Humid Southeast United States', *Applied Engineering in Agriculture*, 21(2), 197–202. doi: 10.13031/2013.18153.
- Yong, C., McCarthy, D. and Deletic, A. (2013), 'Predicting physical clogging of porous and permeable pavements', *Journal of Hydrology*, 481, 48–55. doi: 10.1016/j.jhydrol.2012.12.009.
- Zeileis, A. and Grothendieck, G. (2005), 'zoo: S3 Infrastructure for Regular and Irregular Time Series', *Journal of Statistical Software*, 14(6), 1–27. doi: 10.18637/jss.v014.i06.
- Zhang, W., Min, H. and Gu, X. (2016), 'Temperature response and moisture transport in damaged concrete under an atmospheric environment', *Construction and Building Materials*, 123, 290–299. doi: 10.1016/j.conbuildmat.2016.07.004.
- Zoppou, C. (2001), 'Review of urban storm water models', *Environmental Modelling & Software*, 16(3), 195–231. doi: 10.1016/s1364-8152(00)00084-0.

A Appendices

A.1 Extended tables & figures

	Volumetric water content (θ) [Vol.-%]					
	Cobblestones			Concrete slabs		
	5 cm	15 cm	25 cm	5 cm	15cm	25cm
2016-06	11.46	14.79	18.09	10.18	13.71	17.23
2016-07	11.32	14.74	17.94	9.90	13.53	17.05
2016-08	11.45	14.91	17.94	9.87	13.63	17.07
2016-09	11.14	14.68	17.92	9.53	13.35	16.67
2016-10 [†]	10.91	14.06	18.29	9.32	13.15	16.78
2016-11	9.75	13.48	18.32	8.21	12.60	16.36
2016-12	10.00	13.25	18.06	7.86	12.61	16.16
2017-01	9.88	13.28	18.32	6.74	12.53	16.04
2017-02	10.29	13.44	18.46	7.75	12.71	16.20
2017-03	10.87	13.92	18.74	8.51	13.14	16.80
2017-04	10.69	13.87	18.25	8.66	13.14	16.52
2017-05	11.02	14.27	17.83	9.43	13.60	17.05

[†] No data available for 17 out of 31 days in October 2016

Table A.1: Monthly mean volumetric water content (θ) [Vol.-%] measured at 5, 15 and 25 cm below paver

	Cobblestones				Concrete slabs				T_{air}		
	surface	paver*	5 cm	15 cm	25 cm	surface	paver*	5 cm		15 cm	25 cm
<i>Annual</i>											
Min T [°C]	-8.03	-6.58	-0.80	0.63	0.95	-7.33	-7.17	-1.86	0.49	1.10	-11.30
Mean T [°C]	11.73	10.26	13.28	13.52	13.59	12.81	11.00	13.66	14.01	14.06	10.13
Median T [°C]	9.61	7.85	11.05	11.29	11.50	10.32	8.38	11.20	11.74	11.89	9.20
Max T [°C]	47.23	43.92	39.63	35.57	33.43	51.52	47.12	44.15	38.41	34.62	35.50
<i>Summer</i>											
Min T [°C]	0.75	0.63	5.61	7.08	7.94	1.99	1.23	5.01	7.45	8.68	-0.30
Mean T [°C]	19.62	18.35	21.04	20.96	20.78	21.31	19.46	21.96	21.81	21.47	16.40
Median T [°C]	18.98	18.07	21.90	22.20	22.18	20.09	18.71	22.29	22.83	22.81	16.35
Max T [°C]	47.23	43.92	39.63	35.57	33.43	51.52	47.12	44.15	38.41	34.62	35.50
<i>Winter</i>											
Min T [°C]	-8.03	-6.58	-0.80	0.63	0.95	-7.33	-7.17	-1.86	0.49	1.10	-11.30
Mean T [°C]	4.13	2.47	5.78	6.34	6.66	4.62	2.84	5.64	6.49	6.90	3.76
Median T [°C]	3.75	1.83	5.55	6.29	6.65	4.01	2.00	4.97	6.20	6.70	3.60
Max T [°C]	26.72	24.40	21.54	18.89	17.59	30.73	28.68	26.64	21.57	19.08	24.00

*Measurement underside paver

Table A.2: Hourly surface & soil temperatures T measured on top and within the lysimeter soil column. Hydrological summer May to October, hydrological winter November to April

	Monthly mean temperature [°C]													T_{air}
	Cobblestones						Concrete slabs							
	surface	paver*	5 cm	15 cm	25 cm	surface	paver*	5 cm	15 cm	25 cm				
2016-06	24.18	23.22	25.37	24.96	24.50	26.21	24.63	26.73	26.10	25.38	19.03			
2016-07	23.45	21.83	24.63	24.42	24.10	25.21	23.14	25.81	25.44	24.89	19.77			
2016-08	23.21	21.85	24.34	24.14	23.87	24.61	22.80	25.15	24.87	24.35	18.28			
2016-09	20.43	18.90	21.78	21.84	21.77	21.59	19.72	22.37	22.41	22.23	17.80			
2016-10 [†]	9.54	7.72	11.02	11.57	11.89	10.12	8.09	10.98	11.78	12.24	8.73			
2016-11	3.02	1.21	4.70	5.36	5.76	3.41	1.43	4.45	5.54	6.15	3.56			
2016-12	2.18	-0.03	3.17	3.71	4.00	2.25	0.02	2.85	3.74	4.24	2.61			
2017-01	0.19	-1.63	2.09	3.04	3.61	0.05	-1.68	1.32	2.75	3.42	-1.16			
2017-02	2.81	1.09	4.68	5.45	5.86	2.93	1.19	4.21	5.13	5.856	2.05			
2017-03	7.09	5.62	8.83	9.33	9.61	7.80	6.28	8.83	9.64	9.91	7.22			
2017-04	9.72	8.85	11.60	11.62	11.59	11.49	10.06	12.39	12.48	12.25	8.29			
2017-05	19.88	19.56	21.73	21.28	20.82	23.14	21.46	23.49	22.74	22.03	14.98			

*Measurement underside paver

[†]No data available for 17 out of 31 days in October 2016, T_{air} unaffected

Table A.3: Monthly mean air, surface & soil temperatures T measured on top and within the lysimeter soil column

	Year	Season		Month												
		S	W	1	2	3	4	5	6	7	8	9	10	11	12	
<i>Annual</i>																
κ cobblestones	0.22	0.16	0.30	0.62	0.41	0.29	0.25	0.20	0.11	0.13	0.13	0.13	0.13	0.32	0.35	0.36
κ concrete slabs	0.12	0.08	0.34	0.63	0.44	0.19	0.06	0.08	0.08	0.08	0.08	0.08	0.05	0.29	0.59	1.14
<i>Dry days</i>																
κ_d cobblestones	0.21	0.15	0.33	1.31	0.41	0.26	0.26	0.21	0.08	0.10	0.12	0.12	0.12	0.47*	0.47	0.83*
κ_d concrete slabs	0.08	0.05	0.31	0.61	0.87	0.12	0.05	0.05	0.06	0.05	0.07	0.04	0.38*	0.74	6.13*	
<i>Wet days</i>																
κ_w cobblestones	0.24	0.18	0.28	0.25	0.40	0.42	0.23	0.18	0.21	0.16	0.13*	0.30*	0.20*	0.18	0.24	
κ_w concrete slabs	0.23	0.15	0.39	0.69	0.28	0.37	0.15	0.13	0.14	0.17	0.11*	0.38*	0.09*	0.52	0.64	
number dry days	183	101	82	14	12	15	20	21	16	15	17	27	5	13	8	
number wet days	149	59	90	15	14	15	10	10	14	14	9	3	9	15	21	

*Values based on few data points (< 10 values)

Table A.4: Ratio (κ) of evaporation E of paved surfaces to grass-reference evapotranspiration ET_0 . Based on daily measurements (E) and calculations (ET_0) for yearly, seasonal and monthly data, and for both wet and dry days. Dry days defined as days with $P = 0 \text{ mm d}^{-1}$, all other days considered wet days. S = Summer, W = Winter

hourly air, surface and soil temperatures

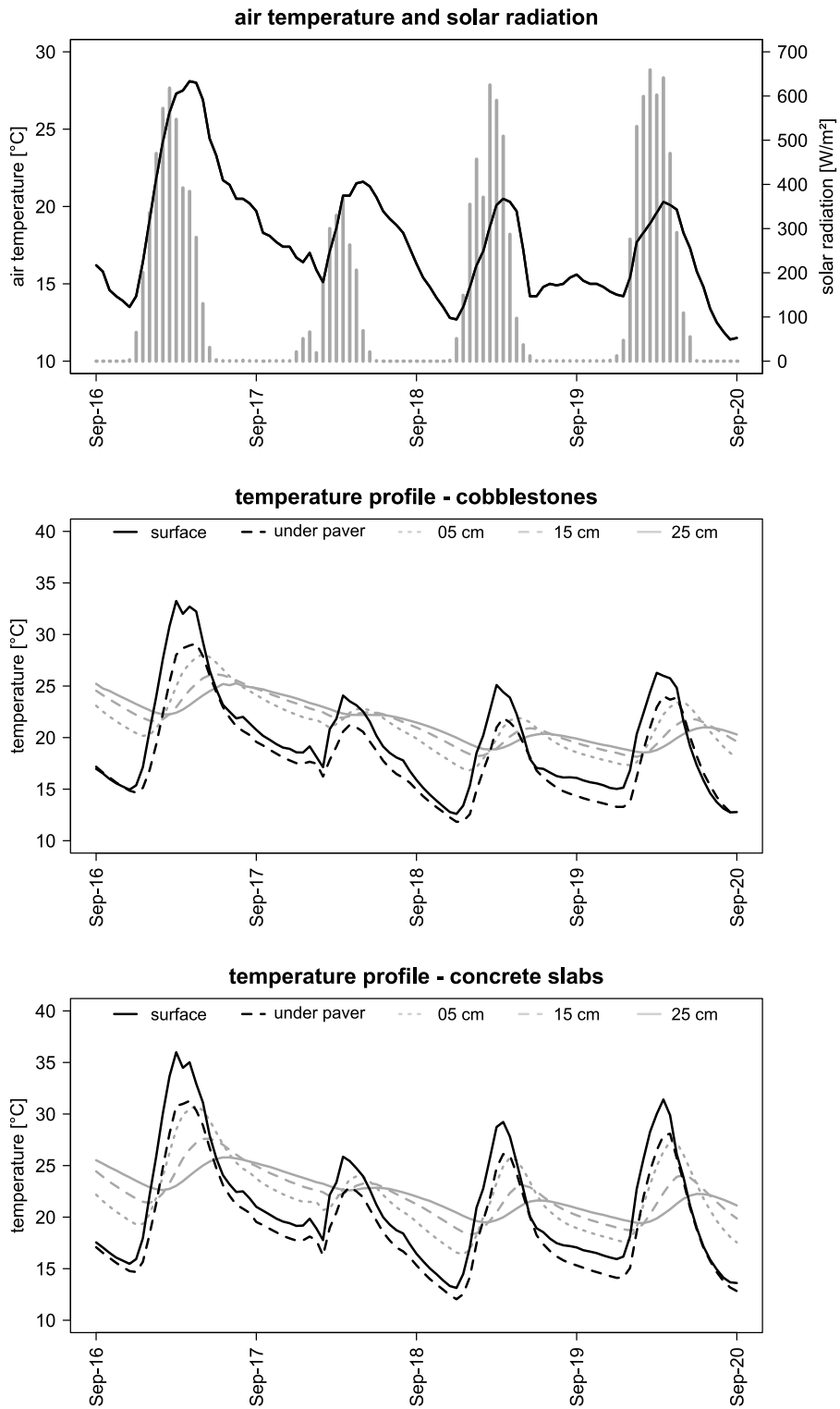


Figure A.1: Hourly air, surface & soil temperatures – period with highest precipitation event from September 16th to September 20th, 2016

monthly κ_w & κ_d derived from air temperature

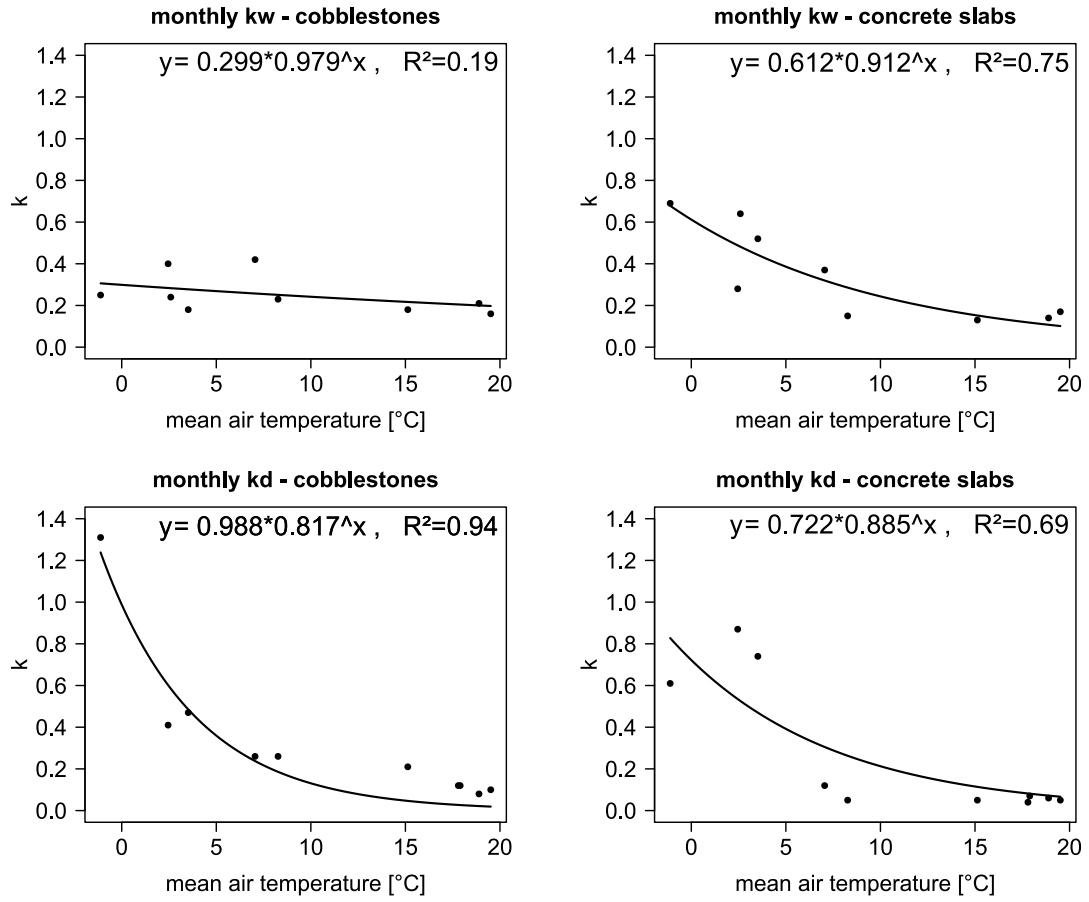


Figure A.2: Deriving median measured monthly wet (κ_w) and dry (κ_d) reduction coefficients from monthly mean values of T_{air}

A.2 Lysimeter reconstruction



(a) empty lysimeter



(b) mesh protecting infiltration outlet



(c) installation of gradient drainage layer



(d) compacting of layers



(e) preparing slope



(f) installation of cobblestone surface



(g) fresh surface – concrete slabs



(h) fresh surface – cobblestones

Figure A.3: Impressions from lysimeter reconstruction in April 2016



Figure A.4: Installation of sensor for soil water content and temperature measurement, sensor is pushed into already compacted soil